Optical Techniques for Multi-point and Variable Wavelength Laser Ignition

Thesis submitted in accordance with the requirements of the University of Liverpool for the degree of Doctor in Philosophy by

Elliott Christopher George Lyon

June 2017

Abstract

The use of laser ignition (LI) in an internal combustion engine as a replacement for traditional spark ignition (SI) has been researched over the last few decades. These studies have shown advantages in using LI over SI, however there is still room for improvement. This thesis presents work on developing optical techniques for creating multi-point and variable wavelength LI, in order to improve engine performance relative to standard LI.

A spatial light modulator (SLM) was used for the first time to generate multi-location LI. Techniques were developed to deliver these multi-beams to the engine and create arbitrary arrangements of foci in three dimensions. Tests were carried out on a single cylinder test engine using two-location LI which showed improved engine performance and stability when compared with single-location LI, especially in lean air-fuel mixtures. Two-location LI ran successfully without misfires at $\lambda = 1.2$, while increasing engine output power by $\approx 10\%$ when compared with single-location LI.

Two wavelengths, 1064 nm and 532 nm, were compared in depth in terms of spark formation and engine performance, however few differences were found. Therefore a technique to achieve LI with continuously tunable wavelength was investigated, which used an optical parametric oscillator. Challenges related to implementing this system are discussed.

Acknowledgements

I would first like to thank my supervisor Geoff Dearden for giving me the opportunity to do this PhD, and for help and support throughout. From the laser ignition project I would especially like to thank Zheng Kuang for help and advice throughout my experiements, as well as Vincent Page, Hua Cheng and Tom Shenton.

I would also like to thank members of the laser group who have supported my research, Stuart Edwardson, Andy Snaylam, Andrea Jones and Walter Perrie.

Finally thanks to Katie and to my Mum and Dad for putting up with me through my endless years of being a student.

Declaration

I hereby declare that all of the work contained within this thesis is my own and has not been submitted for any other qualification.

Signed:

Date:

List of Publications

Journal

Lyon, E., Kuang, Z., Cheng, H., Page, V., Shenton, T., and Dearden, G. (2014). Multi-point laser spark generation for internal combustion engines using a spatiallight modulator. *Journal of Physics D: Applied Physics*, 47(47):475501

Cheng, H., Kuang, Z., Page, V., Lyon, E., Dearden, G., and Shenton, T. (2016). Multiple pulse laser ignition in gdi lean combustion. *International Journal of Powertrains (IJPT)*, 6(1):55–68

Kuang, Z., Lyon, E., Cheng, H., Page, V., Shenton, T., and Dearden, G. (2017). Multi-location laser ignition using a spatial light modulator towards improving automotive gasoline engine performance. *Optics and Lasers in Engineering*, 90:275 – 283

Conference

Cheng, H., Kuang, Z., Page, V., Lyon, E., Dearden, G., and Shenton, T. (2014a). An Investigation of Multi-pulse Laser Ignition in a GDI engine. In *The 2nd. Laser Ignition Conference (LIC'14)*, Yokohama, Japan, Apr. 22 - 24, 2014

Kuang, Z., Lyon, E., Cheng, H., Page, V., Shenton, T., and Dearden, G. (2014). Multi-point Laser ignition of internal combustion engines using a spatial light modulator. In

The 2nd. Laser Ignition Conference (LIC'14), Yokohama, Japan, Apr. 22 - 24, 2014

Cheng, H., Kuang, Z., Page, V., Lyon, E., Dearden, G., and Shenton, T. (2014b). Multiple Pulse Laser Ignition in GDI Lean Combustion. In *PMC2014 2nd Biennial Conference on Powertrain Mapping and Calibration*, Bradford UK

Page, V., Lyon, E., Cheng, H., Shenton, T., Kuang, Z., and Dearden, G. (2014). Calibration of Ignition Location and Pulse Energy in the Laser Ignited Engine. In *PMC2014 2nd Biennial Conference on Powertrain Mapping and Calibration*, Bradford UK

Cheng, H., Vincent, P., Kuang, Z., Lyon, E., Dearden, G., and Shenton, T. (2015). Multiple Pulse Laser Ignition Control Application in GDI Lean Combustion. In *Laser Ignition Conference*, page W2A.2. Optical Society of America

Kuang, Z., Lyon, E., Hua, C., page, V., Shenton, T., and dearden, G. (2015). Diffractive Multi-point Laser ignition of internal combustion engines using a spatial light modulator. In *Laser Ignition Conference*, page W2A.4. Optical Society of America

Page, V., CHENG, H., Shenton, T., Lyon, E., Kuang, Z., and dearden, G. (2015). Neural Network Prediction of Engine Performance for Second Pulse Fire/No Fire Decision Making in Dual Pulse Laser Ignited Engines. In *Laser Ignition Conference*, page Th4A.3. Optical Society of America

Dearden, G., Kuang, Z., Lyon, E., Cheng, H., Page, V., and Shenton, T. (2016). Multi-point laser ignition for in-combustion event feedback control of an automobile engine. In *Laser Ignition Conference*, Yokohama, Japan, May 18 - 20, 2016

Contents

List of Figures

Chapter 1

Introduction

Reducing greenhouse gas emissions and improving fuel economy are of concern to car manufacturers looking to develop new internal combustion engines, due to government regulation and consumer demand. New technologies such as electric vehicles will not fully displace internal combustion (IC) engines for some time, and hybrid vehicles will still require them. Therefore further optimisation of the IC engine remains important, but challenging.

An area that has few possibilities for optimisation is the spark plug. Engine ignition systems based on the spark plug have been produced for automotive engines for more than a century. Over the last few decades alternatives have been researched, including laser ignition. The concept of laser ignition is to either have a compact laser fitted where a spark plug would be, or to deliver the beam here from a remote laser head. The laser beam is focussed into the cylinder via a lens, where the intensity of the light at the focal point creates a plasma, which is capable of igniting the air-fuel mixture.

There are a number of limitations to spark ignition (SI) which might be overcome by using laser ignition (LI). A spark plug will always be in a fixed location close to the cylinder wall, where flame quenching can take place. With LI, the spark can be moved to the centre of the cylinder or wherever is most optimal, with no electrodes intruding into the cylinder. Additionally LI brings new options, including having

multiple breakdown points in space and time, which can be dynamically controlled from cycle to cycle. Comparisons will be discussed in detail in Chapter 2. It is hoped that laser ignition could improve the operation of the IC engine in terms of fuel efficiency, cycle to cycle variation reduction, emission levels and the type of emissions.

Research into laser ignition began around forty years ago, following the invention of the first laser. LI has been used in various applications, such as automotive engines, aircraft engines and gas turbines. The research presented in this thesis is primarily concerned with the application of LI to automotive engines. A variety of lasers have been used for this purpose, but generally they are nanosecond pulsed with millijoule pulse energy. This is due to the threshold in peak power density of $10 \times 10^{11}\,\mathrm{W\,cm^{-2}}$ required for laser air breakdown (Phuoc, 2000a). Extensive research has shown advantages over SI when comparing engine performance. Laser technology has reached a point where achieving LI with a compact laser is not far off, though progress still needs to be made in terms of improving and mass producing these compact lasers. It is also unclear exactly which kind of laser would be best suited for the purpose as there are various potentially useful laser parameters that have not yet been tested in the context of LI.

The aim of this project was to work towards improvements in LI techniques in order to inform the designs for compact lasers in the near future. It was motivated by gaps in knowledge such as there being limited tests of the effect of multi-point LI. Specific objectives were to study multi-point and variable wavelength LI, and to measure their effect on engine performance. This was achieved by developing techniques including using a spatial light modulator, and published in a number of journal articles (Lyon et al., 2014; Cheng et al., 2016; Kuang et al., 2017).

This PhD was part of an EPSRC funded project "Towards In-Combustion Event Feedback (ICEF) control in laser ignition" (EPSRC grant reference: EP/J003573/1). This involves the Laser Group and the Power train Control Group in the Department of Engineering at the University of Liverpool, as well as partners at Newcastle University, Ford Motor Company, and Cambustion. The author's role was focussed on the laser systems, specifically building and testing them, and later using them in engine tests.

The rest of this thesis is structured as follows:

Chapter 2 is the literature review, where relevant background and previous work in the field will be discussed. Gaps in the knowledge that motivated this research will be highlighted.

Chapter 3 describes the experimental methodology and equipment used during the experiments. Basic techniques common to all of the experiments will be covered, with more detail left to the results chapters.

Results are presented in Chapters 4 to 6. Single-point laser ignition experiments are presented in Chapter 4. Laser and engine parameters were varied in order to find the most optimal way to ignite the test engine. Offline work on the laser system and characterisation of the beam are also discussed.

Chapter 5 covers multi-point LI. A spatial light modulator (SLM) was used to achieve this, since it has the capability to move the focal point in three dimensions, as one of the main advantages of LI over SI is that the ignition position can be changed. The SLM can also be used to split the energy of each laser pulse into multiple focus spots. Experiments in this area aimed to implement the technique in an engine environment and measure how it affected the performance.

Chapter 6 details an investigation into the effect of wavelength on LI. Two wavelengths, the Nd:YAG fundamental and second harmonic, were compared in terms of creating a spark in air and engine performance. A system to generate a continuous range of wavelengths using a optical parametric oscillator was tested unsuccessfully, improvements needed to implement this will be discussed.

Finally Chapter 7 will contain conclusions and recommendations for future work.

Chapter 2

Literature Review

This chapter includes relevant background on lasers, optics and engines, as well as a state of the art literature review on laser ignition.

2.1 Lasers

The section will cover background on lasers, optics, and optical techniques, as well as spatial light modulators.

2.1.1 Q-switched Solid State Laser Fundamentals

A laser is a device which generates an intense, collimated, monochromatic beam of light at a certain wavelength, depending on the materials it is made from. There are many possible types of laser, in this research only flashlamp pumped Q-switched lasers were used.

The basic components that make up a flashlamp pumped Q-switched laser are shown in Figure 2.1 (Steen, 1991; Hecht, 2002). The core of a laser is the lasing medium, here an Nd:YAG rod. The requirement for a lasing medium is for it to have a metastable excited electron state, which exists long enough for a large number of electrons to be

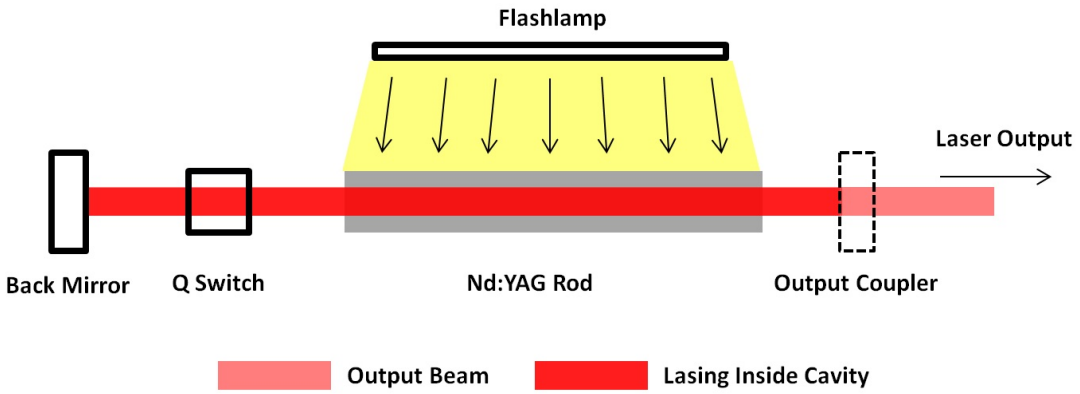

Figure 2.1: Diagram of the basic components that make up a flashlamp pumped Q-switched laser head.

excited into it at the same time.

Adjacent to the rod is a flashlamp, which is capable of producing a short burst of very intense light. When the lamp flashes, much of the light enters the rod, where part of the energy is absorbed by its electrons, allowing them to be excited into the metastable state. The lamp is powerful enough that at some point during the flash, a large proportion of the electrons are at the metastable state at the same time, which is known as a population inversion. Over time, these electrons will spontaneously decay back to the ground state, releasing the stored energy as photons, which have a specific energy for a given lasing medium. Photons produced using a Nd:YAG rod have a wavelength of 1064 nm. When these photons are released, they will travel in a random direction.

Around the Nd:YAG rod are two mirrors, forming a cavity. When one of the photons is spontaneously emitted along the axis linking the cavity mirrors and the rod, it will become trapped and travel back and forth. This stimulates emission in the lasing medium. Stimulated emission is an effect whereby, if a photon with energy equal to that of the metastable state passes the atom, it perturbs it, causing the electron in the state to fall to ground, releasing another photon. As well as the same energy, this photon has the same direction, phase and polarisation as the perturbing photon, and both photons will travel together along the original path. These photons can each cause more stimulated emission as they travel within the cavity, eventually stimulating

emission from all the excited atoms, at which point a laser beam has been formed.

In order to generate a pulsed laser beam, this process has to be held off until the population inversion reaches its maximum point, otherwise a continuous beam is formed. To do this an active Q-switch is used, which effectively blocks any photons from potentially reflecting within the cavity until it has reached the correct population inversion, at which point it opens and allows a pulse to form.

An active Q-switch is based on an electro-optic crystal, which has a refractive index dependent on the voltage applied to it. This is then paired with a polariser plate, which reflects polarisation in a certain direction, and transmits in another. By careful selection of the orientation of these two parts, the Q-switch can be setup so that it normally blocks all light, except for when voltage is applied to the electro-optic crystal, at which point light can pass through freely.

Finally, while one of the cavity mirrors has a near 100% reflectivity, the other, know as the output coupler is deliberately designed to transmit only some of the light incident on it. This small loss allows the laser pulse to leave the cavity.

Once the laser pulse has been emitted, it can be manipulated by optics in order to use it for various applications.

2.1.2 Optics

This section will explain some of the optics used in the experiments presented in later chapters. First some laser properties need to be defined.

Polarisation and Modes

Polarisation is the direction of oscillation of the electric field in which a photon's energy is stored. This determines how it interacts with certain materials, such as those that make up the Q-switch in a pulsed laser. Linearly polarised light has an electric field in a fixed direction, while circularly polarised light has a constantly changing direction,

due to different components of its electric field being out of phase with each other.

Furthermore, wave plates can be used to manipulate the direction of polarisation. Half-wave plates and combinations thereof change the direction of linear polarisation. Quarter-wave plates convert linearly polarised light to circularly polarised and vice versa.

Modes are standing oscillating waves setup inside the cavity, which can be described by their transverse electromagnetic mode (TEM, Steen, 1991). This is what governs the shape of beam, for example TEM_{00} is a Gaussian shape. Higher order modes exist which can be more complex. Many lasers will appear to produce a circular beam shape, which is actually made up of many different modes, which is called a multi-mode beam.

Beam Diameter and Pulse Length

The size of the cross section of a beam, its beam diameter, can be defined in a number of ways. Typically, and in the case of the research presented here, it is defined the $1/e^2$ width, or the width when the intensity has fallen to $1/e^2$ of peak intensity ($\sim 13\%$). Many other measures of beam diameter exist, such as 4σ. In the work presented later in this thesis the $1/e^2$ definition is used, since it contains the majority of the energy within a smaller area.

The laser pulse length is how long a single pulse lasts, which is defined as the full width half maximum (FWHM) of its intensity distribution. Pulsed laser operate at a certain repetition rate, which is the number of pulses generated per second by the laser. Typically every pulse will have the same pulse length.

Divergence and Beam Quality

Laser beams are described as collimated, but over long distance even an ideal laser's beam diameter will increase. Divergence is the angle at which the beam diameter is growing as it travels. Another way of expressing this is beam quality factor (M^2),

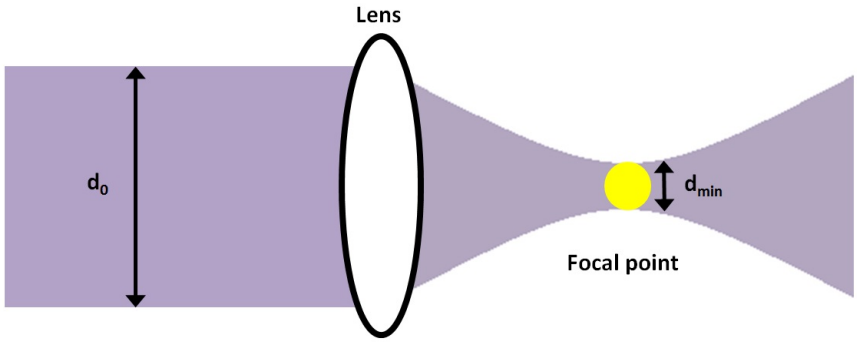

Figure 2.2: Schematic of laser focussed through a lens showing the minimum focus spot size d_{min}.

which is commonly used in laser engineering when analysing a laser (Steen, 1991). It is expressed as a ratio compared with a perfect Gaussian beam (i.e. a Gaussian beam has $M^2 = 1$). M^2 is defined in the equation for half-angle divergence θ:

$$\theta = M^2 \frac{\lambda}{\pi \omega_0} \tag{2.1}$$

Where λ is the wavelength and ω_0 is the beam radius at the beam waist (narrowest beam diameter, usually inside the cavity).

Focussing

A lens can be used to focus or defocus a laser beam. A diagram of a beam focussing through a lens is shown in Figure 2.2. A real beam will focus to a finite sized point, with a diameter dependent on a number of factors.

Equation 2.2 gives the minimum focus spot diameter d_{min}:

$$d_{min} = \frac{4M^2 \lambda f}{\pi d_0} \tag{2.2}$$

For a Gaussian beam with $M^2 = 1$, d_{min} is constrained by the diffraction limit (Hecht, 2002), which means that light cannot be focussed to an infinitesimally small point. It is possible to achieve a diffraction limited focus spot with appropriate optics and laser,

which will be of the order of half the laser wavelength, but in all other conditions the d_{min} is required.

Beam Telescopes

Multiple lenses can be used to form a telescope, which can be used to change the diameter of a beam while keeping it collimated. Two common types of telescope used with lasers are the Galilean and Keplerian. Keplerian telescopes focus the beam, which is not practical when working with lasers capable of creating air breakdown (which will be discussed in a later section), so Galilean were used in most cases during this research.

Telescope magnification M is given by the following equation:

$$M = \frac{f_1}{f_2} \tag{2.3}$$

Where f_1 and f_2 are the focal lengths of the 2 lenses used.

2.1.3 Spatial Light Modulators

A spatial light modulator (SLM) is device which can dynamically alter the phase and amplitude of a laser and therefore can be used to create multi-beam patterns. There are various methods of doing this; it was first done using an SLM by Hayasaki et al. (2005) in the context of material processing. A reflective liquid crystal on silicon (LCoS) SLM is similar to an LCD display with three main layers: a transparent protective layer (usually glass), the array of pixels, and finally a mirror. An incoming laser beam passes through the glass layer, through the liquid crystal pixels, is reflected back through them a second time by the mirror, and finally leaves through the glass.

When a pixel is addressed, the liquid crystal inside it changes orientation, which causes a change in the refractive index (Δn, Efron, 1994; Khoo and Saleh, 2007). Each pixel will have its own refractive index, so parts of the beam incident on different pixels

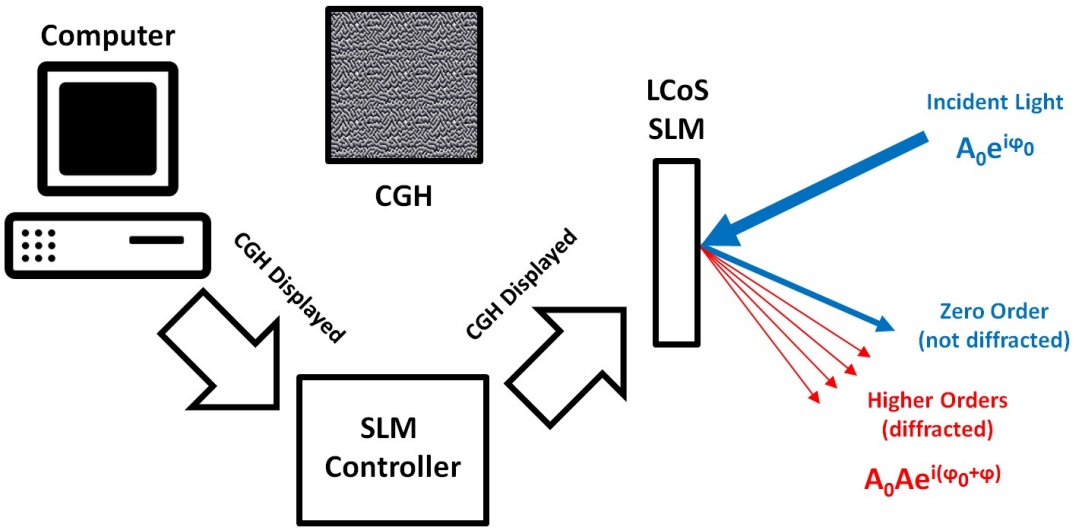

Figure 2.3: Simplified setup for the spatial light modulator.

could have their phase changed by different amounts. Commercial SLMs display in 8bit greyscale, so there are $2^8 = 256$ different levels for each pixel. Grey levels are expressed from 0-255, and each level corresponds to a different phase change, from 0-2π.

Computer generated holograms (CGHs) are displayed on the SLM in order to modulate the incident beam. These are effectively greyscale images, which are created using various algorithms which create a specific type of modulation.

A simplified diagram of a SLM setup is shown in Figure 2.3. A CGH is displayed on the SLM by the attached computer via a controller. Part of the incident light is modulated (higher orders, in red), while part isn't and simply reflects off the surface (zero order, in blue).

The CGHs are created using various pieces of software, some obtained from the SLM manufacturers, which use different algorithms. For example they can create Dammann gratings (Dammann and Grtler, 1971), arbitrary patterns (Kuang et al., 2008), and Fresnel lens phases (Kuang et al., 2009b). The gratings and lenses algorithm is widely used to create multiple beams due to its high calculation speed and accuracy, and has been used for applications such as optical trapping (Leach et al., 2004, 2006) and materials processing (Kuang et al., 2008, 2009a,b, 2012).

Detailed description of the types of CGHs used in the work will be included with the relevant results in Chapter 5.

2.2 Engines

This section describes relevant engine background. The research presented in later chapters is mainly focused on the development of optical techniques, which are eventually compared during engine tests in terms of engine performance.

While laser ignition has been applied to a variety of engines, research described in this thesis was focussed on petrol fuelled car engines. Automotive engines commonly use a four stroke engine cycle (Heywood, 1988), intake, compression, expansion, and exhaust. The complete cycle takes 720° of crank angle rotation.

The intake stroke begins at 0°, with the piston at the top of the cylinder. It begins with the inlet valve opening, as the piston moves downwards it pulls in the air-fuel mixture.

The compression stroke moves the piston back up, ending in the 360° position, or top dead centre (TDC). During the stroke the air-fuel mixture is compressed. Ignition takes place near the end of this stroke. Ignition timing is described in terms of spark advance, or degrees before TDC. Combustion has begun by the end of this stroke. During the compression stroke, the piston is pushed downwards by the force of the combustion. This is where the engine power is generated.

Finally the exhaust stroke begins when the piston again reaches bottom dead centre (BDC). At the beginning of the stroke, the exhaust valve opens, and as the piston moves up, it pushes out the exhaust gases. Once the piston reaches TDC, 720°, the cycle is over and it begins again from the start.

A crank angle sensor relays the position of the piston to the engine control computer.

In a laboratory setting, the power generated has nowhere to go, as the engine obviously cannot move. A dynamometer is used to counteract the torque generated. It is

effectively a large electromagnet which pushes back against the rotation of the engine.

A spark plug is the device typically used to ignite this kind of engine. It consists of two electrodes so that when a sufficient voltage is applied across them, a spark is generated which is able to ignite the air-fuel mixture. This is the device that a LI system aims to replace.

Cylinder pressure, engine speed, and torque are the basic measurements taken to assess engine performance. Other parameters can be calculated from these after further analysis. Indicated mean effective pressure ($IMEP$) is a theoretical expression for the mean pressure exerted on the piston during the expansion stroke of an engine cycle, without taking into account friction. It is defined as:

$$IMEP = \frac{W_i}{V_d} \tag{2.4}$$

where V_d is the displaced cylinder volume; and W_i is the gross work done to the piston over the compression and expansion strokes, which is obtained by circular integration of the pressure P over the strokes with respect to cylinder volume:

$$W_i = \oint PdV \tag{2.5}$$

$IMEP$ is conventionally used in engine calibration work, along with the coefficient of variation in $IMEP$ (COV_{IMEP}), which indicates the combustion stability. COV_{IMEP} is defined as:

$$COV_{IMEP} = \frac{\sigma_{IMEP}}{IMEP_{\text{mean}}} \times 100\% \tag{2.6}$$

where σ_{IMEP} is the standard deviation in $IMEP$ and $IMEP_{\text{mean}}$ is the mean $IMEP$. COV_{IMEP} is expressed as a percentage and gives the variation in indicated work per cycle.

Lambda is the ratio of a given air-fuel ratio to a stoichiometric ratio, which is roughly

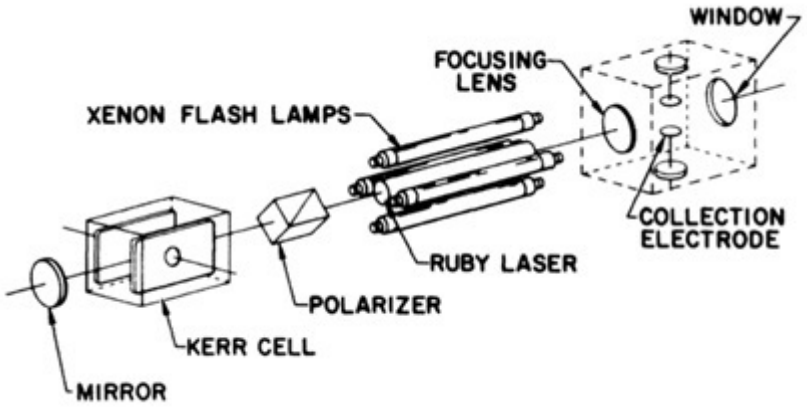

Figure 2.4: Experimental setup from the first laser air breakdown research by Meyerand and Haught (1963).

13:1 air to fuel. So $\lambda > 1$ represents more lean mixtures, $\lambda < 1$ more rich.

2.3 Laser Induced Air Breakdown

Laser induced breakdown (LIB) occurs when laser power density is sufficiently intense to create a plasma. This section covers research in this area and the different mechanisms that can create it. LIB is of interest since it is the mechanism by which a laser ignition system creates a spark in air.

2.3.1 Early Work

The first experiments involving laser air breakdown were carried out in 1963 by Damon and Tomlinson (1963), and Meyerand and Haught (1963). Both used a similar laser arrangement and method of analysis to determine whether air breakdown took place or not. Q-switched ruby lasers were focused to produce air breakdown and a plasma was shown to have been formed by measuring the voltage across 2 electrodes placed either side of the focus position. The change in voltage gave the degree to which the gas had been ionised. One of these set-ups is shown in Figure 2.4.

The theoretical background of how this occurs was developed around the same time

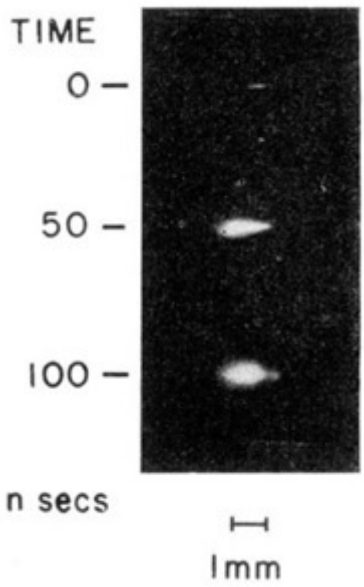

Figure 2.5: Plasma formation due to laser air breakdown from Ramsden and Savic (1964).

by Keldysh (1965) and Gold and Bebb (1965). The equations set out in these articles govern the probability of multiphoton ionisation occurring.

Ramsden and Savic (1964) researched the propagation of the plasma over time. The reason for the plasma expanding in the direction of the focusing lens is that after an initial plasma forms, the laser is continually incident on the side of the plasma facing the incoming beam. A shock wave in the gas created by the initial plasma at the focus spot creates a high pressure front that is more easily ionised. As the shock wave travels back in the direction of the oncoming beam, parts of it are likely to become ionised.

Figure 2.5 shows an image from this work. The laser beam is travelling from the left of the image, and the development of the plasma in that direction from the initial point is clear.

2.3.2 Breakdown Mechanisms

There are four mechanisms that can initiate laser ignition (Ronney, 1994; Phuoc, 2006).These are:

1. Thermal - laser energy deposited as heat onto a target, which heats nearby gas, initiating the combustion.

2. Photo-dissociation - molecular bonds are broken directly with a single high energy photon, which for constituents of air such as oxygen and nitrogen requires wavelengths in the UV range (below 200 nm)).

3. Multiphoton Ionisation (MPI) - high laser peak power density is able to ionise a number of atoms, electron cascade breakdown then creates the bulk of the plasma.

4. Resonant Enhanced Multiphoton Ionisation (REMPI) - similar to MPI but with a wavelength tuned to excite electrons to an intermediate metastable state, which lowers the energy threshold for the initial ionisation step.

The first two have not been widely tested since they are highly impractical; Thermal requires a target which degrades over time, and Photo-dissociation requires a UV laser which brings a host of problems such as being more difficult to build the laser itself, and needing optics made from different materials than those for visible or infrared.

The last two will be covered in detail in Sections 2.3.3 and 2.3.4. The majority of research in the field has used LI via the MPI mechanism.

2.3.3 Multiphoton Ionisation

Multiphoton ionisation (MPI) is the mechanism used in the majority of reported research to date. It is actually the first in a couple of stages which create the plasma, but it's energy threshold is much higher and so determines the threshold of the whole process (Ronney, 1994). The stages of plasma formation via MPI are shown in a simplified diagram in Figure 2.6.

First, MPI is the source of seed electrons, which is widely quoted to have a threshold in peak power density of $10 \times 10^{11}\,\mathrm{W\,cm^{-2}}$. Free electrons readily absorb laser energy, which allows them to ionise further atoms via collision once they have enough energy,

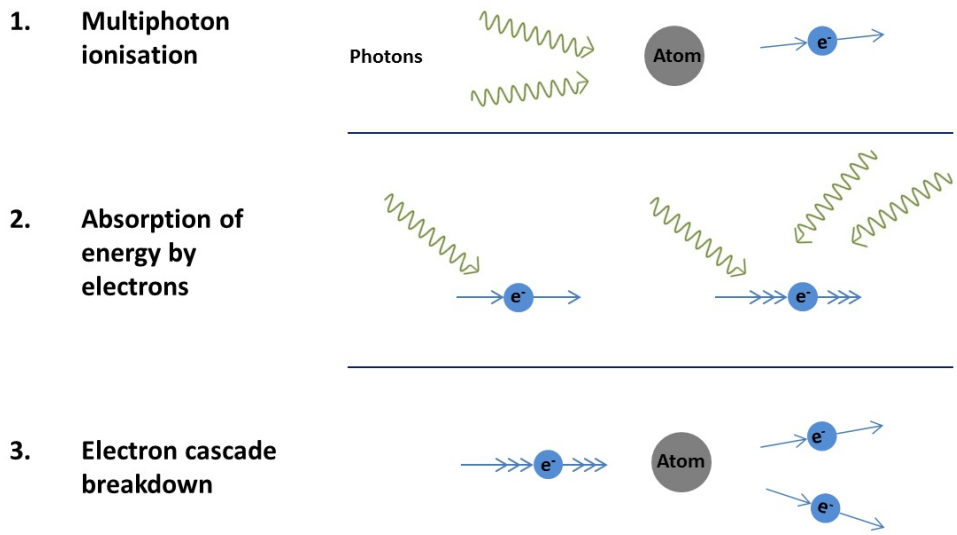

Figure 2.6: The stages of laser air breakdown via multiphoton ionisation.

as shown in the cascade breakdown step. Electron cascade breakdown forms the majority of the plasma.

The minimum energy required to cause air breakdown is often quoted as the minimum pulse energy, however peak power density at the focus spot is another useful definition, as it is independent of the optics and properties of the laser beam used. Air breakdown is a probabilistic process at low energies, until a certain energy is reached at which 100% of pulses cause breakdown. Energy or power density measurements quoted in the results will be those measured at the threshold for consistent 100% breakdown efficiency.

2.3.4 Resonant Enhanced Multiphoton Ionisation

Resonant Enhanced Multiphoton Ionisation (REMPI) is a similar process, except in how it ionises the initial electrons. As shown in Figure 2.7 on the following page, which compares the two types of multiphoton ionisation, the main difference is the intermediate step where an electron is excited to a metastable state before being ionised. The more simultaneous photons are needed for a process, the less likely the process is to take place. Therefore adding an intermediate step should lower the energy

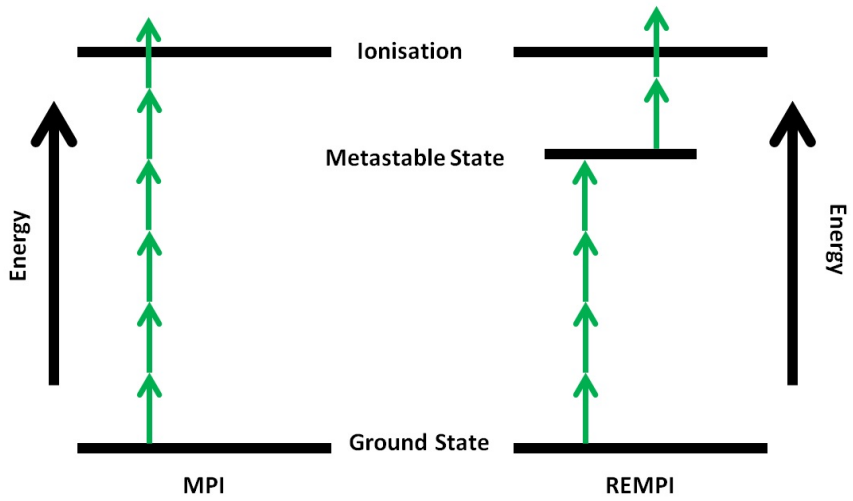

Figure 2.7: Electron energy level diagram for REMPI.

threshold.

REMPI requires a specific wavelength for each type of molecule, so the wavelength required would vary depending on the components of the gas mixture. Air-fuel mixtures usually have nitrogen from the air as their biggest component, but the laser could potentially be tuned to any molecule in the mixture. The biggest limitation of this approach is finding a laser with any specific wavelength output.

Forch et al. were the first to report on using resonant air breakdown for ignition; they ignited H_2/O_2 mixtures via REMPI (Forch and Miziolek, 1986, 1987, 1991; Forch, 1994). Figure 2.8a on the next page shows clearly the potential gains of resonant ignition. By adjusting the laser wavelength to 286.3 nm (the peak on the right), the minimum ignition energy (MIE) was less than half that when using wavelengths 1 nm away. Figure 2.8b shows the width of this resonant effect in terms of wavelength. The graph shows emissions at 777.5 nm which correspond to resonant breakdown. The range of wavelengths at which this effect is seen is roughly 0.2 nm wide.

Air plasma creation via REMPI has also been investigated by Shneider et al. (2007), Thiyagarajan and Scharer (2008),Way et al. (2009) and Hummelt and Scharer (2010). An important point from Way et al. was that air breakdown was achieved at energy intensity of $5.5 \times 10^9\,\mathrm{W\,cm^{-2}}$ using a wavelength where REMPI takes place. This is

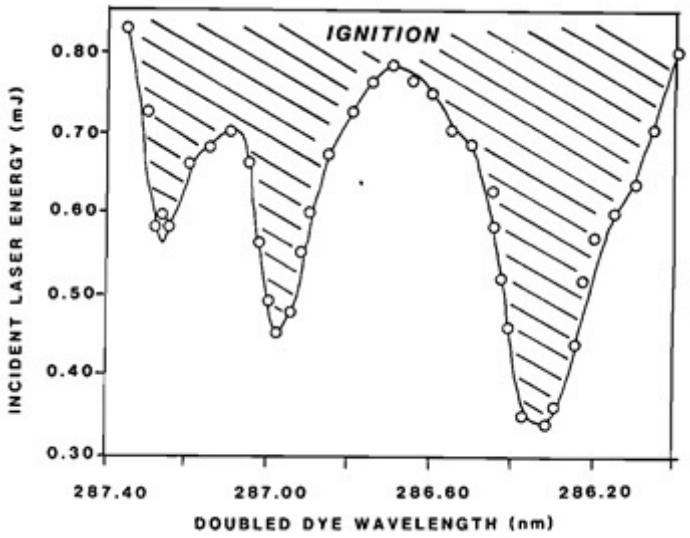

(a) Wavelength dependence on minimum ignition energy (MIE) of a H2/N20 mixture from Forch and Miziolek (1987).

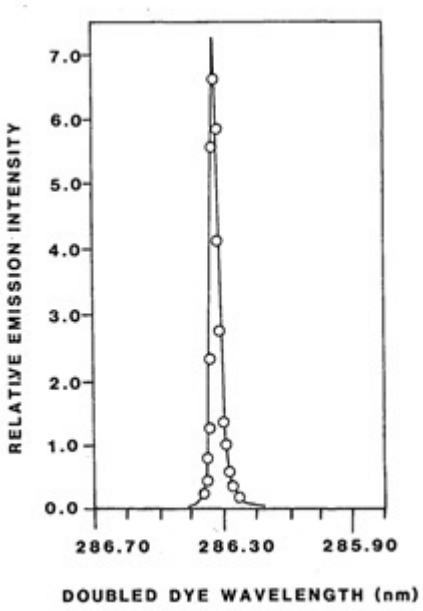

(b) Emission spectrum indicating resonant excitation of O atoms from Forch and Miziolek (1986).

Figure 2.8: REMPI in a H_2/O_2 mixture from Forch and Miziolek (1986, 1987).

2-3 orders of magnitude lower than is typically used for laser ignition experiments using the fundamental Nd:YAG wavelengths.

2.4 Laser Ignition

The concept of laser ignition (LI) is to replace the traditional spark plug with a laser, which when focused down with sufficient energy can cause air breakdown, and in turn initiate combustion.

There has been work in this area since the 1970s, when it was developed following the first demonstration of laser air breakdown, in the early 1960s. Work since then was usually limited to single-point LI using the laser technology at the time, across a small range of laser parameters. A production automotive engine has not yet been produced that uses laser ignition, however compact lasers have recently emerged that might be able to achieve this. First use of the term laser spark ignition appears to be by Lee and Knystaut (1969). A study of the use of lasers for ignition was carried out by Weinberg and Wilson (1971). Dale et al. (1978) were the first to apply LI to an internal combustion (IC) engine in 1978.

A number of papers have reviewed the work on laser ignition: Ronney (1994); Phuoc (2006); Morsy (2012) and Dearden and Shenton (2013). LI has been applied to many different situations, but the focus of this work and therefore of this review will be on IC engines. This section will be divided into categories relevant to the research that will be covered later, including multi-point LI and studies on the effect of wavelength.

When compared to laser ignition, spark plugs have limited possibilities for optimisation, since they are at a fixed point within the cylinder, and have to protrude into it. The electrodes can act as a heat sink and quench the flame kernel, and disturb the otherwise smooth geometry of the cylinder. Laser radiation is non-invasive, it can pass into the cylinder via a transparent window fitted to the shape of the cylinder walls. The position of the spark can also be controlled relatively easily using various optical techniques.

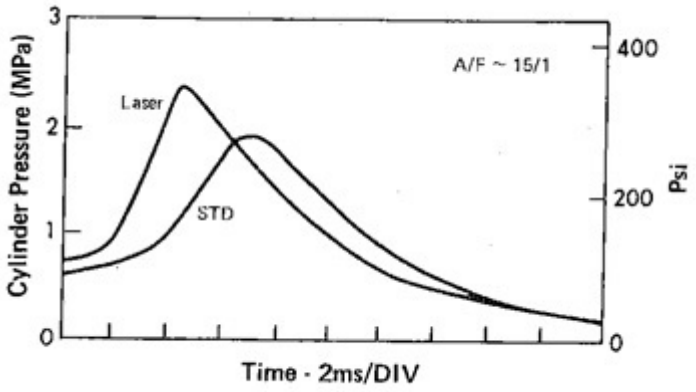

Figure 2.9: Engine pressure trace comparing SI (labelled STD) and LI from Dale et al. (1978).

2.4.1 Engine Studies

As mentioned above, Dale et al. (1978) were the first to carry out an engine study involving laser ignition. An ASTM-CFR single cylinder engine was ignited using a CO_2 laser. It was found that the MIE required was similar to the energy required to breakdown air at pressures equivalent to those inside the engine. In comparison to SI, LI extended operation to leaner air/fuel mixtures. Figure 2.9 is a sample of their data, showing LI increases the peak pressure and decreases combustion time compared with SI.

Various authors have reported on engine studies which showed advantages in certain circumstances to using LI over SI (Weinrotter et al., 2004, 2005b; Schwarz et al., 2010). Liedl et al. (2005) presented results for LI of a single cylinder GDI engine. They determined that the main improvements over SI were freedom of ignition point (rather than fixed at the cavity wall) and reduction in fuel usage. Specifically, laser ignition at a point inside the path of the fuel spray reduced fuel consumption by around 5% compared to SI.

Researchers at the University of Liverpool have previously studied laser ignition using a Ford Boss single cylinder test engine (the same that will be used in research discussed in this thesis) and a Ford Zetec production engine. Carroll et al. (2005) used a nanosecond pulsed, 1064 nm Nd:YAG laser to ignite a single cylinder of a 4

Figure 2.10: Laser and optics fitted to a Ford Zetec engine from Dodd et al. (2007).

cylinder, port fuel injected Ford Zetec engine. The remaining cylinders were ignited using conventional spark plugs. The results were presented in terms of cycle to cycle variations (CCV), the coefficient of variation (CoV) in peak pressure position PPP and in indicated mean effective pressure $IMEP$. Cylinder pressure was measured using a pressure transducer across the entire engine cycle. The laser pulse energy that reached the focal point was kept constant at $7.5 \pm 0.4\,\mathrm{mJ}$, and the focal spot size was varied by using different lenses. It was shown that when the focal spot size was around $100\,\mu\mathrm{m}$, COV_{IMEP} reached values comparable with that of spark ignition. When focal spot size was decreased, the COV_{IMEP} values increased, however values above $100\,\mu\mathrm{m}$ were not investigated.

Dodd et al. (2007) and Mullett et al. (2007) reported further work with this engine. Their experimental set-up is shown in Figure 2.10. The laser head is mounted on a metal plate attached to the engine, and the optics are mounted on a rail above the cylinders (left side of the image). Finally Mullett et al. (2008) demonstrated LI of 4 cylinders of an IC engine. The arrangement for the two laser used is shown in Figure 2.11 on the facing page. Each laser fires into two cylinders simultaneously whenever a pulse is needed to be fired for either cylinder.

2.4.2 Multi-point Ignition

While most LI work has focused on a single ignition point, some researchers have investigated the effect of 2 or more simultaneous ignition points in space. Morsy et al. (1999b) used a conical cavity based on the principle of a beam stop, as shown in

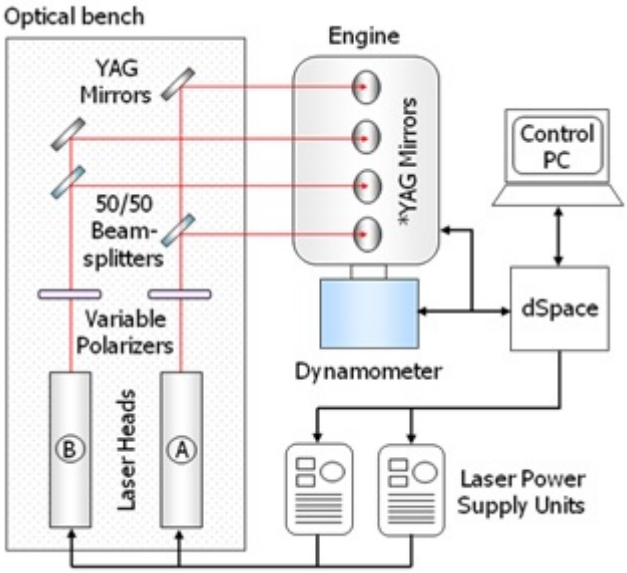

Figure 2.11: Laser set-up for LI of a 4 cylinder IC engine from Mullett et al. (2008).

Figure 2.12. In Figure 2.12 part (b), the cavity creates many smaller focus spots in a line. When the pulse energy is sufficient, this creates a line of breakdown as shown in part (c). The results showed faster combustion speed compared with single-point. Morsy and Chung (2003) later elaborated on this idea with 2 more arrangements of conical cavities. The downside of this approach is that an engine must be designed with these shapes as part of the cylinder geometry.

Phuoc (2000b) used a different approach to multiple ignition points. Two Nd:YAG lasers were used to create sparks simultaneously at either side of a cylindrical chamber, near the walls, as shown in Figure 2.13a on page 25. This was then compared with a single ignition near the wall, and a single ignition near the centre of the chamber. There was a reduced combustion time and increased combustion pressure from the two point ignition.

Weinrotter et al. (2004) presented two different approaches (each compared with single point). As with the previous article, two ignitions occurred at either end of a chamber, and results showed decreased combustion time and increased peak pressure. Three closely spaced ignitions (5 mm apart) in a line had the opposite effect of reducing peak pressure, combustion time remained similar. In another reporting of this work

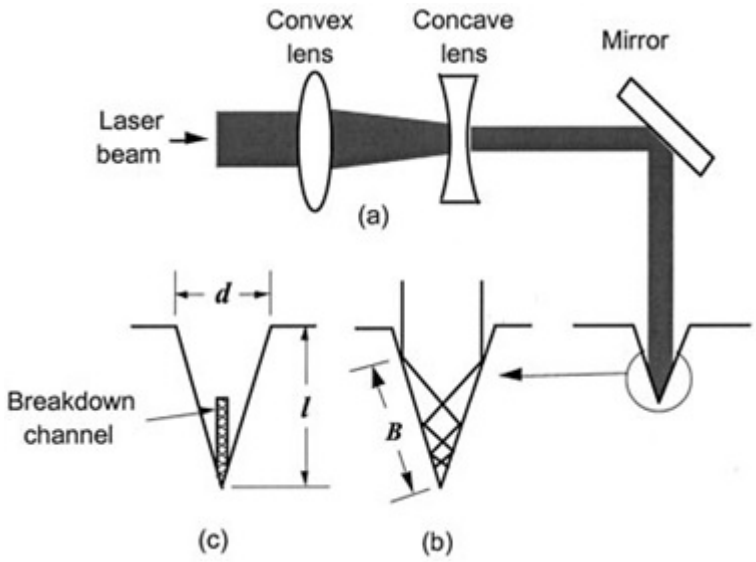

Figure 2.12: Optical arrangement and conical cavity used to generate a breakdown channel (Morsy et al., 1999a).

(Weinrotter et al., 2005a), it is suggested that the reason that the closely spaced multiple ignitions reduce the peak pressure is that the shock waves disrupt each other. Figure 2.13b shows how the expanding shock fronts of the 3 ignitions overlap.

Ryu et al. (2009) used a conical cavity similar to Morsy along with a so called pre-chamber. In their experiments there are 2 ignition points, one in the cavity, and one in the pre-chamber, shown in Figure 2.14. Their results again showed a decrease in combustion time compared with single point ignition. The limitation of this is that it might not be practical to use a pre-chamber in every engine system.

A compact laser was developed which created three simultaneous ignition points (Pavel et al., 2011a,b), but engine results using it were not presented. Compact lasers for LI will be discussed later in Section 2.4.5.

Work on multi-point ignition is still limited, and so further contributions in this area are needed.

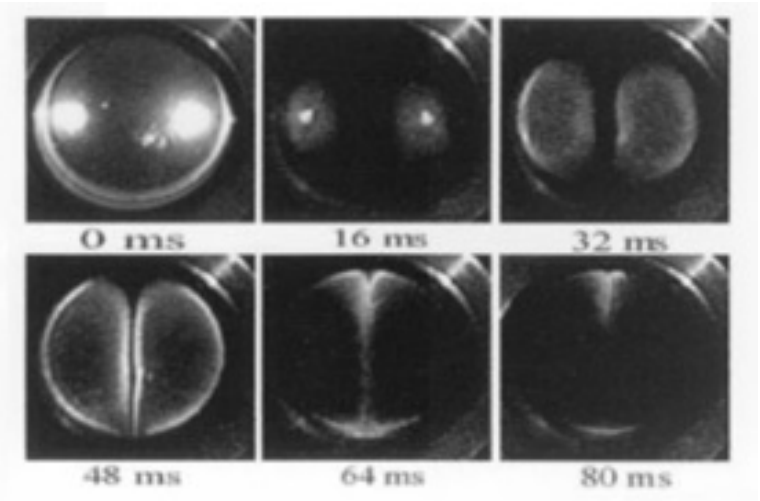

(a) 2 point ignition from Phuoc (2000b).

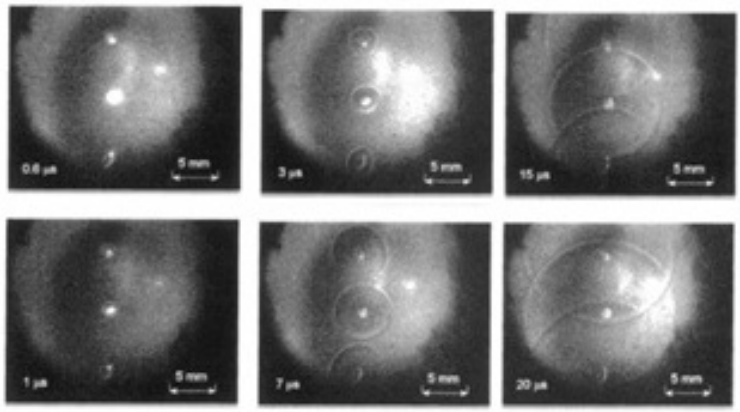

(b) 3 point ignition from Weinrotter et al. (2004).

Figure 2.13: Images of 2 and 3 point ignition in combustion chambers (Phuoc, 2000b; Weinrotter et al., 2004).

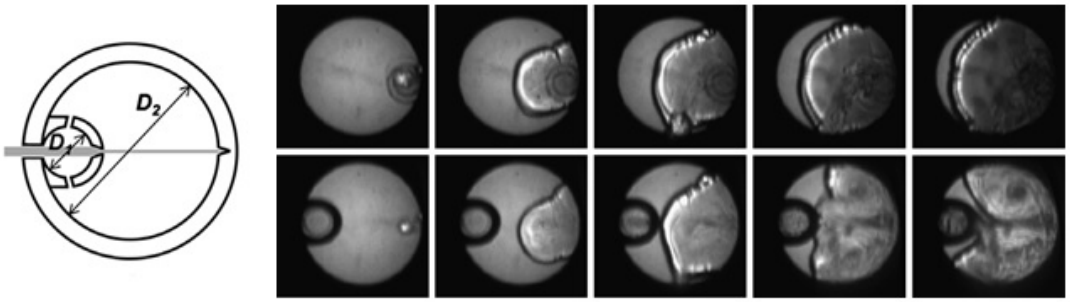

Figure 2.14: Chamber schematic and images of combustion with and without a pre-chamber from Ryu et al. (2009).

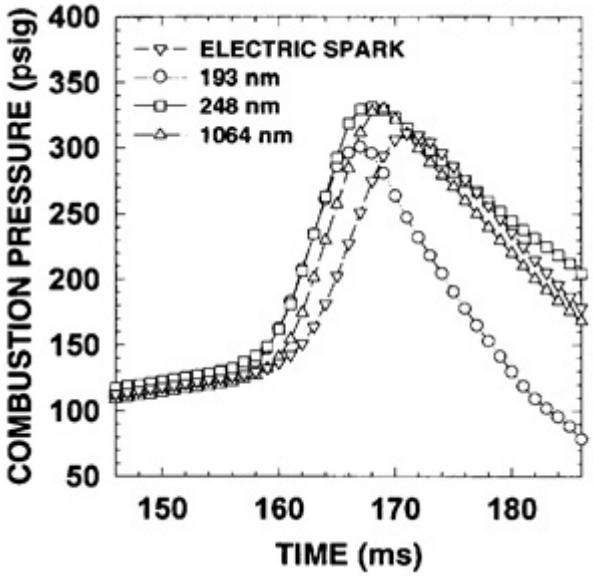

Figure 2.15: Pressure curves for ignition using different wavelengths from Ma et al. (1998).

2.4.3 Wavelength Dependence of LI

The effects of wavelength on LI can be broken down to two main parts: the ability of a particular wavelength to create a spark in the components of the fuel/air mixture, and the amount of energy transmitted through the fuel/air mixture between the entrance window and the focus spot.

Ma et al. (1998) compared laser ignition using three different wavelengths: 193 nm, 248 nm and 1064 nm. Unfortunately they did not compare minimum ignition energy or breakdown intensity threshold. Figure 2.15 shows some of their results, a graph of combustion pressure against time for the different wavelengths and a spark plug. All of the laser ignition results show a decrease in the time to the peak pressure, however in the case of 193 nm, the peak pressure is significantly lower. This suggests a possible issue with LI using very short wavelengths, however more wavelengths would need to be tested as there is not much literature on this topic.

Kopecek et al. (2003) compared the use of another three different wavelengths for LI: 355 nm, 532 nm and 1064 nm. They ignited a methane-air mixture whilst varying wavelength and focus spot diameter. Figure 2.16 on the facing page shows an excerpt

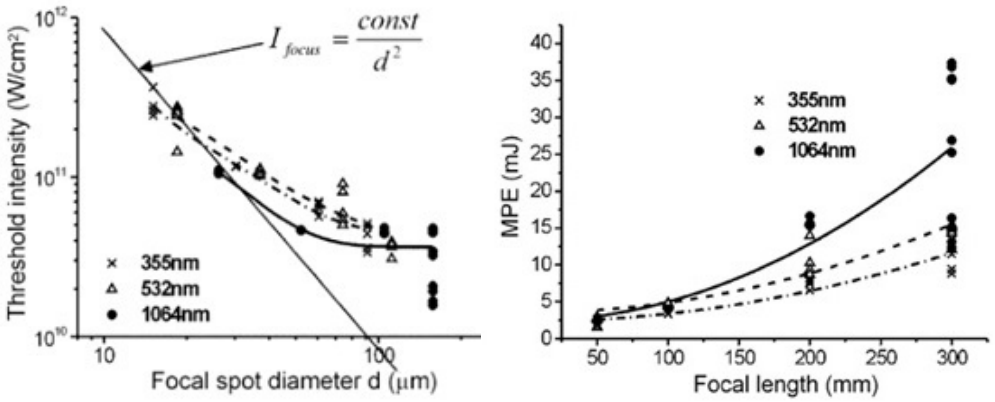

(a) Threshold intensity (Kopecek et al., 2003).

(b) Minimum pulse energy (Kopecek et al., 2003).

Figure 2.16: Wavelength dependence of air breakdown threshold intensity and minimum pulse energy (MPE, Kopecek et al., 2003).

of their results. They concluded that there was little difference between the different wavelengths, but their results mostly focussed on the effect of focussing optics and other parameters. Here, it was shown that 20 µm is the minimum focus spot size that will produce ignition, and that LI was able to ignite leaner air-fuel mixtures than conventional ignition systems.

Figure 2.16a in particular shows the threshold intensity for air breakdown at focus spots of different diameters. This allows a good comparison between wavelengths as the different beam properties are taken into account.

Similar tests have not been carried out for gasoline automotive engines elsewhere in the literature. Overall there is not enough work investigating wavelength comparison to draw any conclusions and so it would be useful to investigate this further.

2.4.4 Fibre Delivery

The majority of reported LI work has been carried out with beams delivered via free space, however some efforts have been made towards delivering the beam with optical fibres. Yalin (2013) reviewed the work on optical fibre delivery for laser ignition systems.

Stakhiv et al. (2004) tested various types of fibres for engine ignition, however none were suitable. Weinrotter et al. (2004) gave further details on this work, explaining that different fibre material would be needed to do this successfully.

Yalin et al. (2005) reported successfully generating air breakdown using a nanosecond pulsed laser delivered using a hollow core fibre. This was successful where previous work was not, because of the coupling optics used where the laser entered the fibre. This allowed the exiting beam to be of sufficient beam quality and intensity to create LIB. This result was true for a perfectly straight fibre, but when a bend was introduced, the transmission through the fibre decreased and spark formation became unreliable. They concluded that solutions to this problem should be explored.

Mullett et al. (2009) carried out a study on fibre delivery, testing four types of fibre: silica step index fibre, sapphire fibre, large mode area photonic crystal fibre and multi-mode ultra-high numerical aperture photonic crystal fibre. Of these 4 types, 400 µm and 600 µm core diameter silica step index fibres were found to be most appropriate, and were used for engine ignition tests. However combustion was unreliable: at best 40% of attempted ignitions were successful. An issue with encountered with the fibre delivery was that the beam profile could be affected by the vibrations of the engine running at certain speeds. In a similar way to how excessive bending can affect the way the beam propagation through a fibre, the beam was significantly distorted as shown in the second row of images from Figure 2.17 on the next page.

Recent work has used new types of fibres with high power handling ability to deliver the required laser pulses. Beaudou et al. (2012) used a type hollow-core photonic crystal fibre to reliably deliver a Nd:YAG laser pulse to create air breakdown. Ignition of a jet of butane gas was demonstrated using a 2 mJ, 9 ns pulse and an 8 mm focusing lens. The relatively low MIE was because the type of fibre used allowed the transmitted beam to keep a high beam quality. Joshi et al. (2012) used large clad silica step-index fibres in order to overcome the problem of high power handling.

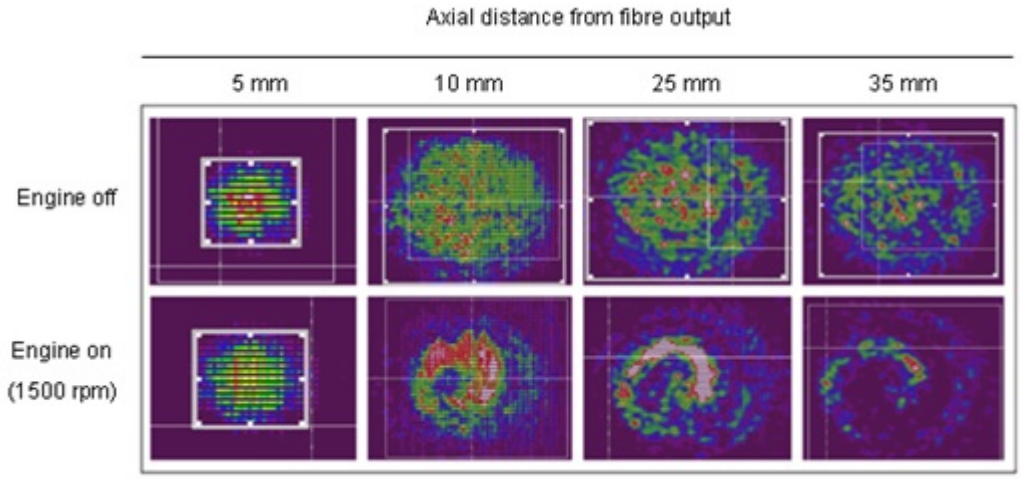

Figure 2.17: Effect on the beam profile of the fibre output with and without engine vibrations from Mullett et al. (2009).

2.4.5 Compact Laser Sources

Fundamental LI research has generally used CO_2 or flashlamp pumped Nd:YAG lasers, however these would not be suitable for implementation into an automotive engine due to their large size and high power requirements. This has led to research into potential compact sources that could be used in an engine. Successful production of a robust, compact laser would be required for a commercial implementation of LI.

The two main approaches have either been a cavity and pump source together attached to the engine, or remote pumping source with cavity close to engine. Another approach might be to have the laser placed remotely, and fibre deliver it to engine, if the issues with fibre discussed in Section 2.4.4 could be resolved.

Taira (2011), Pavel et al. (2011b) and Tsunekane and Taira (2011) reported on a diode pumped Nd:YAG ceramic laser designed for LI in a car engine, shown in Figure 2.18 on the following page. The design consists of the gain media, passive q-switch, cavity mirrors, and focusing optics all contained within a similar footprint to that of a spark plug. The pumping source is an array of diode lasers (not shown) delivered via optical fibre. This diode array would be placed away from the engine. Their passive Q switch was a saturable absorber, which absorbed a portion of the incident light until

Figure 2.18: Compact ceramic laser for LI from Taira (2011).

saturated, at which point a pulse can form.

The size and power requirements of the pump lasers are not mentioned, however Tsunekane and Taira (2013) reported on an improved version of this laser which required a 120 W laser diode for pumping.

Bihari et al. (2015) and Biruduganti et al. (2015) used a similar remotely pumped system to ignite a natural gas engine. A prototype compact laser delivered 2.5 mJ pulses at 10 Hz which was sufficient to offer comparable performance to a spark plug.

Other researchers have built complete compact laser heads using a VCSEL array (vertical-cavity surface-emitting laser) pumping source. A VCSEL is a type of laser diode, an array of which can be combined to output sufficient energy to be a pump source. Manufacturers have begun to produce compact lasers in recent years, for example Princeton Optronics, details of which were published by Leeuwen et al. (2016). Here four VCSEL arrays were combined to form a pumping source with a circular output, with an output power of 750 W. The output pulse energy was as high as 19 mJ with $M^2 = 6$, sufficient to create air breakdown. They mention problems remain in terms of the optical efficiency however.

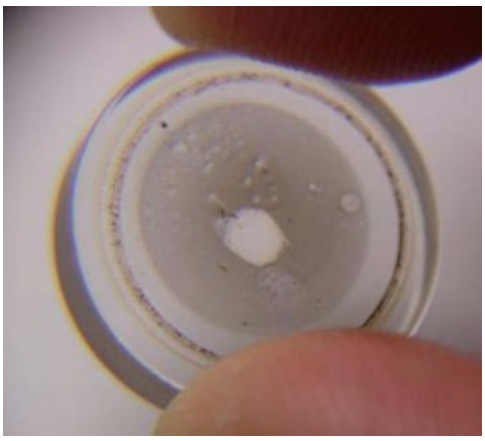

Figure 2.19: Image of the laser cleaning effect from Lackner et al. (2005).

2.4.6 Laser Cleaning Effect

An effect has been observed in LI experiments whereby the window into the engine or combustion chamber is cleaned of soot by some action of the laser pulse. Lackner et al. (2005) observed this effect and reported the performance of different window materials. An example image of this effect is shown in Figure 2.19. A small area of the otherwise dirty window has been kept clean by repeated laser pulses.

Liedl et al. (2005) reported on experiments involving LI of a GDI engine. Calculations has been made to determine the breakdown threshold of air, however it was found that higher pulse energies were required for smooth engine operation, because of the need to clean the entrance window. Figure 2.20 on the next page shows two images, the first is a window after 20 hours of engine operation whilst it was spark ignited. The second shows this same window after 100 laser pulses at energies used for LI. This shows how the laser cleaning effect is sufficient to remove many layers of deposits and leave the window clear.

Ranner et al. (2007) carried out tests to determine how different substances can be removed from a window. They used energy-dispersive x-ray spectroscopy (EDXFS) to determine the chemical make-up of the window deposits. Figure 2.21 shows a cleaned portion of a window, along with an element spectrum. The spectrum shows that the remaining deposits in the clean area are only made up of carbon (the other elements

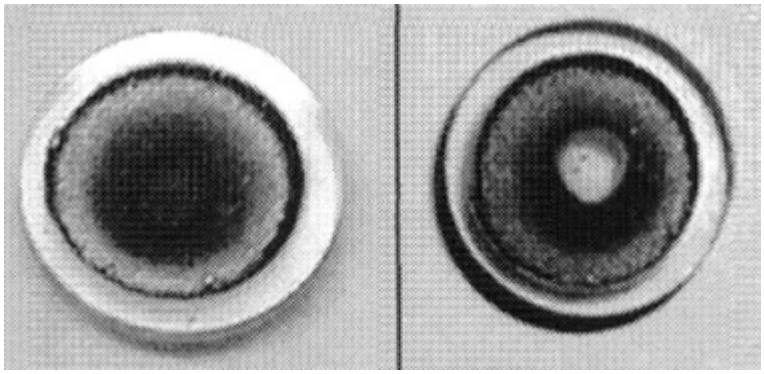

Figure 2.20: Image of the laser cleaning effect from Liedl et al. (2005).

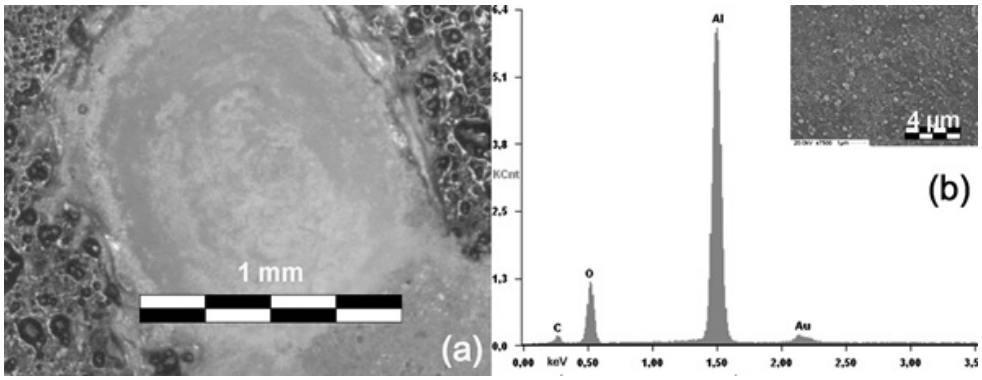

Figure 2.21: Laser cleaning micrograph and element spectrum of the deposits from Ranner et al. (2007).

in the spectrum are those that make up the window itself). Other results show that the uncleaned deposits are made up of a larger amount of carbon, along with other constituents of the fuel and engine oil.

Griffiths et al. (2013) showed that the surface of a glass window was unchanged after repeated deposition and cleaning of carbon, suggesting that long term laser cleaning of a window may be viable. Mullett et al. (2008, 2009) also observed a laser cleaning effect during tests of LI on a IC engine.

The laser cleaning effect is an area that vitally needs to be understood in order to know whether a LI system could function in the long term, tests in the region of hundreds and thousands of hours in an IC engine need to be carried out.

Chapter 3

Experimental Equipment and Techniques

This chapter will cover the equipment that was used during the project, experimental set-ups, and techniques that were used. Basic information common to all experiments will be covered here, specifics will be included in relevant sections of the results chapters.

3.1 Lasers

Two Nd:YAG, flashlamp pumped, nanosecond pulsed lasers were used during the work presented in this thesis.

First, a Litron LPY 764-30 Nd:YAG laser with a built in 2nd harmonic generator. This output at 532 nm, but alternatively could be adjusted to output 1064 nm. It is an oscillator-amplifier system with two flashlamp-rod pairs inside the cavity and another two outside in the amplifier, making four Nd:YAG rods in total. Maximum pulse energy was 500 mJ, beam quality $M^2 \sim 5 - 10$, and pulse length 12.6 ns (all at 532 nm). At 1064 nm maximum pulse energy was 1 J, while other properties were similar. Both modes had a variable repetition rate between 1 and 30 Hz, which allowed

it to synchronise with the engine.

The laser could be controlled either via an attached control box or by externally triggering. When running with the engine, it would be set to external triggering mode, attached to the engine control computer.

The main weakness of this laser was the variability in beam mode and pulse with repetition rate. Due to the high pulse energy, the thermal lensing effect inside the cavity was significant; effectively the Nd:YAG rod would act like a lens depending on its temperature. A telescope within the cavity accounted for this, but not uniformly across all repetition rates, as the temperature of the lamps would vary depending on how often they were flashing. These effects had to be considered in experiments, and accounted for in later analyses.

The other laser was a Spectron Mini-Q Nd:YAG laser outputting at 1064 nm. It had maximum energy 80 mJ, $M^2 \sim 3$, and pulse duration 10 ns. This laser could run at repetition rates between 1 and 50 Hz, and could also be controlled either manually or by external trigger like the Litron. This laser avoided the problem of thermal lensing at the cost of much lower energy output. It also didn't have a harmonic generator option.

3.2 Optics

The basis of the optical setups used in the work were simple mirrors and lenses. Mirrors were coated for maximum reflectance at a given wavelength and lenses for maximum transmission. Typically these are $\sim 99\%$ reflecting or transmitting, which meant total losses in the system were kept low. Beam telescopes were used, usually to reduce beam diameter, and were typically $2\times$ beam reducers built from $f = -100$ mm and $f = +200$ mm lenses. See further discussion in Section 2.1.1.

The pulse energy output by the lasers was generally much more than needed, so this had to be addressed. It was possible to control energy by affecting the laser directly, with the controller it was possible to change the voltage applied to the flashlamps,

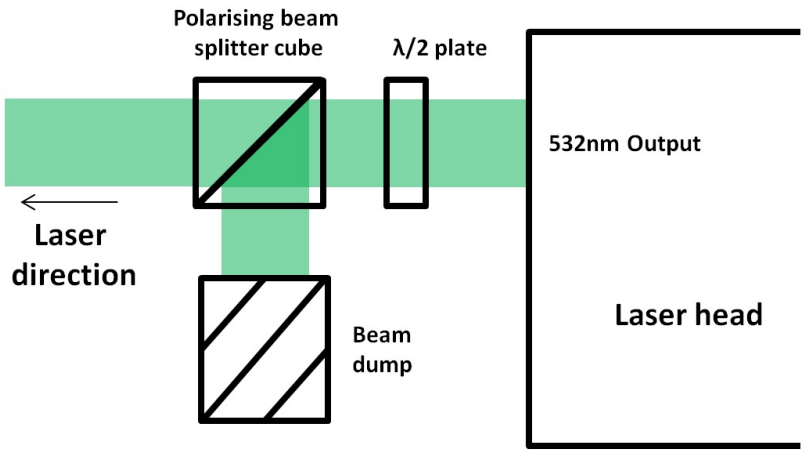

Figure 3.1: Schematic of the optical arrangement used to build a laser energy attenuator.

which in turn controls energy. However this has the side effect of seriously affecting the mode and divergence, especially at low voltage. Therefore it was best to attenuate the energy outside of the laser head instead.

An energy attenuator was built using a half-wave plate, polarising beam splitter cube, and a beam dump. The optical arrangement for the attenuator is shown in Figure 3.1.

The output laser is linearly polarised, and its polarisation direction can be changed by rotating the half wave plate. When the beam is incident on the cube, horizontal polarisation is transmitted and vertical is reflected. When a polarisation somewhere between these two directions is incident on the cube, part of the energy will go either way according to the size of the vertical and horizontal components of the beam relative to each other. Unwanted energy is contained by a beam dump, which is important for safety reasons since up to 500 mJ can be attenuated.

It is not necessary to know anything about the polarisation state of the beam in practice. When adjusting the attenuator, the energy meter was used to measure the pulse energy in real time, and the half-wave plate was rotated until the desired energy was measured.

Laser-induced damage thresholds (LIDTs) varied between components. At maximum output, the raw beam of the Litron laser had an intensity of $\approx 1\,\mathrm{J\,cm^{-2}}$, but typically only 10% of this was used, so only the attenuator and mirrors had to meet this

requirement.

The polarising beam splitter cube in the attenuator had a high threshold of $10\,\mathrm{J\,cm^{-2}}$, the half-wave plate was the same. Some of the wave plates used in other areas had lower thresholds of around $1\,\mathrm{J\,cm^{-2}}$. Coated N-BK7 lenses used had LIDTs of $7.5\,\mathrm{J\,cm^{-2}}$, while the mirrors had LIDTs of $5\,\mathrm{J\,cm^{-2}}$. The uncoated sapphire lenses had LIDTs around $10\,\mathrm{J\,cm^{-2}}$.

3.3 Laser Analysis Equipment

This section will cover equipment used to characterise the properties of lasers used, and analysis of the data obtained using them.

A Gentec-EO QE25 energy meter was used to measure laser pulse energy E_p. It was calibrated for 532 nm and 1064 nm, with power handling capability in excess of the maximum output of the laser. Readings were generally taken for ~ 30 seconds, during which time the meter would record every pulse. The laser would be left to warm up before this, then kept at a steady state for the measurement to make sure the value was representative. The energy meter was connected to a computer, where it would output a file in the form of a time-stamp and energy reading for every pulse detected. Timing is not generally important; it only provides the repetition rate, which is controlled already. E_p readings are the mean of all pulses measured. The uncertainty ΔE_p is calculated by summing in quadrature the statistical variation between pulses as measured by the standard deviation of the set of energies (σ_{E_p}); and the measurement error, which according to the manufacturer is 3%:

$$\Delta E_p = \sqrt{\sigma_{E_p}^2 + \Delta_{measure}^2} \tag{3.1}$$

The laser was imaged using a Thorlabs BC106-VIS beam profiler camera. The camera was based on a CCD sensor with a pixel size of 6.45 µm. It was attached to a translational stage with travel distance of around 150 mm. Both the stage and camera were

connected to a computer and controlled by the manufacturer's software. The sensor was protected by a set of neutral density (ND) filters to reduce laser energy incident directly on the sensor.

The camera was mounted on the stage, meaning each beam diameter measurement could be linked to a stage position. Plotting beam diameter against stage position produced a curve, the minimum of which gives the minimum focus spot size (d_{min}). Therefore in order to measure M^2, the laser was focused using a long focal length lens ($f > 100\,\text{mm}$), which would give a large enough focus spot that the camera would not be damaged. Measuring the size of a focus spot used to create air breakdown directly would severely damage the camera.

As discussed previously, the minimum focus spot size is given by:

$$d_{min} = \frac{4M^2\lambda f}{\pi d_0} \tag{3.2}$$

This can be rearranged for M^2, and used to calculate it as all other parameters are known:

$$M^2 = \frac{d_{min} d_0 \pi}{4\lambda f} \tag{3.3}$$

The software had a built in function to take an automated M^2 measurement, which didn't always work due to an issue with the automatic adjustment of the gain and measurement time. Therefore some M^2 measurements were automated by the software, others were calculated manually from the raw data.

In the case of manual measurement, M^2 was calculated using Equation (3.3), from a spot sized measured by manually adjusting the stage position to the focal point. The software did the same calculation but using a minimum spot size found by fitting a curve though the plot of beam diameter mentioned earlier.

A Thorlabs DET36A/M photodiode with a 14 ns rise time was used for sensing the laser air breakdown spark in various circumstances. This was only a measurement of

the presence or absence of a spark, not any analysis of the intensity. To do this it was paired with various standard oscilloscopes. The photodiode was mounted near to the focus but away from the path of the laser to avoid detecting it.

A different photodiode, the Thorlabs DET025A/M, with a 1 ns rise time was used for measuring the laser pulse length. This was connected to a Tektronix TDS 3054C oscilloscope with a 500 MHz frequency, in order to display the nanosecond order signals. The shortest time interval was 4 ns, other settings were auto-adjusted to find the peak.

The external trigger from the laser power supply was attached to the DET025A/M for timing. For these measurements, the laser was attenuated to a very low energy and scattered off a white cardboard target, since the diode has a very low damage threshold.

A Thorlabs CCS200 CCD spectrometer was used to measure the laser wavelength. It had a spectral range of 200 nm to 1000 nm, so it was not suitable for measuring the fundamental output of the Nd:YAG lasers, and a resolution of 2 nm. Results were recorded using a computer attached via USB cable, with the software provided by the manufacturer.

3.4 Spatial Light Modulator

Two different spatial light modulators (SLMs) were used in experiments related to generating multi-point air breakdown. Relevant background was discussed earlier in Section 2.1.3 on page 10.

In early experiments a HOLOEYE LC-R 2500 was used, a liquid crystal on silicon (LCoS) device with 1024×768 pixels, phase and amplitude modulation capabilities, reflectance $\eta > 80\%$, and a broadband metallic coating which made it compatible with both 532 nm and 1064 nm lasers. The majority of experiments presented used Hamamatsu X10468 LCoS SLM, with phase only modulation, 800×600 pixel display and 532 nm dielectric coating that gave reflectance at 532 nm of $> 99\%$. Another SLM

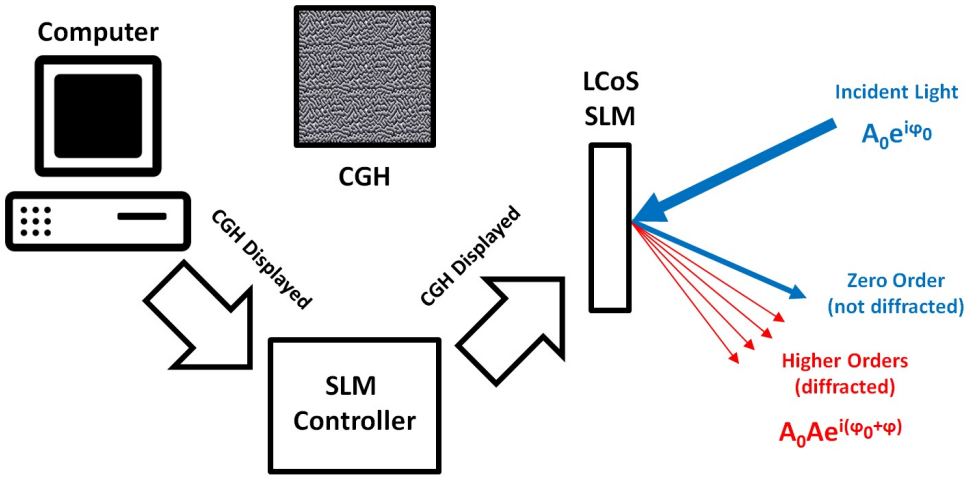

Figure 3.2: Spatial light modulator schematic - applying a CGH using attached computer, which diffracts part of the incoming light.

used was the

Figure 3.2 shows a simplified SLM setup. A computer is used to calculate the computer generated holograms (CGHs), then displays them as it would display an image on a monitor. The SLM controller bridges the SLM itself to the computer, and provides power to it. The laser light incident on the SLM surface will be diffracted depending on what is displayed. Imperfections in the SLM are accounted for by the deformation correction pattern, which is supplied by the manufacturer. These correct for the surface not being perfectly flat and are implemented by combining them with the CGH to be used.

As mentioned a CGH is a digital image. Two broad categories of CGHs exist (and are discussed further as part of the results in Chapter 5): representations of prisms, gratings or lenses, which have an effect on the laser similar to that of their physical counterpart, and Fourier transforms of arbitrary images, which cause the modulated beam to focus in the shape of the original image.

Modelling of the optical systems related to the SLM experiments was done using the ZEMAX software package, which can simulate how a beam propagates through an optical system. Off the shelf optics from major manufacturers can inputted into the simulation, in order to work out what is needed before purchases are made. It was

possible to input multiple beams equivalent to those produced by the SLM; further explanation will be included with the results of these experiments in Chapter 5.

3.5 Optical Plug

An optical plug is a device which holds the focusing lens, which creates the spark and acts a window into the cylinder through which the laser can travel. It physically replaces the electric spark plug, is of a similar size, and screws into the same opening. It is a cylindrical steel tube, with an outer thread to screw into the engine, and an inner thread to allow a screw top to hold the components in place. The experiments discussed in this thesis used a plug containing only a sapphire focusing lens.

Figure 3.3 shows the plug along with a diagram of the contents. Beginning at the front of the plug, which will be flush with the cylinder wall, the components are typically as follows: copper washers and/or spacers to move the lens to the correct position and create a seal; the sapphire lens, with the flat side facing into the engine; another copper washer to protect the lens surface from the spacer; more spacers; and finally the screw lid to hold everything in place. The inner thread is wrapped in PTFE thread seal tape to stop it loosening. Once the entire object is built and screwed into the engine block, there are no issues with leakage or components moving.

A simpler fixed design could easily be built, but tests required different lenses and lens positions, and this design was more flexible to those needs.

Early versions had a sapphire window at the very front, with the lens a short distance behind, however the positioning and focal lengths required inevitably led to back reflections from the window focusing back onto the lens, so this design was abandoned. Unfortunately the solution to this (just using a lens) created a small cylindrical cavity which the air-fuel mixture could enter. This didn't affect the engine in any way as far as was seen, but is not ideal.

The design of this evolved through the experiments and two different sizes were used in the results presented. The second was just a shorter version, which made align-

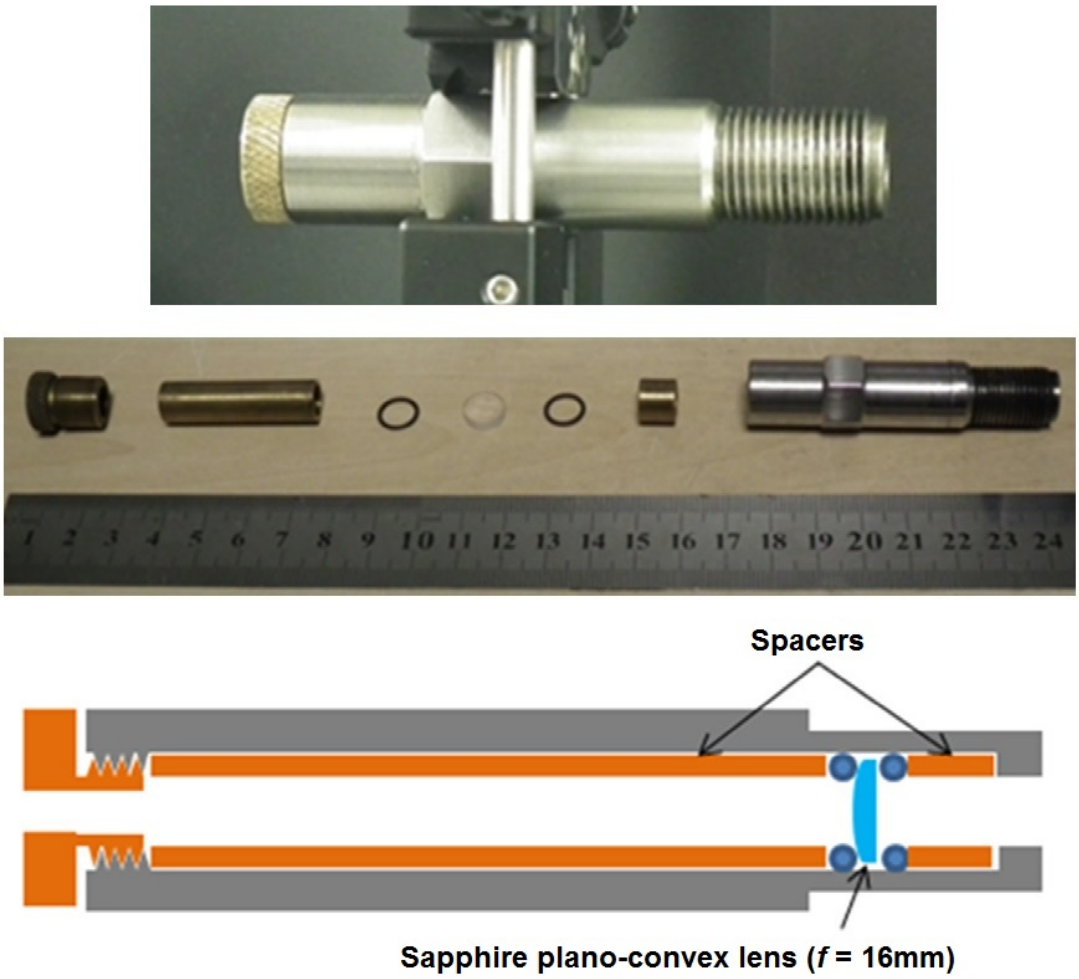

Figure 3.3: Photograph and diagram of the long optical plug.

ment more straightforward. A photograph including internal components is shown in Figure 3.4. Results chapters will note relevant details of the plug used.

There are slight variations between each experiment, but typically the plug would have a lens with focal length $f = 16\,\text{mm}$, and a clear aperture of at least 6 mm through the entire length. The target beam size at the opening to the plug was therefore 6 mm, but varied slightly as the output beam diameter at the laser varied slightly around 10 mm as different parameters were adjusted.

The proportion of laser energy transmitted through the optical plug needs to be known. The useful quantity is the energy delivered to focus, not the energy input to the optical plug, however it is not always practical to measure directly. It is simplest to measure the input and apply a transmission factor.

Figure 3.5 shows the two energies measured to find transmission, the energy at the focus (E_p), and the energy at the input (E_{input}). These are measured at low energy so that the focused light does not damage the energy meter. The plug transmission percentage T is therefore given by the following equation:

$$T = \frac{E_p}{E_{input}} * 100 \tag{3.4}$$

The main factor influencing transmission is the reflection from the uncoated surfaces of the lens. There is also some energy lost due to slight clipping since the laser is a similar size to the clear aperture. This leads to typical transmission of 80% in practice.

3.6 Engine

The engine used was a single cylinder Boss prototype test engine provided by Ford Motor Company (FMC), with a 776 cc swept volume, compression ratio of 9.2, and 100 bar maximum pressure. It is a gasoline direct injection engine (GDI), however this function was not used in these experiments, it was instead used in homogeneous charge mode. Previous University of Liverpool researchers received the engine block and

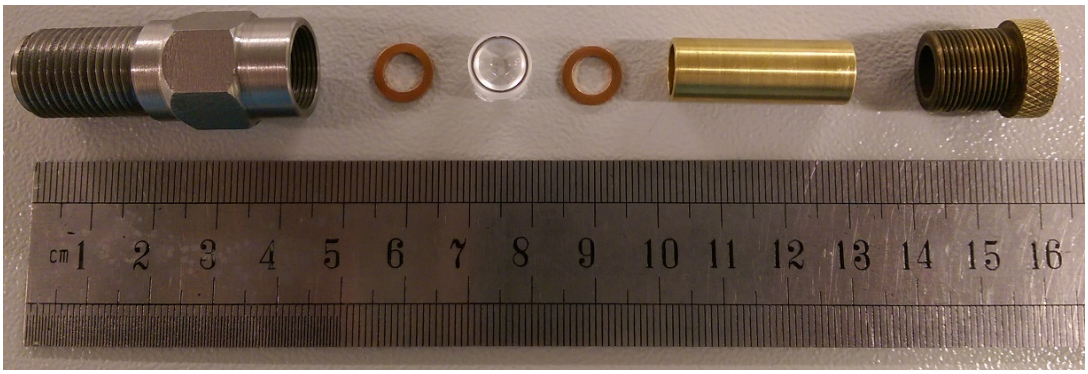

(a) Deconstructed optical plug using copper washers for engine testing.

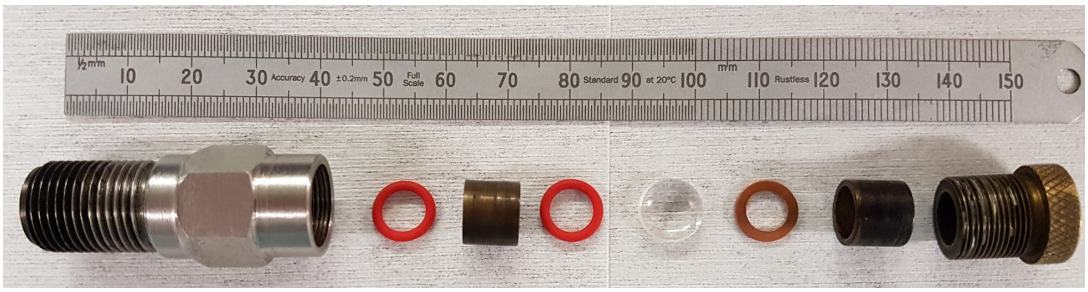

(b) Deconstructed optical plug showing the rubber rings which form an airtight seal.

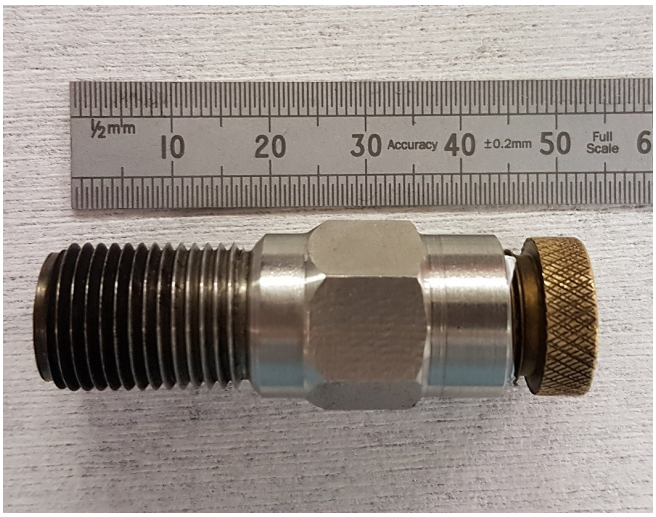

(c) Constructed optical plug.

Figure 3.4: Photographs of the short optical plug and its internal components.

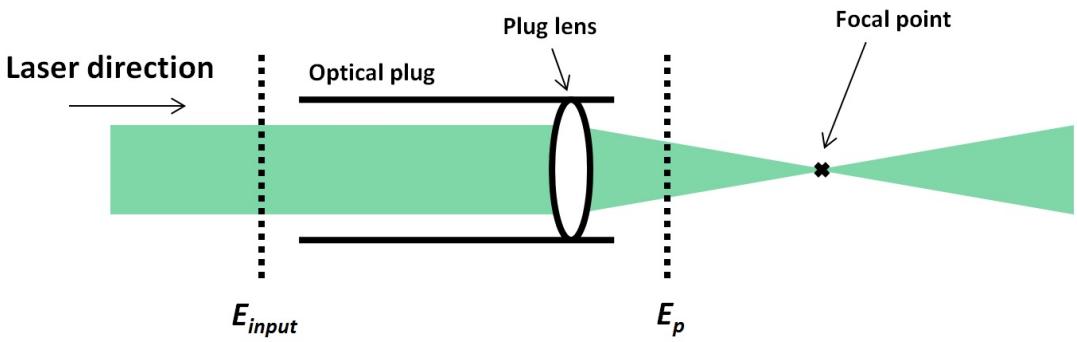

Figure 3.5: Schematic showing a beam focussed through the optical plug lens, indicating energy measurements made in relation to the transmission percentage.

custom built much of the rest of the system, so there is not extensive documentation. The engine is controlled by a dSPACE control box, which is connected to a computer through which the user controls the engine.

Photographs of the engine system are shown in Figures 3.6 and 3.7. The engine block is silver, the dynamometer green, and the starter motor blue. In Figure 3.6 specifically the engine mirror can be seen on top of a post. The laser was input from the right of the picture and reflected down into the opening below, where the optical plug was attached.

Figure 3.8 shows the entire engine control system. As mentioned, the dSPACE control box is linked to all other equipment, and addressed from a computer. In short, the motor, dynamometer, fuel injection system, laser trigger, and throttle are all controlled; other signals are measured data being reported back.

Further information on the operation of this engine is discussed in an article by Cheng et al. (2016). Engine running details will be given in each results chapter, in relation to the test being ran.

3.7 Pressure Chamber

A pressure chamber was used, with the same internal dimensions as the test engine cylinder. It was custom made for use during this project, and also designed to be

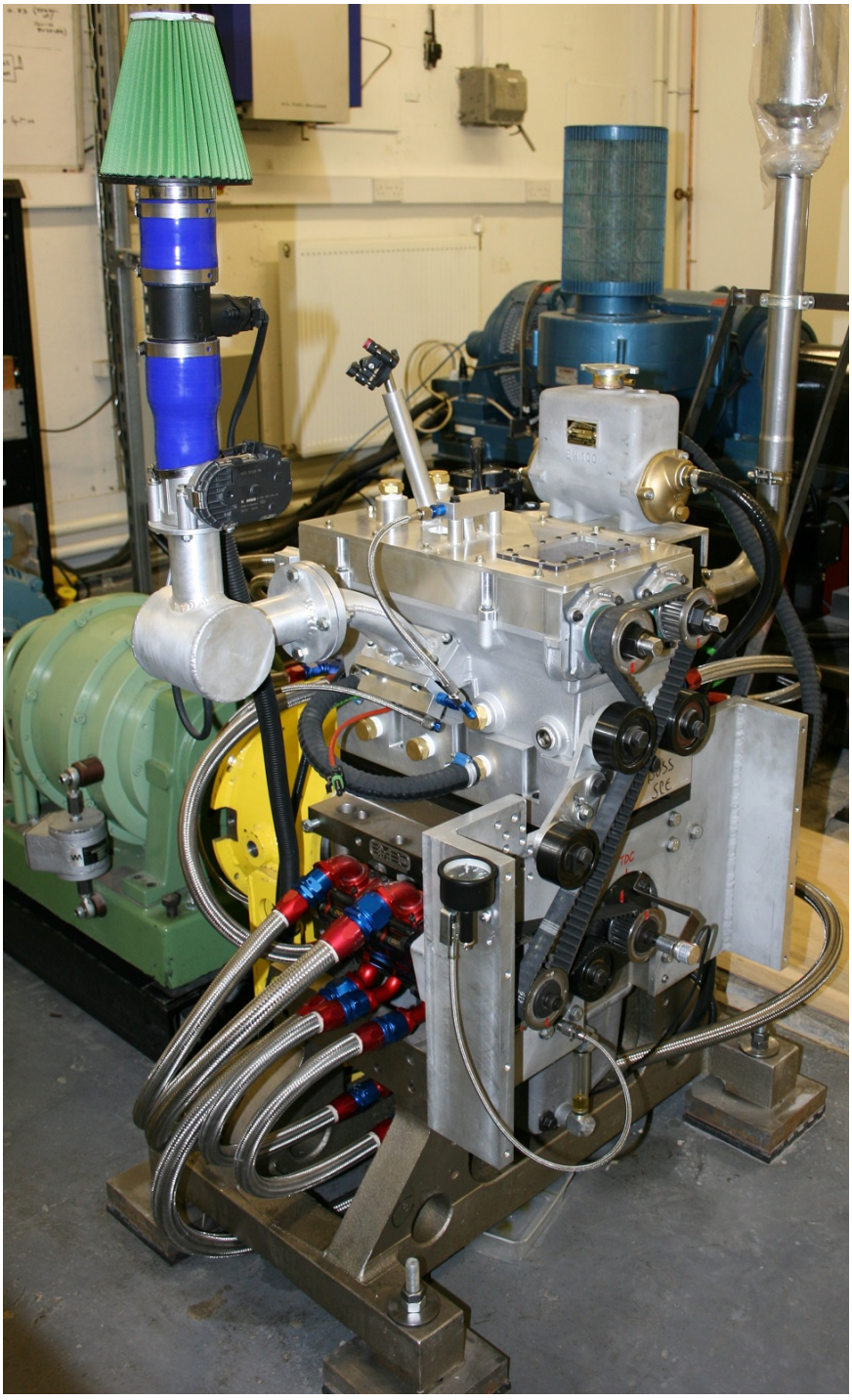

Figure 3.6: Photo of the single cylinder Boss test engine. The dynamometer and stater motor are to the left of the image.

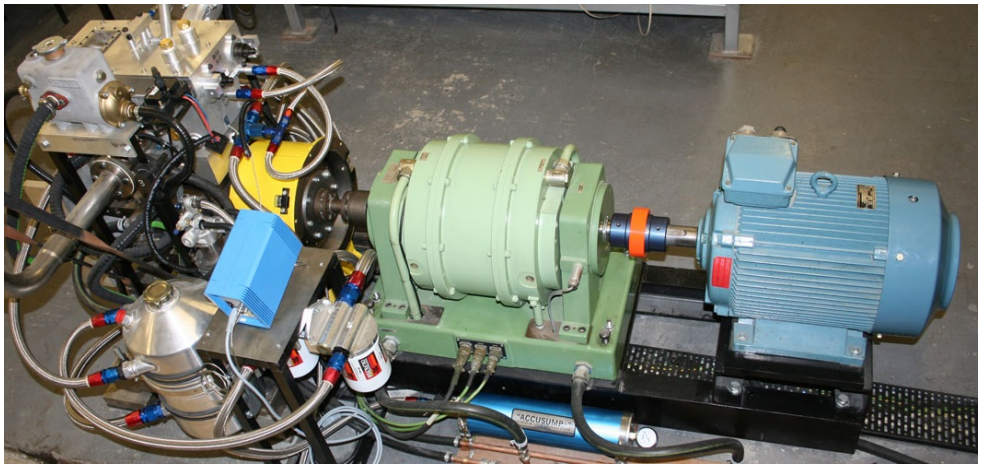

Figure 3.7: A different view of the single cylinder engine, with the dynamometer (middle, green) and the starter motor (blue, right) visible.

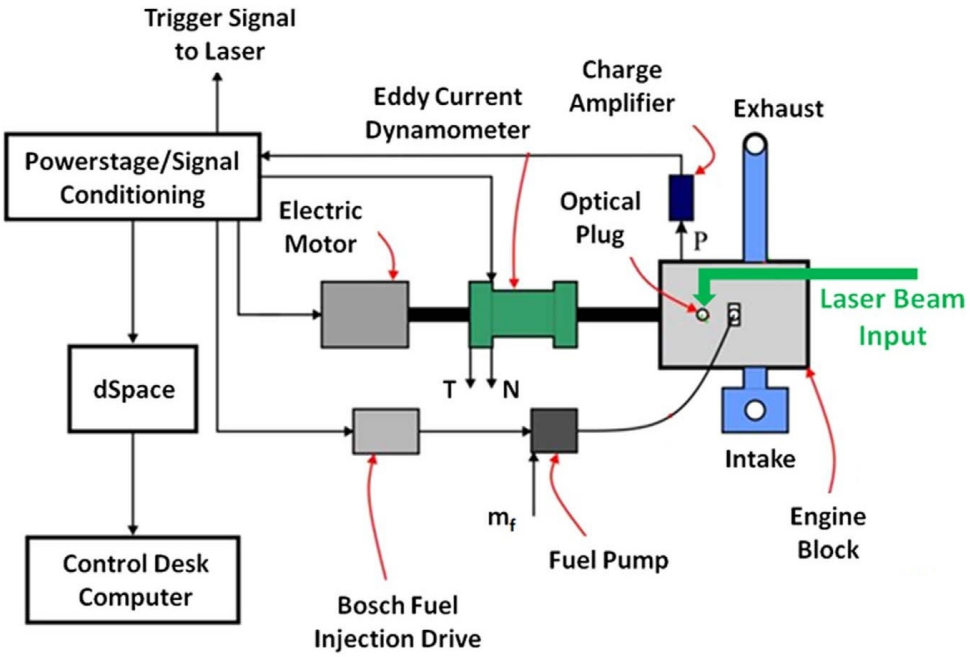

Figure 3.8: Schematic of the engine control system used in the experiments.

usable as combustion chamber, but this function was not utilised for any of the results presented in this thesis.

It operated at up to 10 bar, and was pressurised by the compressed air supply available in the laboratory, which was at 7 bar. Safety valves were set to 4 bar during testing, so no higher pressures than this were used. It could be accessed via a screw hole made to fit the optical plug. A manual screw valve increased the pressure; opening the release valve reduced it. The gauge on the intake was used to take measurements once pressure had equalised. The main body was made of transparent material, which allowed observation of what was happening inside, for example to see if air breakdown took place or not.

Figure 3.9 shows a photograph of the pressure chamber, looking from the optical plug side, which is screwed in near the centre.

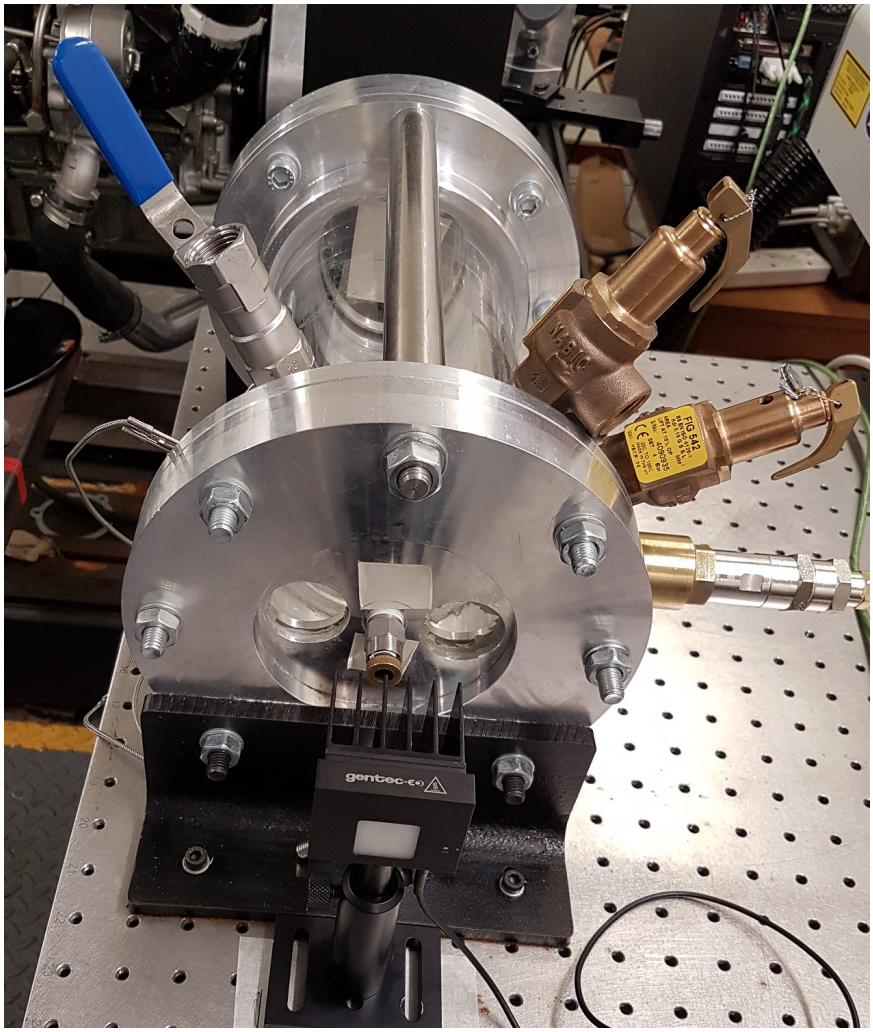

Figure 3.9: Photo of the pressure chamber. The laser energy meter is in front of the optical plug, safety valves and the air intake can be seen on the right.

Chapter 4

Single-point Laser Ignition

This chapter describes the results of a study into single-point LI of an IC engine and associated offline work and characterisation that led up to it. Online and offline refer to experiments carried out using the engine and in air respectively. Laser and engine parameters were varied in order to find the most optimal way to ignite the engine using the laser.

The starting point for this work was that LI has been established as an effective technique with advantages over SI. Research on comparing these two and optimising the laser for ignition has been done in the past.

The objective here was to find the ideal single-point parameters to ignite the test engine. This would then give the best simple case from which to work on new techniques later.

4.1 Offline Tests and Experimental Setups

This section describes the experimental setup and laser calibration work that preceded the engine testing.

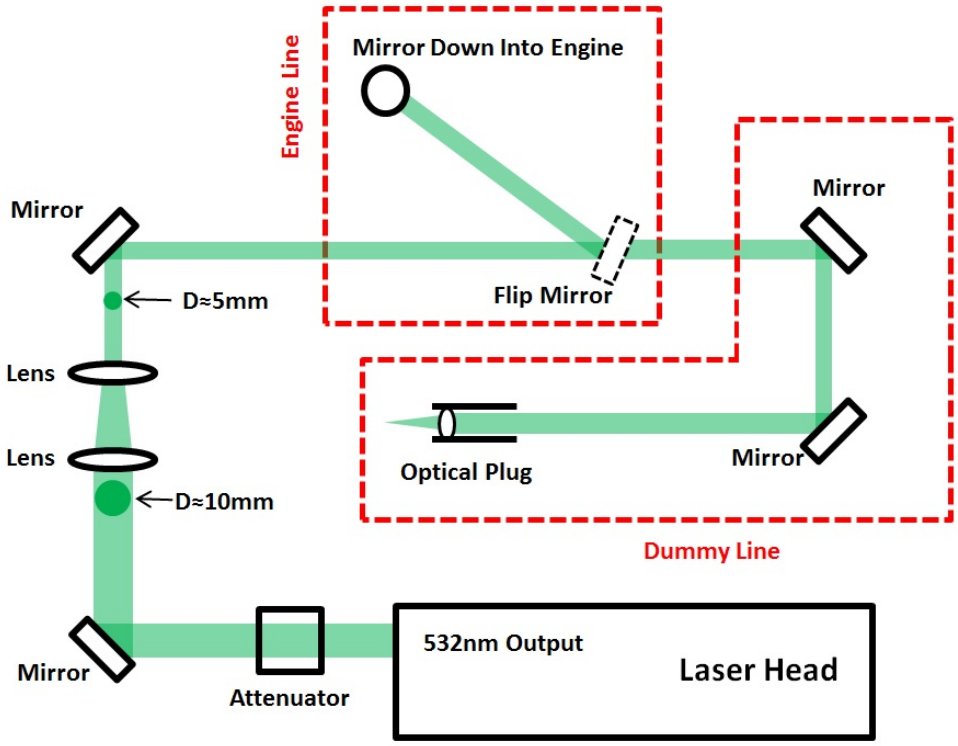

Figure 4.1: Schematic of the experimental setup used for single-point LI, showing the engine and dummy lines.

4.1.1 Experimental Setup

The laser used was the Litron LPY 764-30 Nd:YAG, running in 532 nm mode. A range of energies and repetition rates were used that will be described later.

Figure 4.1 shows the complete experimental setup. The path to the engine is referred to as the "engine line", while an optically equivalent path in free space on the table is referred to as the "dummy line". The dummy line is useful since the engine is effectively a black box as the spark cannot be analysed inside the cylinder.

On either line, the first beam passed through the attenuator, followed by a beam reducing telescope that reduced the beam diameter in order to fit into the optical plug. Then, in the case of the engine line, the beam hit the flip mirror that was moved into position, then the engine mirror which reflected it down into the optical plug below. For the dummy line, the beam was reflected from two identical mirrors and into the optical plug, having travelled the same distance as to the engine.

A Gentec-EO QE25 energy meter, and a Thorlabs BC106-VIS beam profiler camera were used to measure the pulse energy, beam size and beam quality, as described in Section 3.3.

The optical plug used was the original longer version, with the standard $f = 16\,\text{mm}$ sapphire lens. The transmission varied slightly between tests due to fouling and self-cleaning of the lens surface due to combustion. Transmission was measured between each engine run to account for this. One of the variables tested was spark distance, or the distance from the end of the plug to the focal point. This was varied by changing the number and size of spacers and washers between the lens and the end of the optical plug.

The engine used was the Ford single cylinder test engine, ignited using the Litron laser and controlled as described previously in Section 3.6. During start-up, the engine was run for around 30 minutes to warm before beginning any experiment. Data was collected at each set of fixed parameters for ~ 500 engine cycles and each data point presented is the average of such a test.

4.1.2 Laser Characterisation

The properties of the laser beam were measured for conditions relevant to the planned engine tests.

Figure 4.2 shows variation in E_p and M^2 over a range of repetition rates. E_p was fairly stable at repetition rates above 10 Hz, but varied greatly below this level. This was not a significant issue, however, as rates below 8 Hz were not needed. M^2 increased linearly with repetition rate, which was somewhat concerning as it affects spot size significantly. Fortunately in the region of interest (around 8 Hz) it remained steady at $M^2 = 10$. It should be noted that the reason for this is that the manufacturer optimised the laser to work best in this area, it could in principle be optimised for any parameters close to these by making adjustments to the cavity.

These variations were accounted for in testing by setting the pulse energy after the

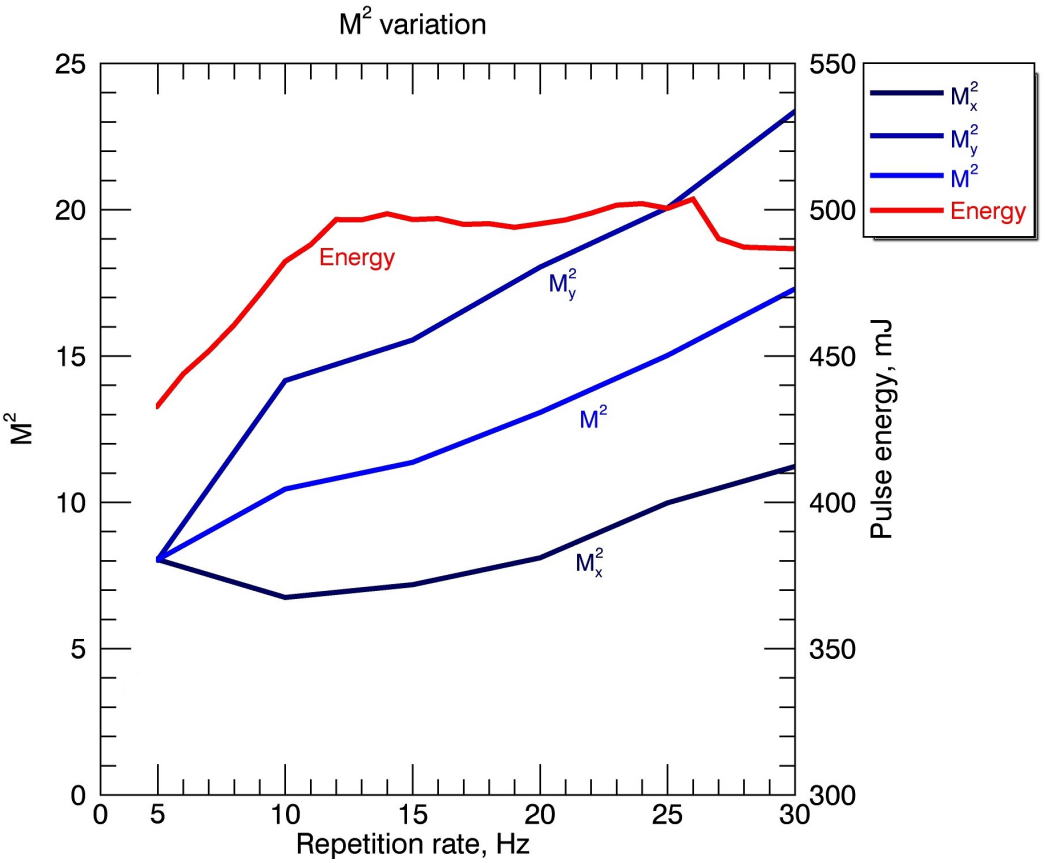

Figure 4.2: Laser output variation with repetition rate of pulse energy (E_p), beam quality (M^2), and the x and y components of M^2.

repetition rate, which kept the energy measurements for each engine run accurate.

Beam profile images at 8, 10 and 12 Hz can be seen in Figure 4.3. The scale shown is in 1000 µm increments. These are shown as they are equivalent to the engine speeds tested in the 1000 to 1500 rpm range. The general shape is slightly oval with three peaks down the middle so is clearly a multi-mode beam. As repetition rate increases, the beam diameter decreases slightly, and some of the energy shifts from the bottom peak to the top peak.

Laser pulse length measurements were provided by the manufacturer, for repetition rates tested it was 10 ns.

The minimum pulse energy required for consistent spark formation in air was measured to be approximately 30 mJ, therefore 40 mJ was used as the baseline energy in testing

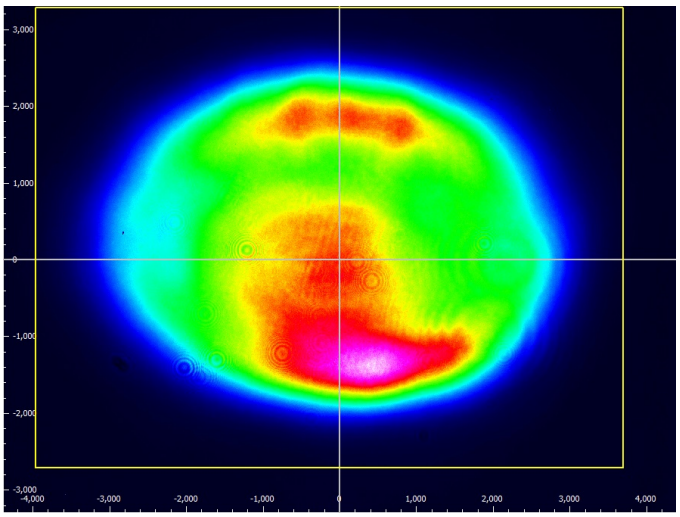

(a) 8 Hz

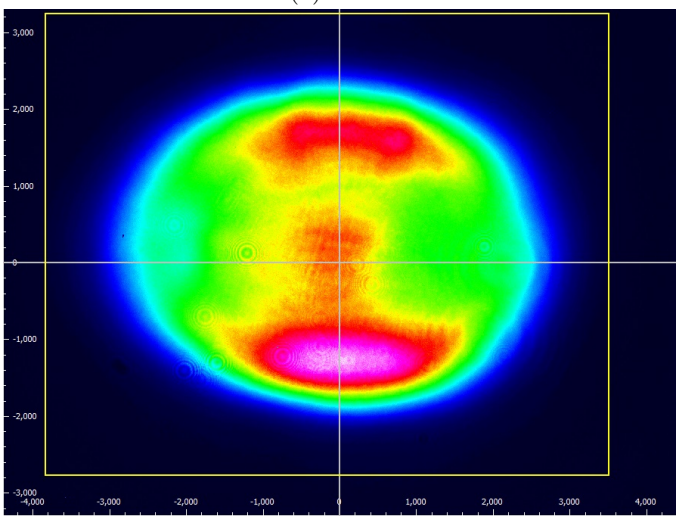

(b) 10 Hz

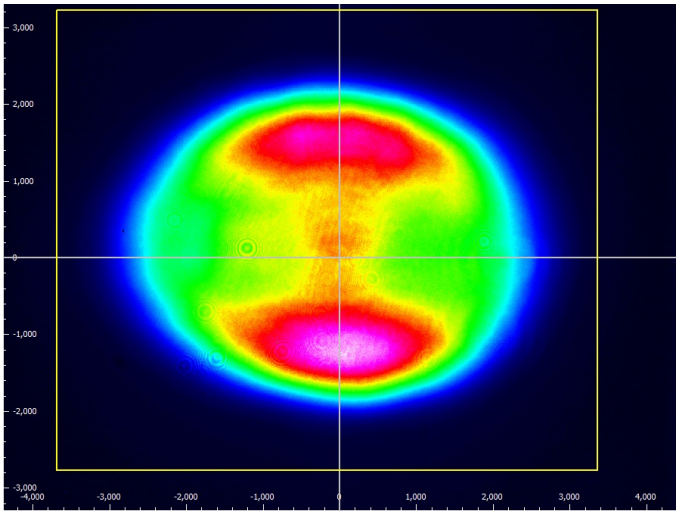

(c) 12 Hz

Figure 4.3: Litron LPY 764-30 beam profiles at 532 nm across different repetition rates.

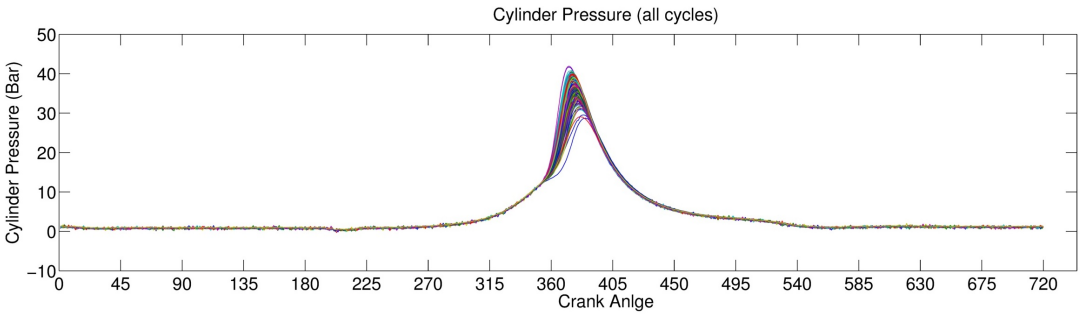

Figure 4.4: Example raw pressure data from 500 cycles at $E_p = 50\,\text{mJ}$, spark advance of 20°, and 1000 rpm.

to ensure consistent ignition.

4.2 Engine Test

Engine tests investigated two main parameters, the laser pulse energy E_p used for ignition, and the distance from the end of the plug to the focal point, or spark distance.

Engine performance was compared in terms of engine output power and $IMEP$, while engine stability was compared in terms of COV_{IMEP}. An example of the raw pressure data is shown in Figure 4.4, from a test where $E_p = 50\,\text{mJ}$, and spark advance (SA) was 20°. Parameters such as $IMEP$ are calculated and averaged over all cycles in each data set.

Results presented here were taken at 1000 rpm, which is the design speed of the engine.

4.2.1 Variation in Laser Pulse Energy

The first set of tests measured the effect of varying pulse energy, from the minimum required in this engine of 40 mJ, up to 90 mJ. The maximum energy was chosen for safety reasons, as it was the maximum that the protective equipment in the lab could handle.

Figure 4.5 shows the power output at various pulse energies and ignition timings. The power output peaks at around 20° and 50 mJ to 60 mJ. $E_p = 50\,\text{mJ}$ gives the highest

output power across all timings.

The reason that the higher energy pulses, particularly 80 mJ and 90 mJ, perform worse is not explained directly by the data, but a possible reason comes from the differences in the spark formation at higher energies. As part of the plasma formation a shockwave is created in the air around the plasma travelling outwards. The more energetic plasma, the larger it is, and the larger the shockwave. This shockwave could potentially disrupt the combustion, perhaps extinguishing parts of the flame front.

The cylinder in the test engine is a black box, without imaging the combustion it is not possible to know for certain how the shockwave interacts with the combustion at high pulse energies.

The $IMEP$ as shown in Figure 4.6 shows similar trends, not surprisingly due to the equivalence between this and power output. Again the two highest energies perform worst of all. COV_{IMEP} is effectively the error on $IMEP$ and power in percentage terms, but is also a measure of engine stability. This is plotted in Figure 4.7. There is a spread of around 0.5%, with the lower half of the energies having the best stability.

Looking at this data set, 20° and 40 mJ to 50 mJ seem to be the ideal parameters to choose.

4.2.2 Variation in Spark Position

With the ideal E_p for these test conditions established, a new test was carried out to determine the ideal position for the single spark. Spark distance is the distance from the focal point to the end of the optical plug, which is flush with the cylinder wall. In these tests engine speed was fixed at 1000 rpm, and pulse energy at $E_p = 50$ mJ.

Figure 4.8 shows variations in engine power output for various spark positions and ignition timings. The power varies by around 150 W or 5% depending on spark distance, which is a significant effect. Again there is a strong advantage for the 20° SA, with a spark distance of 6 mm clearly ahead of the others. Looking closely at the timing of the highest output power for different spark distances, there appears to

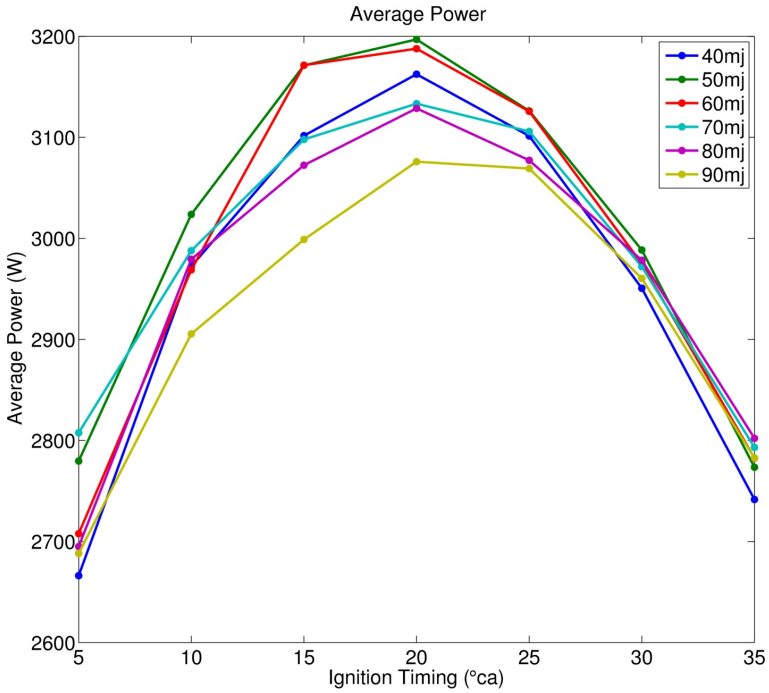

Figure 4.5: Average power output for a range of pulse energy and ignition timings.

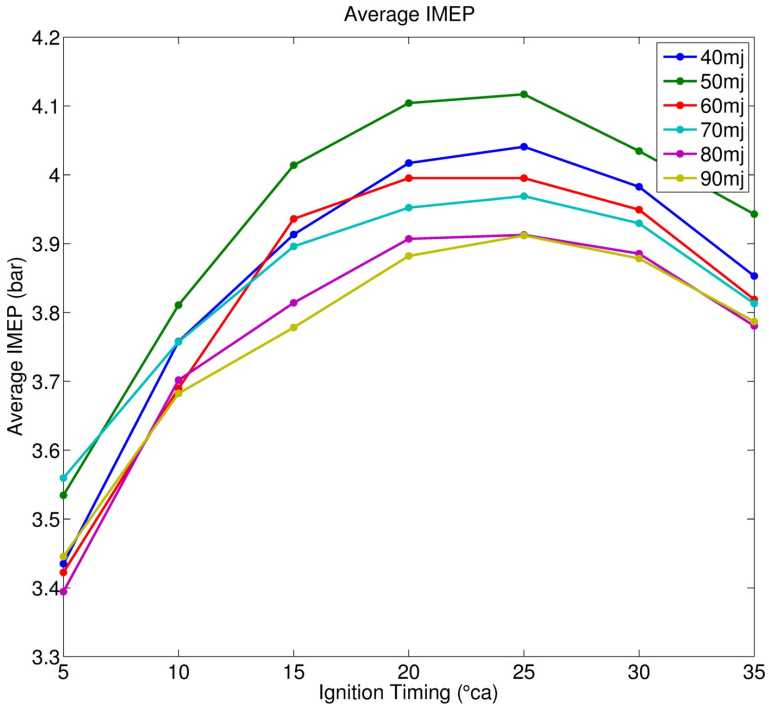

Figure 4.6: $IMEP$ for a range of pulse energy and ignition timings.

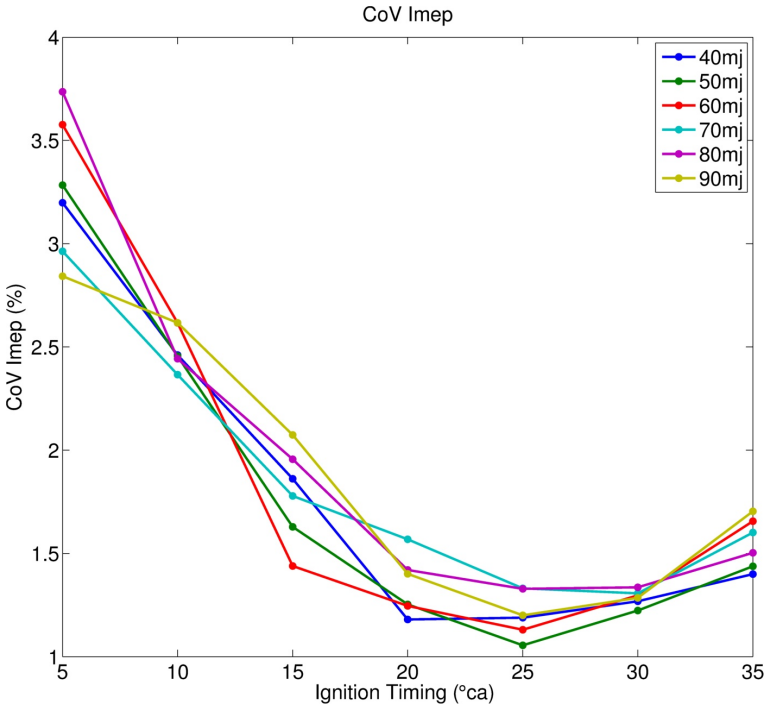

Figure 4.7: COV_{IMEP} for a range of pulse energy and ignition timings.

be a correlation where longer distances prefer shorter SA. This makes sense, as the purpose of having a spark advance is so that the flame has propagated to the edge of the piston at around the time it reaches top dead centre. Longer spark distance means less distance to the piston, so a shorter time is needed for flame propagation (lower spark advance is a later timing).

Turning to COV_{IMEP} , which is shown in Figure 4.9, the difference between the distances is less clear. The 6 mm spark is once again the significantly best performing across the majority of values of SA, apart from the the lowest. It falls slightly short at the previous best performing SA value of 20°, and indicates a slightly different best performing SA value of 25°.

4.3 Chapter Summary

This presented results of a number of engine tests which aimed to find the best way to ignite this test engine using a single laser spark. Spark advance, pulse energy and

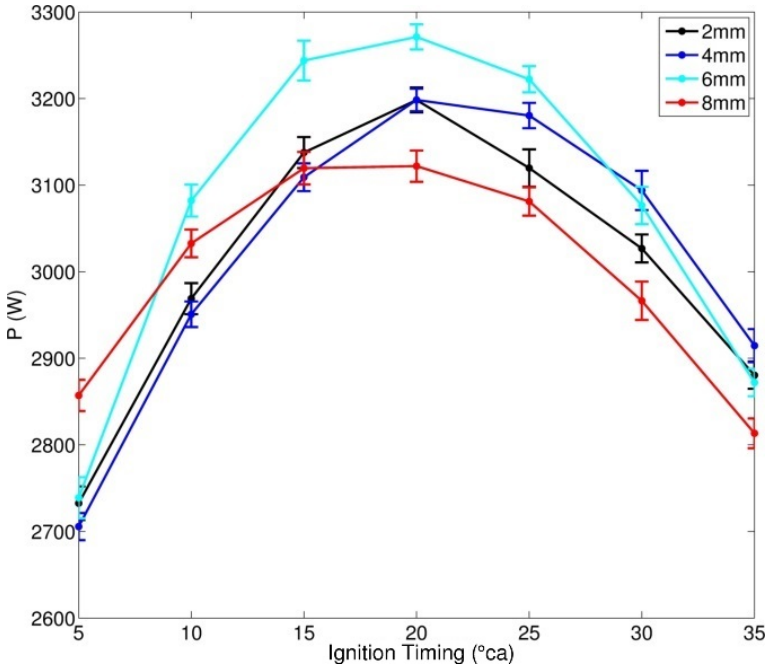

Figure 4.8: Average power output for a range of spark positions and ignition timings at a fixed pulse energy and engine speed.

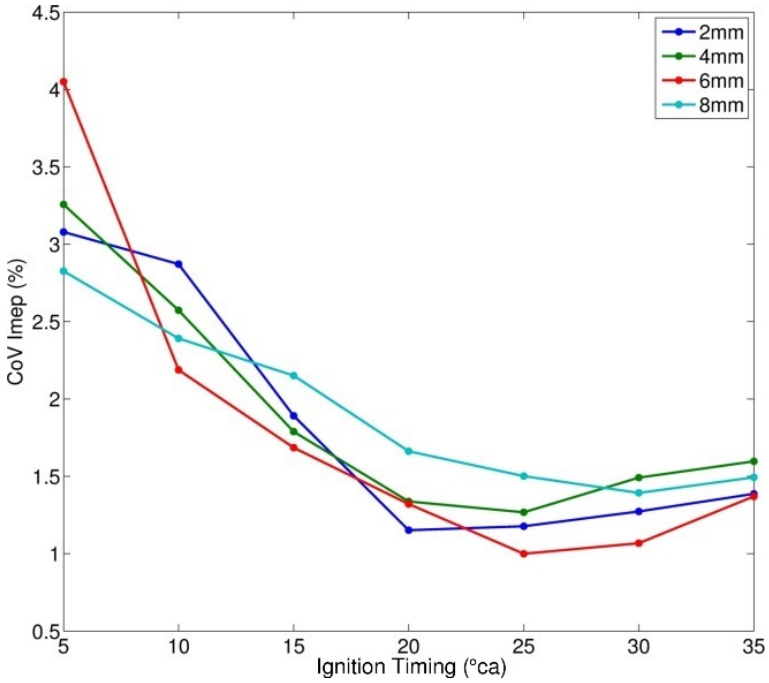

Figure 4.9: COV_{IMEP} for a range of spark positions and ignition timings at a fixed pulse energy and engine speed.

spark distance were varied at fixed speed, all of which significantly affected the engine output power and stability. The best ignition conditions of those tested were found to be $E_p = 50\,\text{mJ}$, 20° SA, and 6 mm spark distance. These gave a baseline when choosing parameters to test and compare with in later experiments.

Chapter 5

Multi-point Laser Ignition

Multi-point laser ignition refers to the idea of having multiple sparks beginning or maintaining each combustion event, in contrast to the usual method of one point of ignition beginning the combustion, which is then left to develop on its own. This can be divided into multi-location for spatial variation, and multi-pulse for temporal variation. As discussed in the literature review, specifically in Section 2.4.2 on page 22, one of the potential advantages of laser ignition over using a spark plug is the freedom to distribute the laser energy around the cylinder in order to create multiple ignition locations. There has been some work in this area, but the methods used could only produce two or three sparks in fixed locations (Morsy and Chung, 2003; Pavel et al., 2011a).

This chapter describes work on an experimental technique which can be used to produce several sparks with arbitrary spatial location in three dimensions within an engine cylinder These are created by variable diffraction of a pulsed single laser, which is focused inside the cylinder by an optical plug. Diffractive multi-beam patterns were generated using a spatial light modulator (SLM) by reflecting the laser beam off of it during its path to the engine. The diffraction was dependent on which computer generated hologram (CGH) was displayed. The first section describes initial work on this technique, the next the application of it to the engine. The chapter will conclude with a summary of the findings.

Much of the work discussed in this chapter was published in two journal articles (Lyon et al., 2014; Kuang et al., 2017). This was the first time this technique was applied in relation to engine ignition.

5.1 Multi-location breakdown in air and development of the technique

This section covers an initial study into multi-location air breakdown.

5.1.1 Experimental Setup and Methodology

The laser used was the Spectron Mini-Q flashlamp pumped Q-switched Nd:YAG, manufactured by GSI Group. This was operated at the fundamental wavelength of $\lambda = 1064\,\text{nm}$, and at pulse length $t_p = 10\,\text{ns}$. The pulse energy was set by controlling the voltage to the flashlamp using a built in controller. More details on the laser and other equipment were explained in Chapter 3. The SLM used was a HOLOEYE LC-R 2500, a liquid crystal on silicon (LCoS) device with 1024×768 pixels, and with a broadband coating. At $\lambda = 1064\,\text{nm}$ and a 0° angle of incidence, its reflectivity is $\eta > 80\%$. The SLM was controlled by an attached computer, this was discussed in Section 3.4.

Figure 5.1 on the facing page shows the experimental setup used. The laser output passed through a half wave plate used for adjusting the linear polarisation direction, since polarisation should be aligned with the direction of array of pixels on the surface of the SLM, in order to maximise efficiency. Next is a beam expander, with a magnification factor $M \approx 4$. The expanded beam then illuminates the SLM, at a < 10 degree angle of incidence. Different computer generated holograms (CGHs) could be displayed on the SLM to creative different diffractive multi-beam patterns.

The multi-beam pattern then reached an optical plug and was focused by a 2 mm thick sapphire plano-convex lens $f = 12\,\text{mm}$ into multiple focal points. See Section

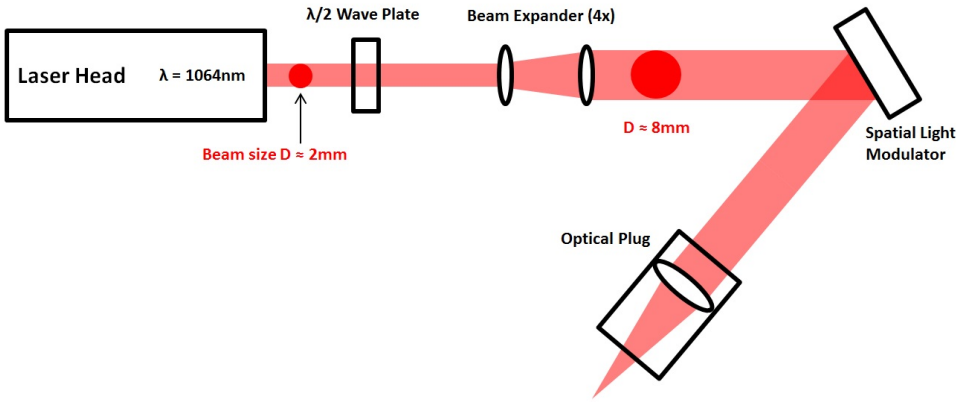

Figure 5.1: Schematic of the experimental setup used to generate axial multi-location air breakdown, as well as other tests described in Section 5.1.

3.5 for details on the optical plug.

A Gentec-EO QE25 energy meter was used to measure laser pulse energy. Energies given in this chapter refer to the energy delivered to the focal point, with transmission and other effects taken into account, unless otherwise specified.

The CGHs used to create diffractive multi-beam patterns were calculated by a gratings and lenses (GL) algorithm. The HOLOEYE software provided by the SLM manufacturer used these algorithms to create the CGHs, in the form of black and white image, which is displayed on the SLM as an image would displayed on a computer screen. By combining the phase of basic optical components; prisms or gratings (producing lateral shifts); and lenses (producing axial shifts); the GL algorithm can generate three dimensional arbitrary multiple beam patterns. The next subsection will explain how this works in detail. Relevant background was covered in Section 2.1.3 on page 10.

5.1.2 Multi-beam pattern creation by superposition of prismphases to achieve lateral shifts

The equations and theory that follow give the mathematical basis of GL algorithm. An optical beam can be represented by a complex field ψ, which can be written as:

$$\psi_0 = A_0 e^{i\phi_0} \tag{5.1}$$

The modulus A_0 is the amplitude of the field and ϕ_0 is the phase. The phase only hologram acts as a transmission function ψ_t, expressed as the following, which modifies only the phase of the beam:

$$\psi_t = e^{i\phi_h} \tag{5.2}$$

When the beam given by equation 5.1 is incident on the SLM, ψ_h, the complex amplitude profile of the beam after the modulation of the phase hologram, will be:

$$\psi_h = \psi_0 \cdot \psi_t = e^{i(\phi_0 + \phi_h)} \tag{5.3}$$

If the hologram plane has an inclined phase front, the spot in the image space will be laterally displaced from the optical axis. This is equivalent to passing the light through a prism with a small angle that introduces a linearly increasing phase delay ψ_{prism} across the beam. The prism phase at the hologram plane required to produce a lateral shift $(\Delta x, \Delta y)$ in the position of the focused spot is given by:

$$\phi_{\text{prism}}(x_h, y_h) = \alpha(\Delta x x_h, \Delta y y_h) \tag{5.4}$$

Where α is a coefficient that depends on the imaging characteristics of the SLM and the laser's wavelength.

To generate diffractive multiple beams with lateral shifts, the phase at the hologram plane ϕ_h, should be the complex superposition of the prism phases, each of which shifts a focused spot onto one of the requested positions, $(\Delta x_i, \Delta y_i)$. This is visualised in Figure 5.2 on the facing page. When the laser is incident on one of these superposition, different parts of the laser "see" different elements of the hologram, and are diffracted accordingly.

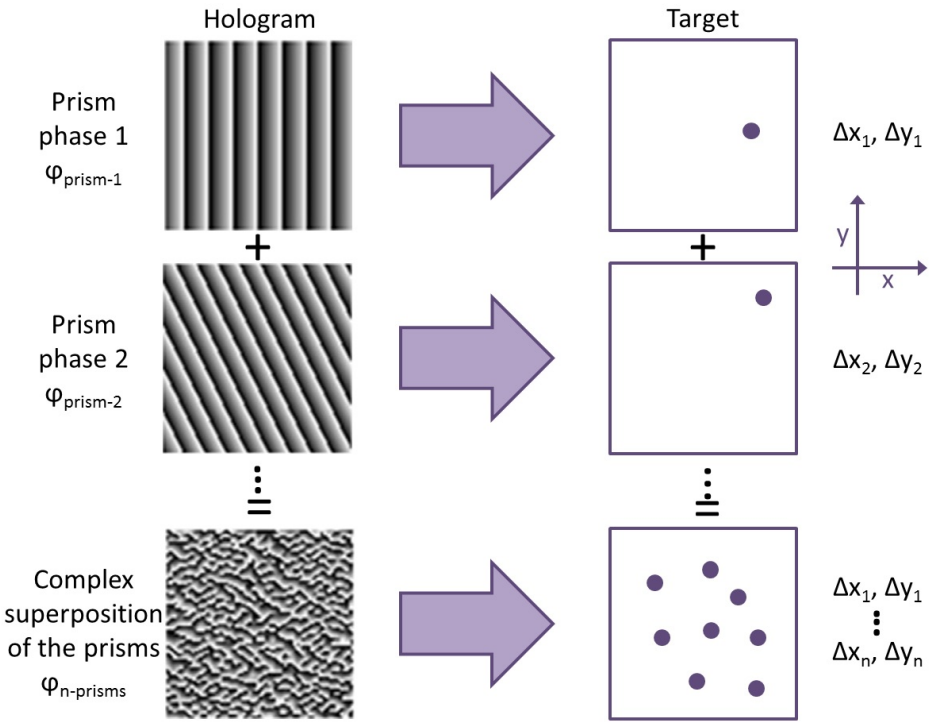

Figure 5.2: Representation of a complex superposition of prism phases generating a diffractive multi-beam pattern.

In this case ϕ_h can be expressed as:

$$\phi_h = \left(\sum_{i=1}^{n} \phi_{\text{prism } i} \right) \bmod 2\pi \tag{5.5}$$

The distance of lateral shift Δl (where $\Delta l^2 = \Delta x^2 + \Delta y^2$) is defined by the diffractive angle θ. According to the grating equation, $\sin\theta_m = m\lambda/\Lambda$, the diffractive angle is $\theta = \lambda/\Lambda$, where $m = +1$ is the diffraction order, λ is the wavelength of the input laser (here 1064 nm), and Λ is the grating period. Since the size of the SLM pixel is $\sim 20\,\mu$m (per the manufacturer's specifications), the minimum grating period is $\Lambda > 2$ pixels $\sim 40\,\mu$m, and hence the maximum diffractive angle is $\theta_{max} \approx 0.025$ rad ≈ 1.4 degrees. As the sapphire plano-convex lens (f = 12 mm) in the optical plug was used to focus the diffractive beams, the maximum lateral shift is $\Delta l_{max} \approx 2f \tan\theta_{max} \approx 0.6$ mm.

Figure 5.3 on the next page shows a CGH which was displayed on the SLM to create 6 diffractive beams in a hexagonal pattern, each with the same diffractive angle $\theta =$

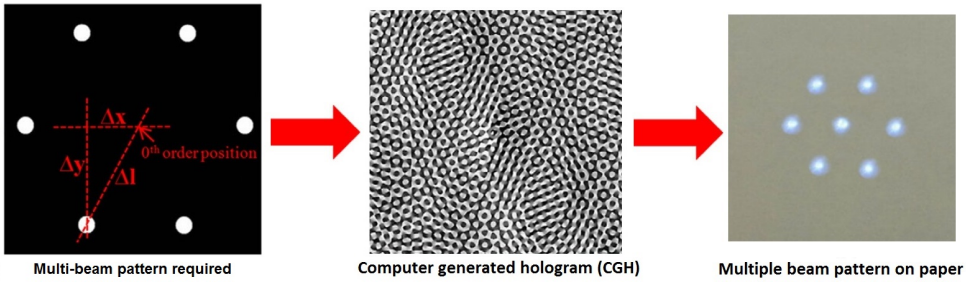

Figure 5.3: The multi-beam pattern required, with lateral shift Δl labelled (left), the CGH displayed on the SLM (middle), and a photograph of the multi-beam pattern focused onto a paper target (right).

0.01 rad.

The 0^{th} order beam is the portion of the laser that has not been diffracted, which will focus to the normal focal point of the lens. At the focal plane of the optical plug lens, the lateral shift of each diffractive beam from the 0^{th} order beam position was $\Delta l \approx 2f \tan\theta \approx 0.24\,\text{mm}$.

When this 6 beam pattern was focused with the optical plug lens, a single air breakdown spark formed which was indistinguishable from one formed by a single laser beam. Since the lateral shift, $\Delta l \approx 0.24\,\text{mm}$, is smaller than the typical spark size ($\sim 0.5\,\text{mm}$), it is not possible to see any separation between the different beams. A displacement of a quarter of a millimetre is also very small on the scale of the engine (cylinder diameter $\sim 100\,\text{mm}$).

A lens with $f = 300\,\text{mm}$ was then used to focus the multiple beams instead of the optical plug lens. Thus, the lateral shift from the 0^{th} order beam increased to $\Delta l \approx 2f \tan\theta \approx 6\,\text{mm}$ at the focal plane of the lens.

Figure 5.3 shows this pattern on the surface of a paper target at the focal plane of the lens (the target is to illustrate the shape, since there isn't sufficient energy to create a spark with this lens). The brighter spot in the centre was created by the non-diffracted 0^{th} order beam, while the other 6 bright spots with a geometrical shape which matches the computational reconstruction of the CGH (also Figure 5.3) were created by the diffracted beams.

With a fixed lens focal length as we have in the engine, there are two ways left to increase the lateral shift displacement. One is using higher diffractive orders (e.g. 2^{nd} or 3^{rd}) to create sparks. According to the grating equation, a higher diffractive order has a larger diffractive angle, and hence gives a larger lateral shift displacement. However CGHs that produce higher order beams have lower efficiency, since part of the energy will still be left at the 0^{th} and any other lower orders. The other way is to use an SLM with a higher resolution and therefore a smaller pixel pitch. Later in the chapter further results of lateral multi-point sparks using a different SLM will be reported on.

5.1.3 Multi-beam pattern creation by superposition of Fresnel lens phases to achieve axial shifts

To shift a focal spot axially, i.e. along the the direction the beam is travelling, a lens phase should be added. Similarly to Equation (5.4) on page 64 which gives the prism phase ϕ_{prism}, the lens phase ϕ_{lens} can be given as:

$$\phi_{\text{lens}}(x_h, y_h) = -\frac{k}{2f}(x_h^2 + y_h^2) \tag{5.6}$$

Here f is a function of the axial shift distance and $k = 2\pi/\lambda$ is the wave number of the light.

The beam being modulated by such a CGH is equivalent to passing the light through an additional lens with focal length f. With both prism and lens phases added, the focused spots are displaced not only laterally and but also axially, i.e. three-dimensionally. In order to obtain a multiple beam pattern in three dimensions, a superposition of lens and prism phases is needed. The phase of the beam at the hologram plane is required to be the sum of ϕ_{prism} and ϕ_{lens}:

$$\phi_h = \left(\sum_{i=1}^{n} \phi_{\text{prism } i} + \phi_{\text{lens } i} \right) \bmod 2\pi \tag{5.7}$$

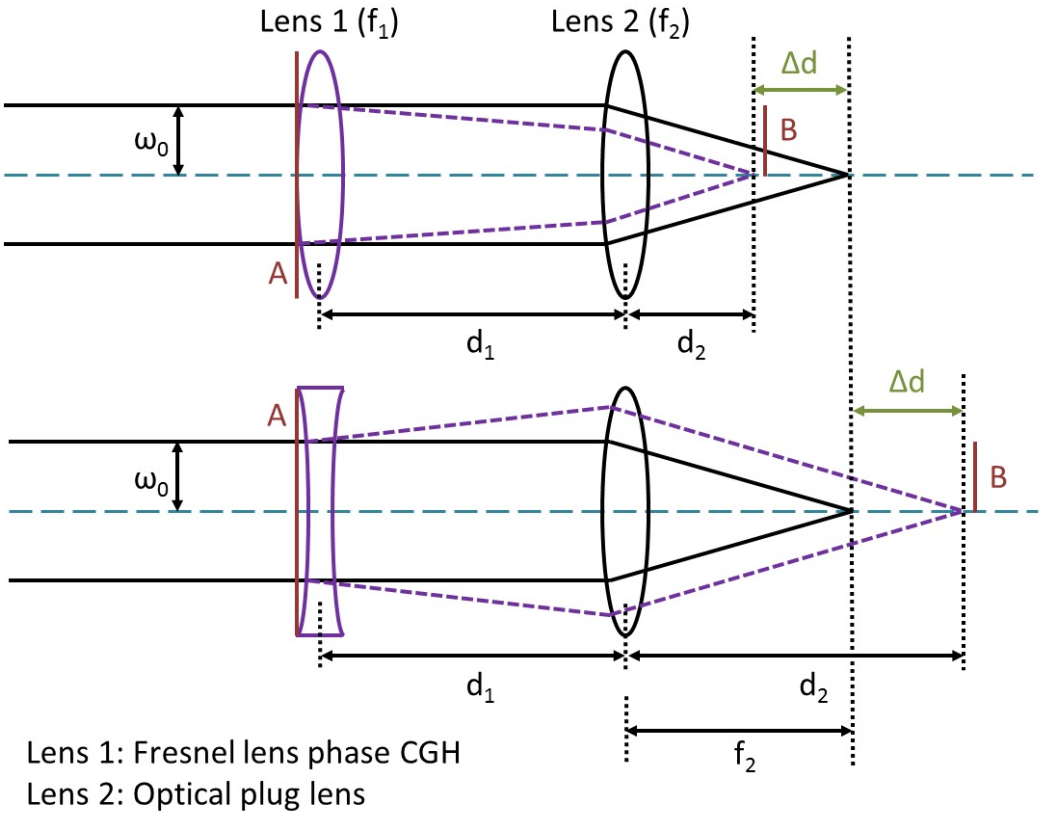

Figure 5.4: Representation of how Fresnel lens phase CGHs modulate a beam. The added Fresnel lens phase, lens 1, can work as either a positive lens (upper) or negative lens (lower).

Figure 5.4 shows the effect of the Fresnel lens phase. Only the diffracted beams were converged ($f > 0$) or diverged ($f < 0$), while the non-diffracted 0^{th} order beam was unaffected. The distance between the two foci is Δd, as shown in Figure 5.4. The following beam matrix equation describes the propagation of the diffracted beam from the SLM surface (A) to its focal plane (B):

$$\begin{pmatrix} X_B \\ tg\theta_B \end{pmatrix} = \begin{pmatrix} 1 & d_2 \\ 0 & 1 \end{pmatrix} \times \begin{pmatrix} 1 & 0 \\ -\frac{1}{f_2} & 1 \end{pmatrix} \times \begin{pmatrix} 1 & d_1 \\ 0 & 1 \end{pmatrix} \times \begin{pmatrix} 1 & 0 \\ -\frac{1}{f_1} & 1 \end{pmatrix} \times \begin{pmatrix} X_A \\ tg\theta_A \end{pmatrix} \tag{5.8}$$

where f_1 and f_2 are the focal length of the added Fresnel phase lens and the real focusing lens respectively; X_A and X_B are the distances of the beam from the axis; $tg\theta_A$ and $tg\theta_B$ are the gradients of the beam with respect to the axis at the position A and B. Since $tg\theta_B = 0$ and $X_A = 0$, the axial shift (Δd) can be calculated by the following equationderived from the beam matrix equation:

$$\Delta d = |d_2 - f_2| = \left| \frac{f_1 f_2 - f_2 d_1}{f_1 + f_2 - d_1} - f_2 \right| \tag{5.9}$$

where $d_1 \approx 10\,\text{mm}$ was the distance between the SLM and the real focusing lens, and $f_2 \approx 12\,\text{mm}$ was its focal length.

As shown in Figure 5.5, three axial air breakdown sparks were created. This CGH was generated by a superposition of two Fresnel lens phases. The spark nearest to the plug was created by the non-diffracted 0^{th} order beam. Each lens phase then created a focal spot with an axial shifts $\Delta d_1 = 5\,\text{mm}$ and $\Delta d_2 = 10\,\text{mm}$. The three air breakdown sparks were created in air when the input pulse energy was $E_p \approx 60\,\text{mJ}$.

The energy distribution between the different beams can be adjusted by rotating the half wave plate which controls the polarisation direction of the beam incident on the SLM. This changes the diffraction efficiency and therefore changes the proportion of energy going to the 0^{th} order beam or the 1^{st} order diffracted beams. Trial and error was used in rotating the half wave plate, until all three sparks appeared to be the

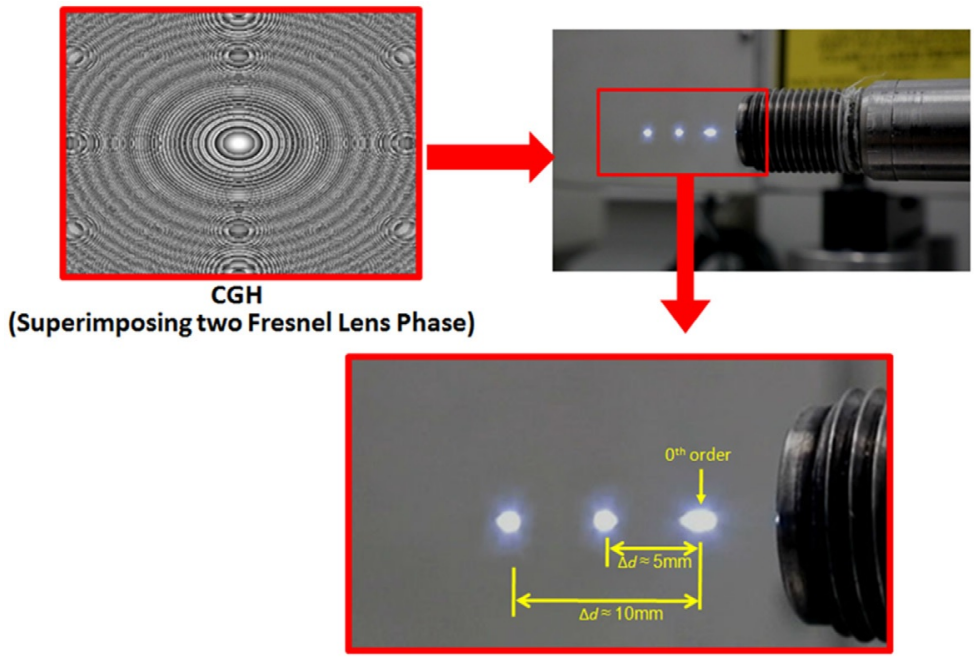

Figure 5.5: Air breakdown sparks created by axial shifts, with spark distance labelled.

same size and brightness, and so have the same energy. The minimum input pulse energy for stable sparking was $E_p \sim 60\,\text{mJ}$. There is no way to independently measure the energy at each focus since the beams overlap, but assuming each has $E_p \sim 20\,\text{mJ}$ seems reasonable since this is approximately the minimum energy for a single spark with this laser and optical plug lens.

Different axial shifts can be created by varying the focal length of each added Fresnel lens phase. Figure 5.6 on the next page shows first single point air breakdown, then multi-location air breakdown with different CGHs displayed.

5.1.4 Engine application of the HOLOEYE LC-R 2500 SLM

The limitation of the axial multi-location spark is that the multi-beam pattern must be focused fairly close to the SLM surface, within around $\sim 300\,\text{mm}$. Otherwise, the different elements of the beam will separate, as the 0^{th} order is collimated, and the higher orders are either diverging or converging at different rates. Due to the design of the test engine used, and the SLM not being robust enough to handle the heat

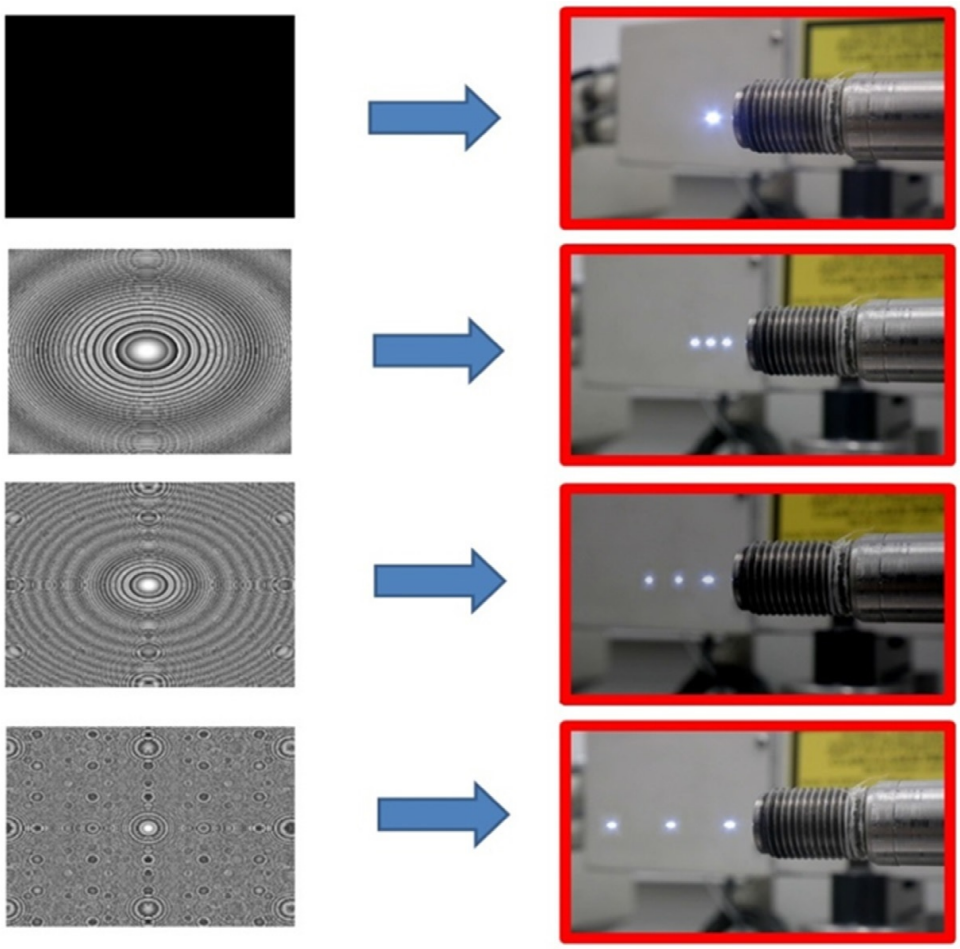

Figure 5.6: Breakdown sparks with variable separation created by axial shifts.

and vibration of the engine, it was not possible to get the SLM close enough to the engine to apply this technique to ignition tests. Lateral multi-beam patterns can be maintained over long enough distances to reach the engine, however the HOLOEYE LC-R 2500 SLM was not suitable to do this, as explained in Section 5.1.2.

The next section (5.2) describes a follow-up to this experiment using a higher quality laser and SLM that aimed to achieve multi-location ignition.

5.2 Multi-location engine ignition and associated experimental challenges

The aim of the next experiment was to use multi-location technique for ignition. This section presents the results. New equipment was used to overcome the limitations of the previous SLM.

5.2.1 Experimental Setup and Methodology

Figure 5.7 shows the optical system that was designed to generate the multi-beam pattern and deliver it to the engine. The "engine line" is the path it takes to the optical plug at the top of the cylinder The "dummy line" is an alternative path, which can be used by moving a mirror into place, which is optically identical but focuses the beam in air, testing that the system works, and for observation and analysis of the spark. There is no way to see inside the engine cylinder, which makes the dummy line necessary.

The laser used was a Litron LPY 764-30 Nd:YAG with a 2^{nd} harmonic generator. The output energy was up to 500 mJ, and the pulse length was 10 ns. The SLM used was a Hamamatsu X10468 LCoS device. It had a 800×600 pixel display and a 532 nm dielectric coating (reflectivity at 532 nm of $> 99\%$). As before, CGHs were generated using a computer, then displayed on the SLM. A Thorlabs PDA10A Si photodiode was used to detect the presence or absence of sparking, both in the engine and in

air. A glass neutral density (ND) filter was attached to this sensor to protect it from damage. Various lenses are mirrors were used, coated for 532 nm. The optical path was designed and simulated using the ZEMAX software package. This was used both to find the required optics, and to find the expected properties of the focused beam.

A $4f$ optical system consists of 2 focussing lenses and a distance of 4 focal lengths, with the lenses positioned after the first and third focal lengths. A collimated beam input to the system will be focussed at the mid-point by the first lens, then re-collimated by the second. When the multi-beam pattern created by the SLM passes through the $4f$ system, each lens performs a Fourier transform on the pattern, so the system as a whole recreates the initial pattern in another location. The final pattern is inverted, however since the ones created by the SLM in this work are symmetrical, there is no change. A $4f$ system is needed in the experiments described here because the laser must travel a significant distance between the SLM surface and the final focussing lens in the optical plug, over which the multi-beam pattern would be lost without any optics.

Following the beam from the SLM (as shown in Figure 5.7), it passes through a series of optics. First, a magnification $M = 2$ Keplerian telescope (lenses 1 and 2), which reduced the beam diameter to 4 mm, in order to later pass through the optical plug's 6 mm aperture cleanly. Next the beam passes through two $4f$ optical systems (lenses 3 and 4, then either lenses 5 and 6 in the dummy line, or lenses 5' and 6' in the engine line). The image plane (A) is the point immediately after the SLM where the beam is in its diffracted state, and would optimally be focused at. The $4f$ system reconstructs the image plane further away from the SLM. The reconstructed image plane is labelled A' at the end of the dummy line, and A" at the end of the engine line. As shown in the diagram, the conditions of the engine (J to A") and dummy (J to A') lines are identical, both in terms of optics and the distances between them.

Finally the multi-beam pattern passes through the optical plug, containing the standard lens used (2 mm thick, 10 mm diameter sapphire plano-convex lens with $f = 16$ mm). The optical plug used was the short version described in Chapter 3, this slightly modified designed was created to make alignment of multi-beam patterns into

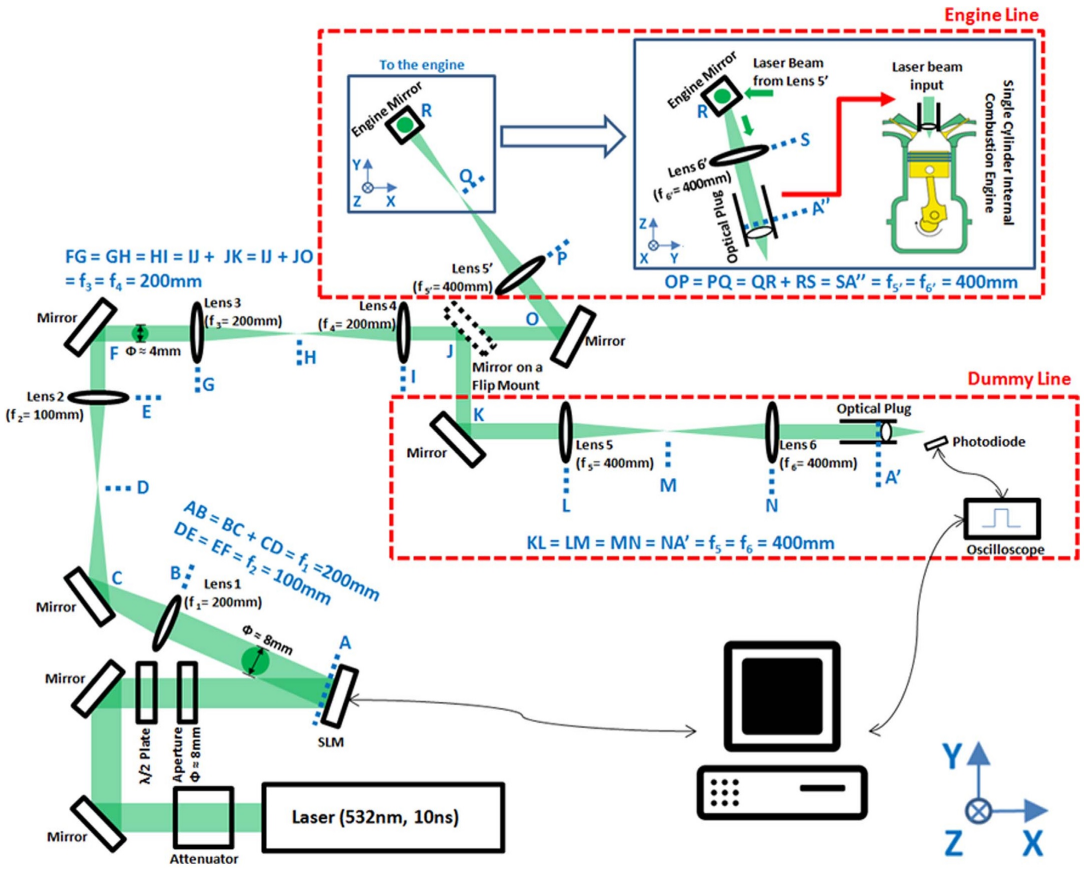

Figure 5.7: Schematic of the experimental setup used to generate lateral multi-location sparks both offline and for engine ignition (Kuang et al., 2017).

the plug lens simpler.

Figure 5.8 on the facing page shows the engine control and data acquisition system. The engine used was a single cylinder Boss prototype provided by Ford Motor Company (FMC), with a 776 cc swept volume and compression ratio of 9.2, and 100 bar pressure. It is a gasoline direct injection engine (GDI), however this was not used for the tests described here. The ignition was timed so that the air fuel mixture was homogeneous. The pressure sensor used in the cylinder was a AVL M5, used with a Kistler 5011 charge amplifier. The dynamometer was used to measure the engine output power.

The engine was controlled by a dSPACE prototyping system. As shown in the diagram, this controlled the electric motor, dynamometer, fuel system and triggered the laser. It also received all of the recorded data. The dSPACE computer was in turn controlled

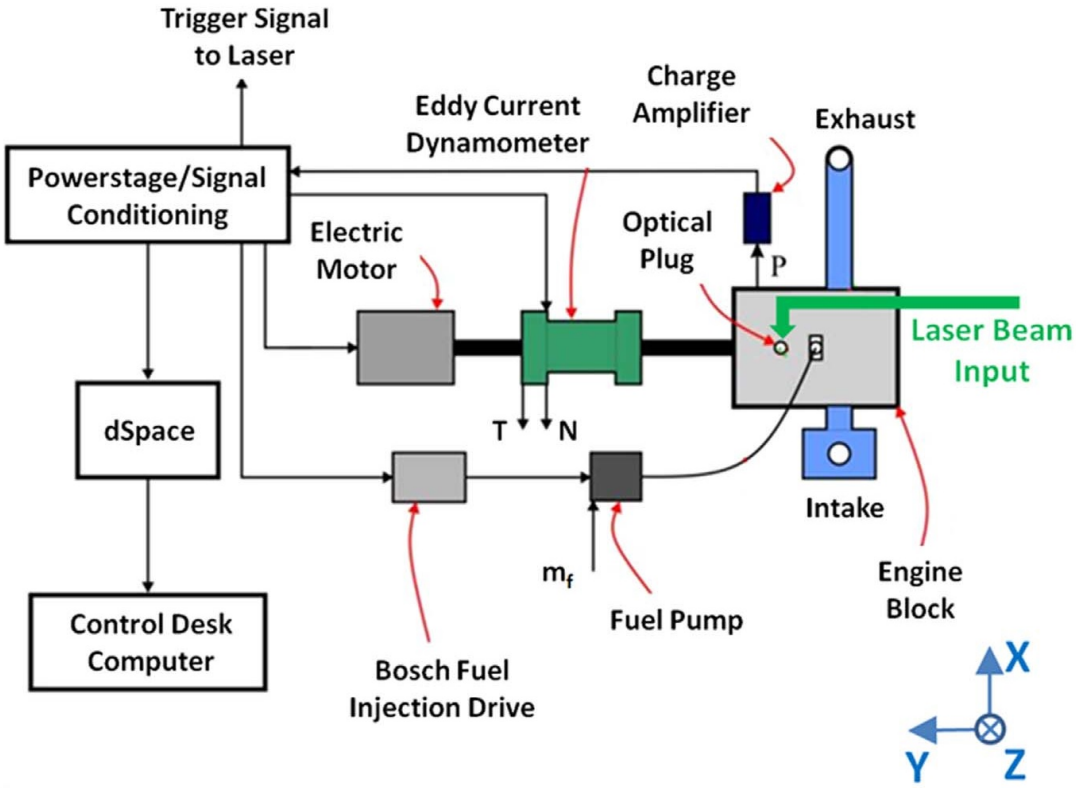

Figure 5.8: Schematic of the engine control and data acquisition system.

by a desktop. During LI operation of the engine, the laser was set to external trigger mode. The timing signal that would be sent to a spark plug was simply sent to the laser instead. The spark advance was fixed at 20° before top dead centre (BTDC) in theses tests. This follows the earlier engine tests as described in Section 4.3. At this stage in the compression stroke the cylinder height was $\approx 15\,\text{mm}$. More details on the engine were included in Section 3.6.

5.2.2 Design and Simulation

As discussed earlier, the SLM is not robust enough to be attached to the engine. Due to this and space constraints in the laboratory, the laser would have to travel $\sim 1.5\,\text{m}$ in free space to reach the optical plug inside the engine. If the multi-beam pattern was left to propagate over such a distance, it would separate and be much larger than the optical plug's 6 mm aperture. Therefore the $4f$ system was required.

E (mJ)	R (Hz)						
	1	5	10	15	20	25	30
78							
80							
82							
84							
86							

Table 5.1: Result of the optical damage tests on LCoS SLM samples. Green indicates no visible damage, red indicates damage.

In order to design this, the ZEMAX software package was used. One function of this software allows a series of commercially available optics to be input, then a simulated multi-beam can be passed through them. The main constraints were to contain the beam at the optical plug lens to within a 6 mm diameter, and for the foci to be sufficiently small and separate The limitation of the software is that it doesn't take into account divergence or beam mode, both of which are poor in the case of the Litron LPY 764-30 laser used. Enough leeway was included in the design to allow for the divergence of the real laser.

Figure 5.9 on the next page shows the simulation developed of the dummy line (5.9a) and the engine line (5.9b). The multi-focus shown has three distinct focal spots. The experimental setup was procured and built following the simulation closely. Figure 5.12 on page 82 is a photograph of the optical table setup as shown in the dummy line simulation. The laser has been made visible by spraying smoke in its vicinity. The multi-beam pattern is clearly visible in the centre of the $4f$ system.

5.2.3 Damage Threshold Tests

The next step was to determine the damage threshold of the SLM. Typically nanosecond lasers are not used with SLMs, so the damage threshold was unknown. Optical damage tests were carried on LCoS samples provided by the manufacturer Hamamatsu Photonics to determine this threshold. All LCoS samples tested were identical to the equivalent part in the SLM used, including coating.

The specific concern was the possibility of damage to the SLM during engine tests

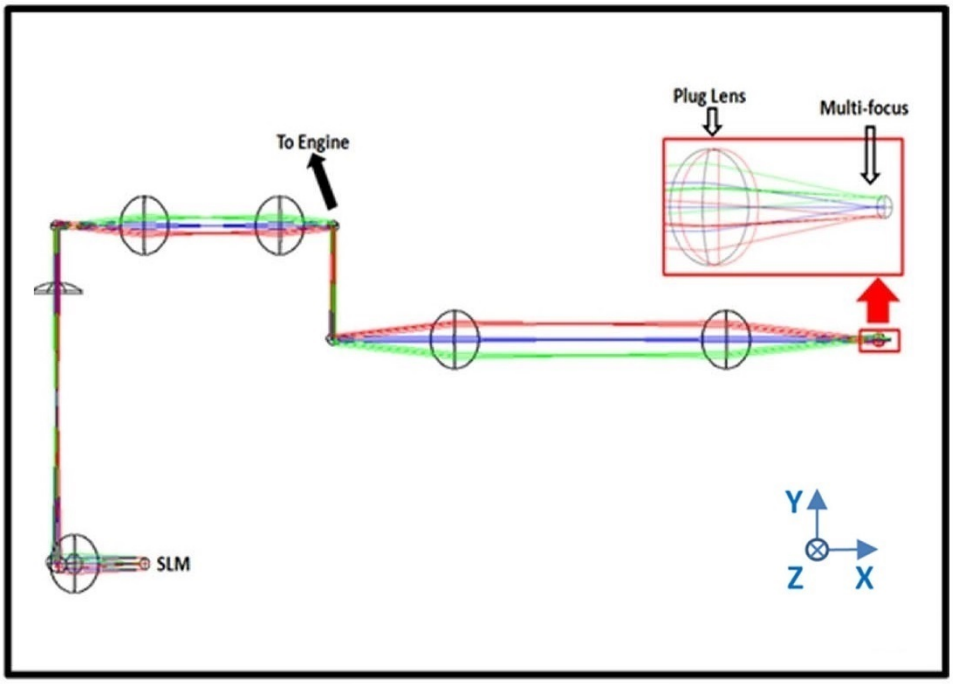

(a) Dummy line simulation.

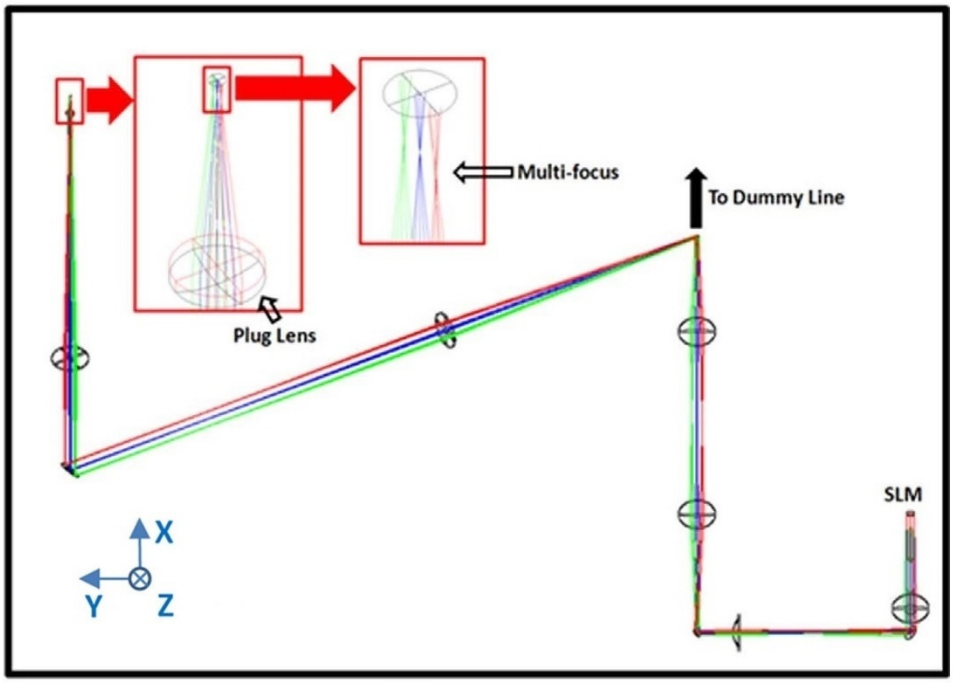

(b) Engine line simulation.

Figure 5.9: ZEMAX simulation of the optical arrangement used for multi-location LI.

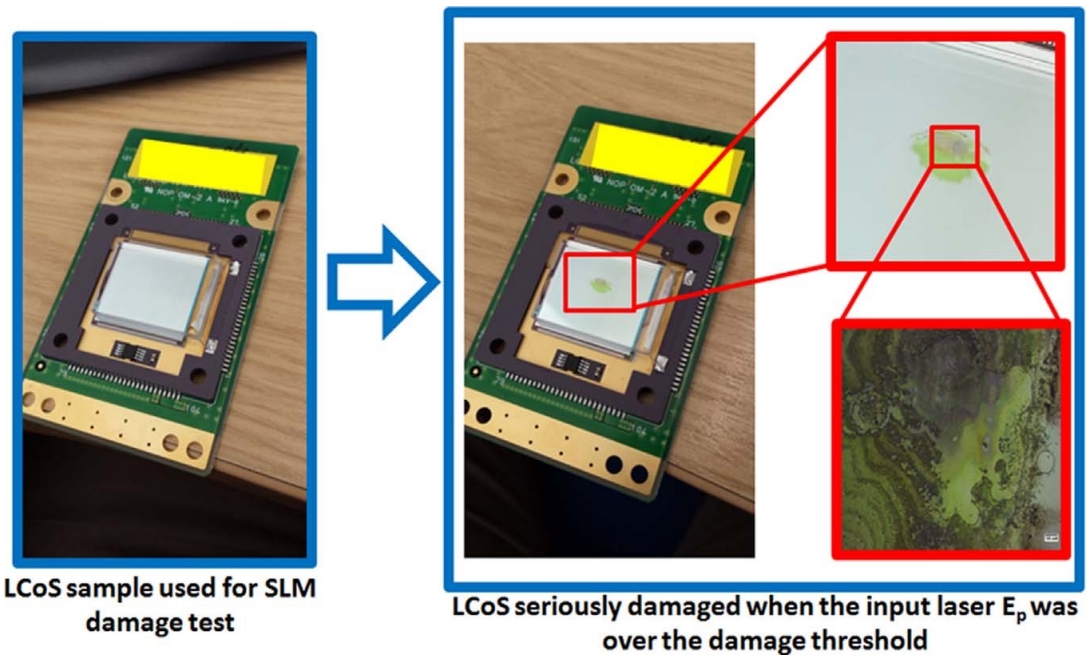

Figure 5.10: Optical damage on the surface of a SLM sample.

like those described in this thesis, so optics were arranged as if one were being done. The SLM was replaced with one of the samples. The input beam diameter was 8 mm, because of the aperture Pulse energy E_p was varied using the attenuator, and measured immediately before the sample. Beginning with low E_p, a constant beam was maintained on the surface for 10 minutes. If the sample remained undamaged, E_p was increased and kept constant for another 10 minutes. In this way the test tried to account for damage due to peak and average laser power. This was then repeated for each repetition rate (R). Thermal lensing within the Nd:YAG rod had a significant effect on the beam mode in the Litron laser, and it was optimised by the manufacturer to be best at around 15 Hz. With varying engine speed the laser could be running across the whole range, so the SLM had to be safe at all R.

The results are given in Table 5.1 on page 76, where green indicates a pass without damage, and red indicates damage at some point during the 10 minute period. The test was stopped after damage first occurred at each frequency, red squares below that are assumed to cause damage (e.g. 1 Hz and 86 mJ). As shown, the damage threshold for the LCoS sample was between 80 mJ and 86 mJ. The highest threshold

corresponded with the best beam mode at around 15 Hz. The lowest occurred at $R = 30\,\text{Hz}$, but was only 4 mJ lower than at $R = 1\,\text{Hz}$, despite the average power being 30 times higher. This suggests that the damage mechanism is related to peak power. Using the convention of expressing this in energy density, 78 mJ to 80 mJ is $0.039\,\text{J}\,\text{cm}^{-2}$ to $0.043\,\text{J}\,\text{cm}^{-2}$, with slight variation across R. This contrasts with the coated mirrors and uncoated sapphire lenses used elsewhere in the setup, with damage thresholds above $0.5\,\text{J}\,\text{cm}^{-2}$ (see Section 3.2).

Figure 5.10 shows a photograph and microscope image of one of the damaged samples. The time before damage occurred in the failed test was not precisely measured, but was around ~ 10 seconds. Analysis using the microscope showed the damage occurred on the pixels themselves. On some of the samples, the glass cover above the pixels was cracked, possibly due to a heating effect after the initial damage.

These tests were not exhaustive, however there were only a limited number of LCoS samples available. E_p was kept at 60 mJ or below in all subsequent tests with the SLM, and there were no instances of damage. This energy limit would ultimately restrict the number of simultaneous sparks that could be created.

5.2.4 Variable focal length single-location spark

As an aside to the work towards engine ignition, Fresnel lens phase CGHs (as discussed in Section 5.1.3 on page 67) were used to generate variable focal length single-location air breakdown. Figure 5.11 on page 81 shows photographs of how a CGH consisting of a single Fresnel lens phase can shift a single-location spark. A CGH with only one lens phase has a reasonably high efficiency, and hence there is not enough energy left at the 0^{th} order to cause air breakdown. With the correct CGH, any focal point could be chosen along this range, although the minimum pulse energy would increase as the effective focal length increased. The pulse energy used here was $E_p \approx 50\,\text{mJ}$. The optical arrangement used was similar to that shown in Figure 5.1 on page 63, except for using the newer laser and SLM combination described in this section. The size of the shift here is $d \sim \pm 5\,\text{mm}$, which is dependent on the focal length of the plug lens.

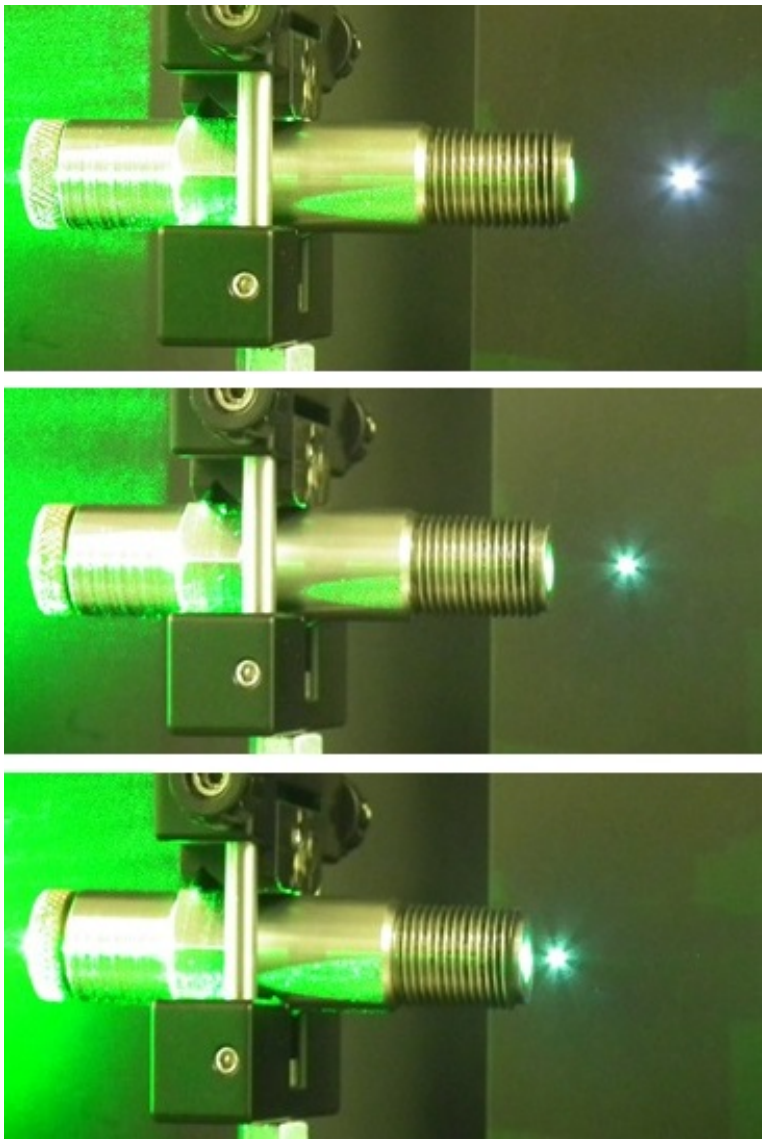

Figure 5.11: Varying the position of a single spark using Fresnel lens phase CGHs. Top and middle are two different CGHs, bottom is without any CGH displayed.

As with the previous Fresnel lens phases shifts, they could not be applied to the engine without a suitably robust SLM, since the Fresnel CGH requires the near field of the SLM, or a physical Fresnel lens

5.2.5 Offline tests with multi-location sparks delivered via a $4f$ optical system

Once the SLM damage threshold was established, and the $4f$ optical system was designed and setup as in Figure 5.7, a suitable CGH had to be generated.

1×2 and 1×3 beam arrays can be made using binary linear grating CGHs, while larger arrays (i.e. 1×4 and higher) using Dammann grating CGHs. This is described by the grating equation:

$$d(\sin\theta_i + \sin\theta_m) = m\lambda \tag{5.10}$$

where d is the grating period, θ_i is the angle at which the laser is incident on the SLM, m is the order of the diffraction, and θ_m is the angle at which that order is diffracted.

This rearranges to:

$$\theta_m = \arcsin\left(\frac{m\lambda}{d} - \sin\theta_i\right) \tag{5.11}$$

When such a multi-beam array is focused down, the separation between the foci is dependent on θ_m, which is in turn dependent on d. We can therefore control the separation by changing the CGH.

Photographs in Figures 5.12, 5.13, and 5.14 show a 3 beam array successfully delivered to the optical plug on both the dummy and engine line. Here E_p was kept low enough to prevent sparking in order to align and photograph the system.

The first experiment carried out on this setup was to determine the minimum breakdown energy per spark, which would set a limit on how many beams could be used

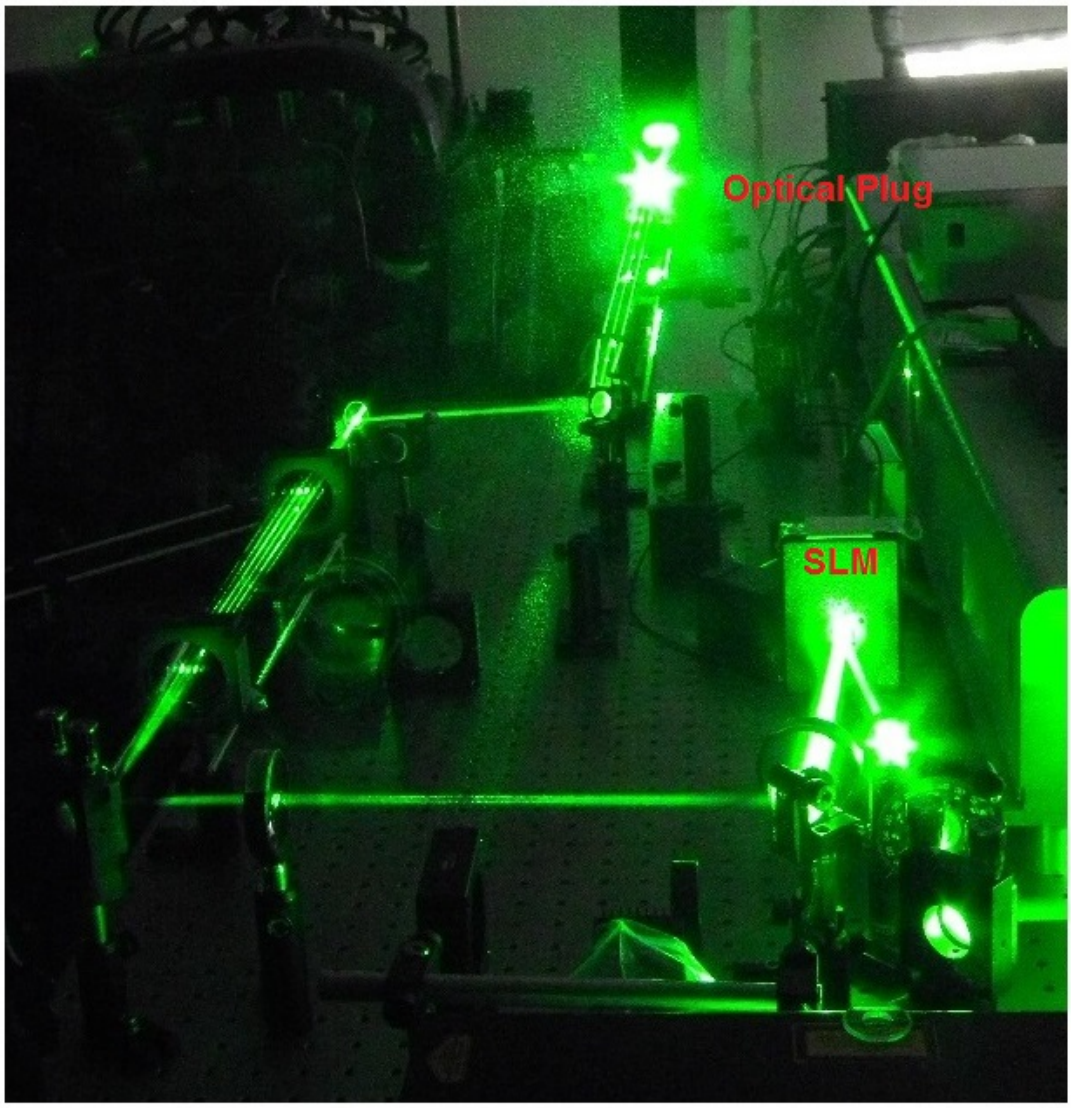

Figure 5.12: Complete laser beam path from SLM to optical plug for the dummy line.

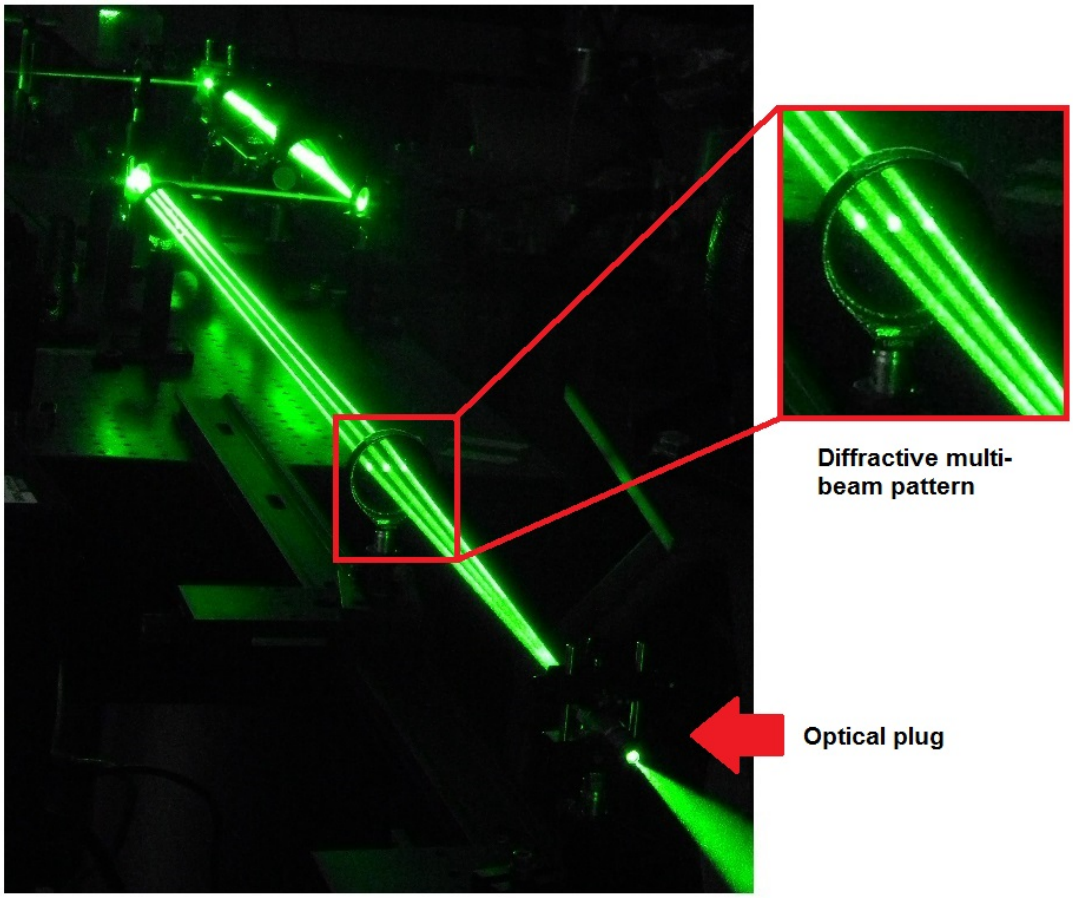

Figure 5.13: Multi-beam delivery to the optical plug on the dummy line.

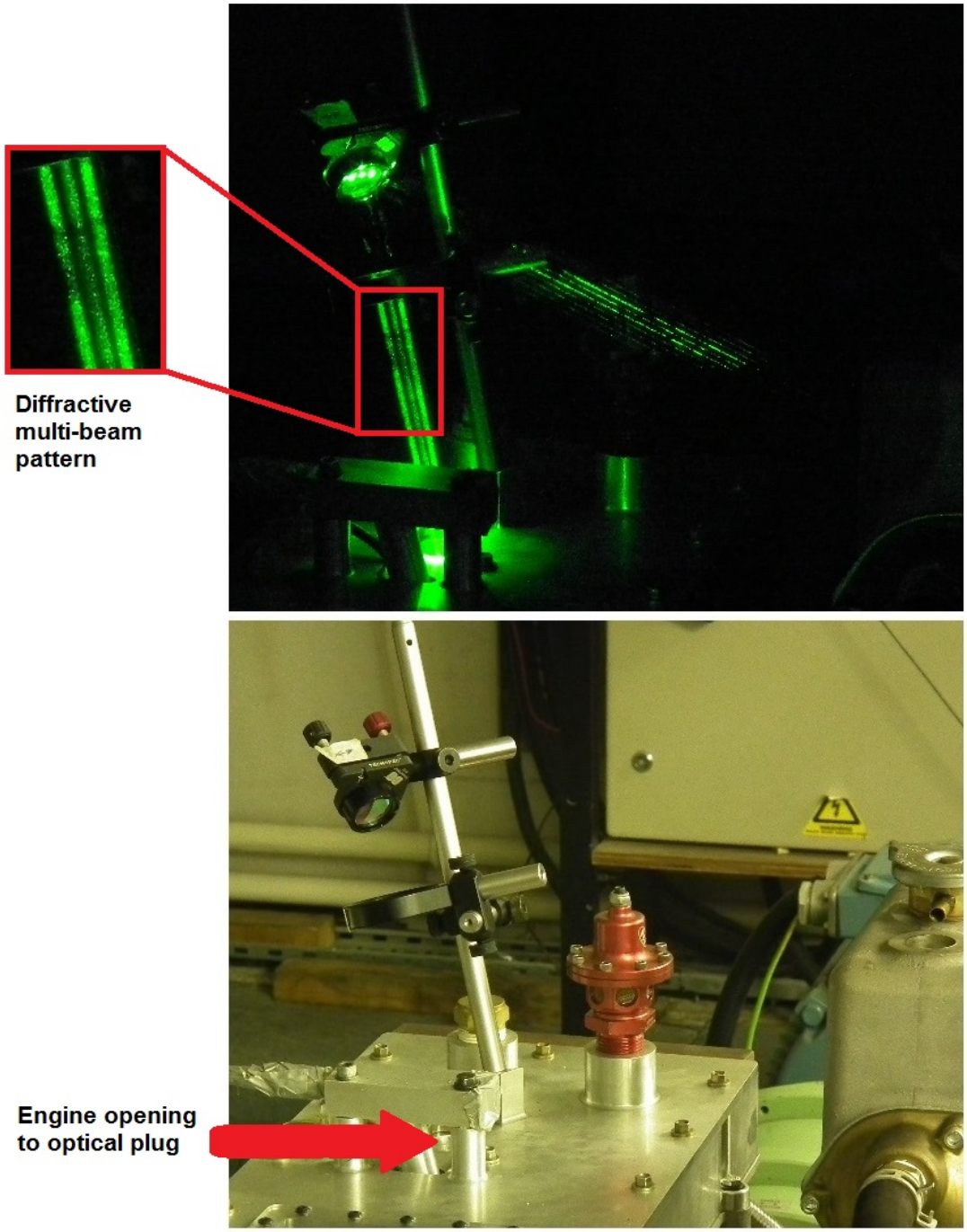

Figure 5.14: Multi-beam delivery to the optical plug on the engine line.

simultaneously for LI of the engine. The stability of laser air breakdown was measured at various combinations of E_p and different CGHs, using a photodiode connected to an oscilloscope

The photodiode was placed near the focus of the optical plug lens, perpendicular to the beam so that it would measure the light emitted by the spark, and not the laser beam itself. The captured signals recorded whether air breakdown occurred or not with each laser pulse. In the case of multi-location spark, it would detect any individual spark, and not clearly differentiate between all locations sparking or just one. Consistent sparking at all locations had to be verified visually.

From this data an air breakdown probability was calculated. Through this test, E_p was gradually increased until the minimum 100% breakdown energy was found. As discussed previously, 100% breakdown probability is the useful measure for engine LI.

A similar diagnostic was later used in the engine, to measure instances of misfiring.

In the case of a single spark (i.e. no hologram displayed on the SLM), the graph in Figure 5.15 plots air breakdown probability against E_p, at various R. The probability was calculated by taking the ratio between the number of peaks representing sparks as measured by the photodiode, to the number of peaks in the laser trigger signal that was simultaneously measured. This trigger signal was output from the laser power supply for every laser pulse, independently of the optical system being used. At $E_p = 18\,\text{mJ}$ and $R = 10\,\text{Hz}$, infrequent sparking began, which became stable at $\approx 22\,\text{mJ}$.

When a binary grating CGH was applied, and the laser set to $E_p = 60\,\text{mJ}$ and $R = 10\,\text{Hz}$, multi-location air breakdown was successfully achieved on the dummy line. Figure 5.16 on page 87 shows this in detail. Row (a) is the binary grating CGH displayed (first column is the SLM left blank), row (b) shows the beam profile of the laser when left unfocused in the far-field, and row (c) is a photograph of the spark formed. The first column shows an intense single spark, since in this case the energy at the focus is far in excess of the threshold energy. Other columns show the laser split into two, three and five diffracted beams of near identical energy, due to the

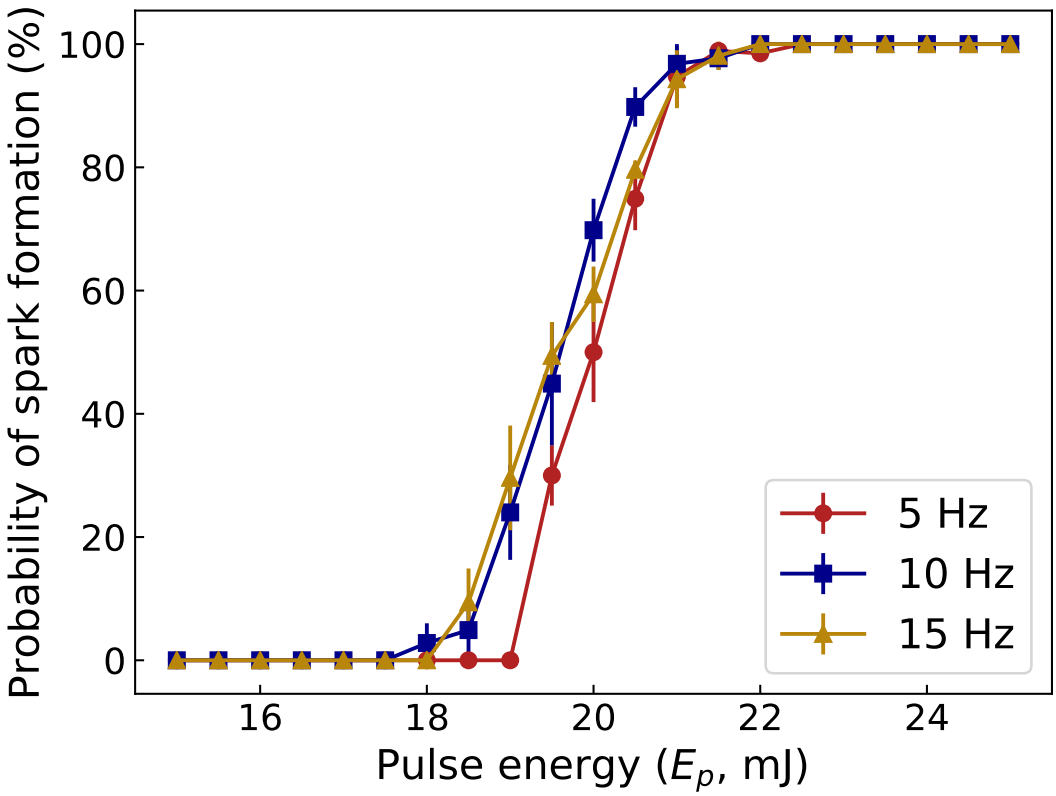

Figure 5.15: Plasma formation stability for single-location air breakdown, over a range of repetition rate and pulse energy.

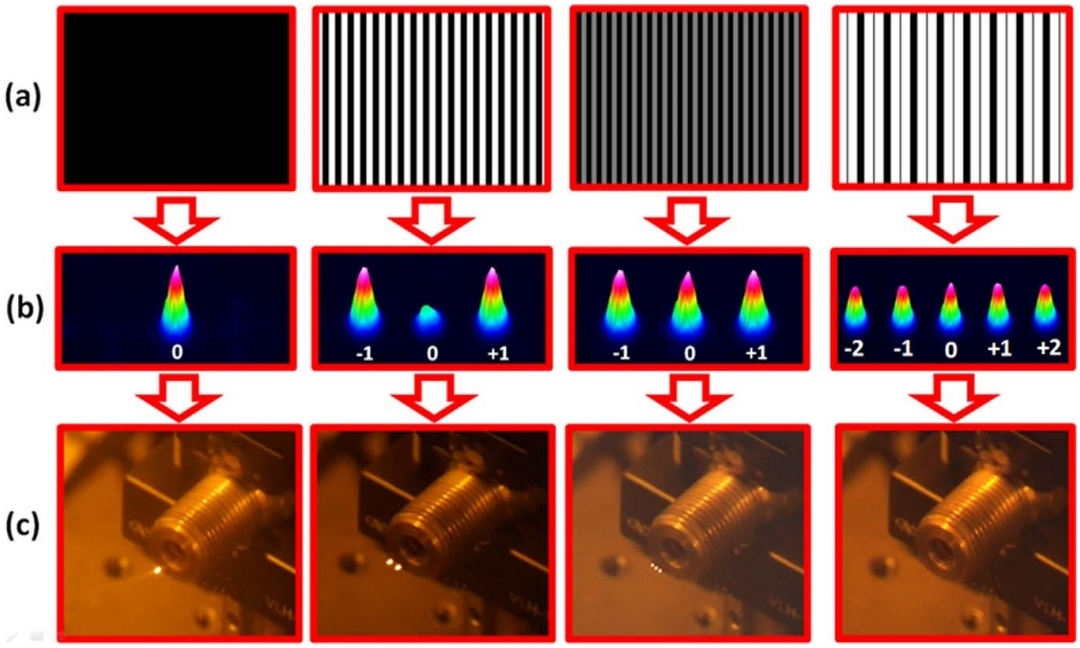

Figure 5.16: Multi-location air breakdown created by binary Dammann grating CGHs: (a) the CGH displayed on the SLM; (b) unfocused, far-field beam profile; (c) photograph of the air breakdown.

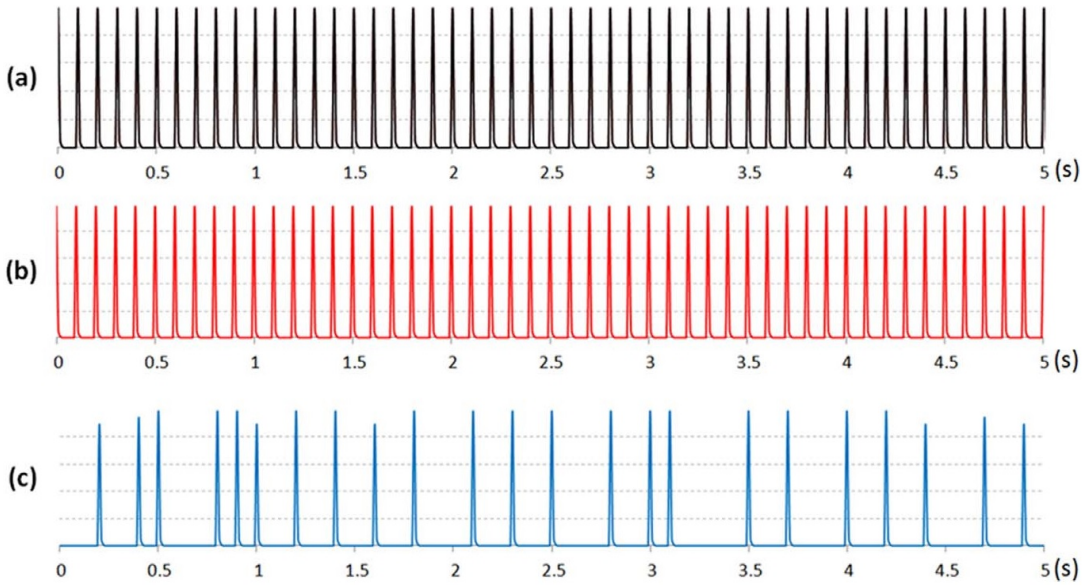

Figure 5.17: Sample photodiode trace showing the stability of (a) single-, (b) two-, and (c) three-location sparks.

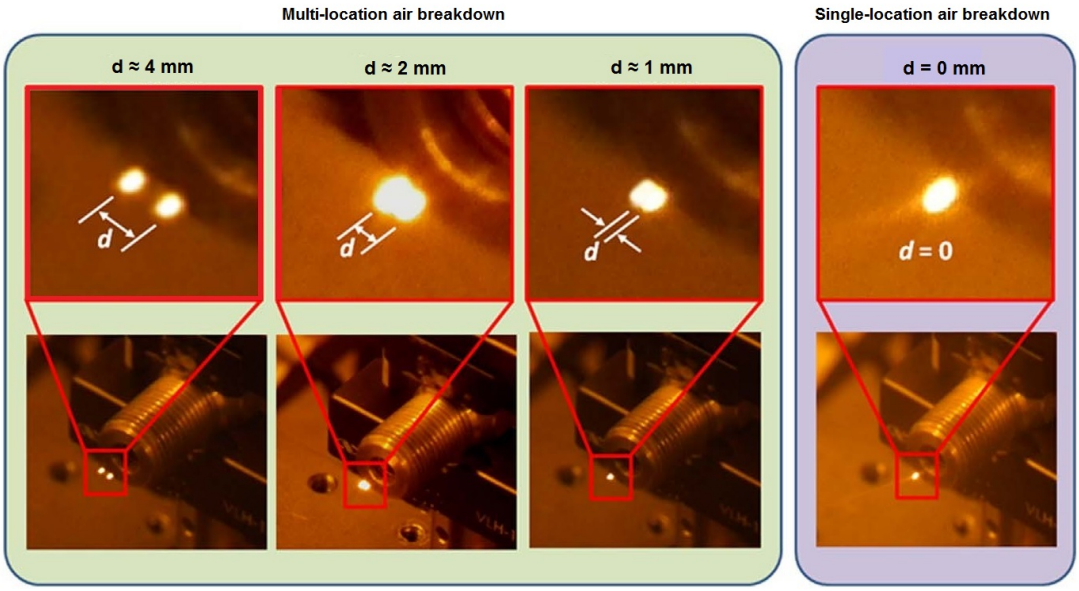

Figure 5.18: Two-location air breakdown with variable spark separation, compared with single-location.

different binary gratings being displayed. Air breakdown occurred in the two and three location cases, but not in the five, since the energy was insufficient at each foci.

However while one and two location air breakdown were stable, three was not. Figure 5.17 shows sample photodiode traces from the spark formed in each case. This shows that there was not plasma formation for every pulse. In the two-location case, the energy of each spark was measured at $E_p = 27\,\text{mJ}$, high enough for 100% air breakdown according to the single-location breakdown probability test. However in the three-location case, $E_p = 19.5\,\text{mJ}$, slightly under enough for 100% probability. This effectively limited the experiment to studying two-location LI. Pushing to enough energy energy for three might have damaged the SLM. The spacing between the two points was the next variable tested.

This lateral spacing could be varied arbitrarily by using different CGHs, limited by the specifications of the SLM. Figure 5.18 shows photographs of two-location air breakdown with spacing d of 1 mm, 2 mm, and 4 mm. These were obtained by varying the grating period as discussed with equations 5.10 and 5.11 earlier in this section.

Single-location is shown for comparison. Diffraction efficiency is similar for each CGH

(within $< 2\%$), so the energy at each of the two-location foci is approximately the same. The total energy is 60 mJ in all of these cases, and energy at each two-location focus was 27 mJ, enough for 100% breakdown probability.

In the $d = 1$ mm and $d = 2$ mm, the plasmas may have started individually but merge into a single plasma. Typical plasma diameter is ~ 1 mm anyway so this is to be expected. Therefore a spacing of $d = 4$ mm was chosen to the engine LI experiments. Otherwise the tests would effectively be of single-location LI. Larger d values can be achieved via the same method, however this would have made the multi-beam pattern too large to fit into the optical plug without clipping the edges.

5.2.6 Engine tests with multi-location sparks delivered via a $4f$ optical system

Once two-location with $d = 4$ mm was established to work, it was tested inside the engine. The objective was to see if multi-location was able to ignite the engine, and how it compared with single-point ignition. In the literature review (see Section 2.2), commonly used parameters for describing performance such as COV_{IMEP} and $IMEP$ were explained. The raw engine data was analysed according to those methods.

The engine was ran at a constant speed of 1000 rpm, which corresponds to a ignition frequency of 8.33 Hz. The variables tested were λ and number of ignition locations, everything else was as kept constant as possible. Parameters such as engine speed vary slightly no matter what, since combustion is a stochastic process. Large data sets should eliminate the effect of this on the results. When comparing single- and two-location LI, the total laser energy input into the cylinder is kept the same, with each of the two-location foci having half the energy of the single-location focus.

A sample cylinder pressure trace is shown in Figure 5.19 on page 91 as an example. This compares single- and two-location LI at air-fuel ratio $\lambda \approx 1.2$. Leaner air-fuel mixtures were used in this experiment since being able to operate in this area is one of the advantages of LI over spark plugs in general.

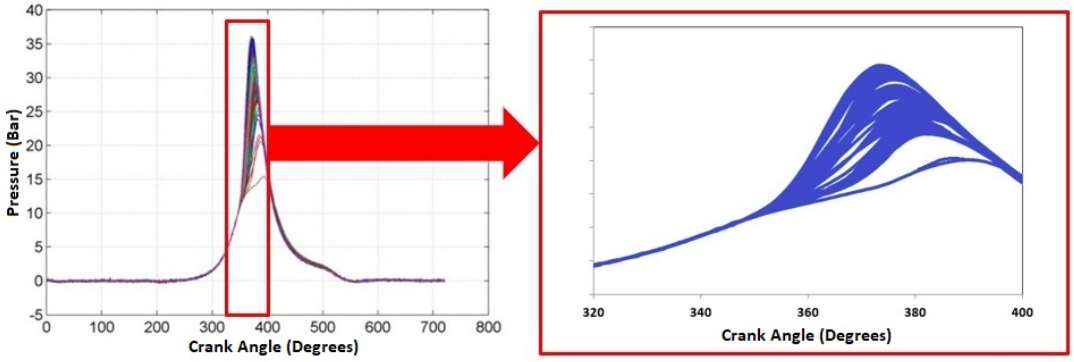

(a) Single-location LI engine pressure.

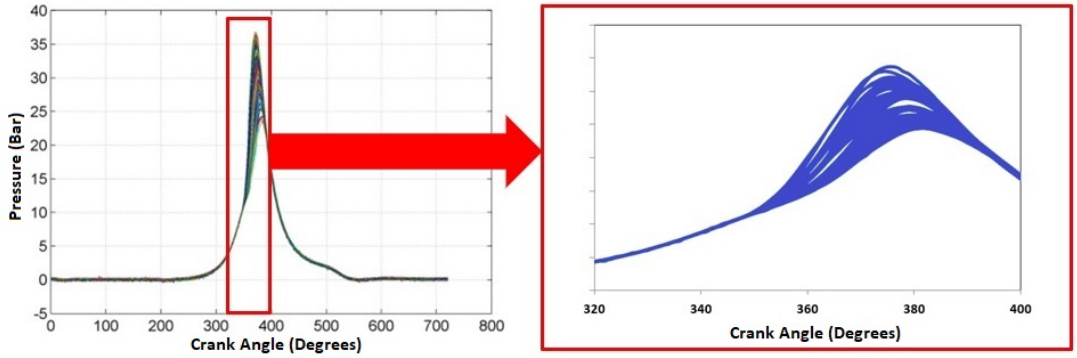

(b) Two-location LI engine pressure.

Figure 5.19: Pressure traces (engine cylinder pressure against crank angle) for single- and two-location laser ignition at air-fuel ratio $\lambda = 1.2$, showing ~ 500 engine cycles.

Pressure data is recorded in real time at every crank angle by the dSPACE system, so each curve is based off ~ 720 data points. At each combination of λ and ignition location, the engine is ran for ~ 5 minutes in order for it to reach a steady state, then ~ 500 engine cycles of data are recorded. Figure 5.19 is one such data set.

Comparing the single- and two-location traces, misfires (no combustion) and more poor combustion events can be seen for single-location, which can be seen as shorter peaks. The variability in the combustion is mainly because the air-fuel mixture is lean. As for why the two-location has fewer poor combustion cycles, it might be due to the fuel distribution not being homogeneous If some locations in the cylinder are more stratified, and they happen to be near to the spark, then combustion will be better that cycle. This is a stochastic process, so the more spark locations, the more chance of good combustion.

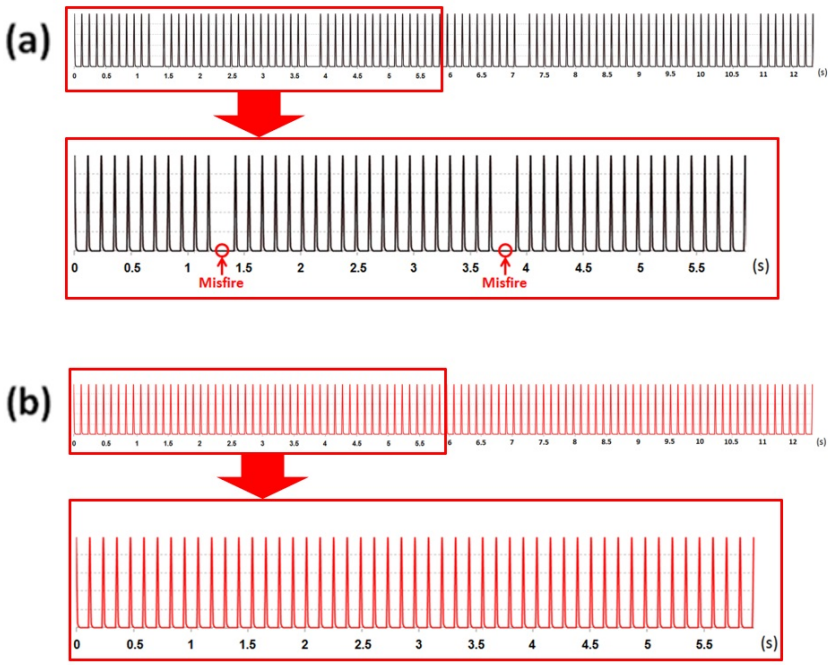

Figure 5.20: Sample photodiode trace showing ignition and misfire events from single-location (a) and two-location (b) laser ignition at air-fuel ratio $\lambda = 1.2$.

Figure 5.20 shows sample photodiode data measured during engine operation, at the same parameters as before, $\lambda = 1.2$. The photodiode is placed behind the engine mirror (labelled R in 5.7), and is able to detect the occurrence of sparks. In (a), the single-location LI shows clearly a number of misfires, while in (b), the two-location LI shows none. Figure 5.21 shows a complete set of this photodiode data across the parameters tested. The percentage of attempted combustions that were misfires is shown against air-fuel ratio for single- and two-location.

First of all, there is a general trend of an increasing number of misfires as the air-fuel ratio becomes leaner, as expected. At near stoichiometric air-fuel ratios there are no misfires for either case, but two-location has a clear advantage as it becomes more lean. $\lambda = 1.2$ is of note since two-location maintains 0% misfires. In a commercial engine only 0% misfires and stable running would be acceptable. In previous tests on this particular engine (Cheng et al., 2016), it could not be ran at all at $\lambda = 1.2$ using a spark plug, so even poor quality running at very lean conditions is an achievement for LI.

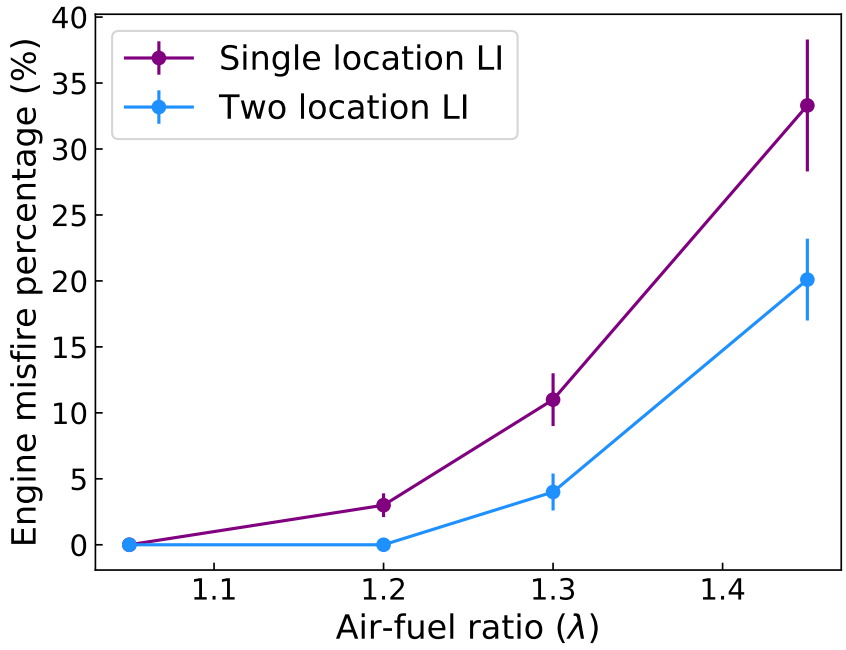

Figure 5.21: Percentage chance of misfire against λ for single- and two-location LI, from photodiode data such as in figure 5.20.

Returning to the data from the engine itself, Figures 5.22 and 5.23 show engine output power and COV_{IMEP} for varying λ with single- and two-location LI. As mentioned earlier, each point is an average over a large number of engine cycles. In terms of power, the two-location LI gives an increase of 300 to 400 W. Some of this increase will be due to fewer misfires, however in terms of percentages, the increase in power is larger than the increase in the number of successful combustion cycles, suggesting there is also an improvement to the successful combustions. At $\lambda = 1.05$ there is no difference however. Looking at COV_{IMEP} , again there is improvement for two-location at higher λ. As a measure of stability, COV_{IMEP} is strongly affected by misfires, the trend in data closely matches that in the misfire data (Figure 5.21).

Higher output power suggests that more of the fuel was burnt and/or the fuel was burnt at a more optimised rate. The fact that there is no change near stoichiometric, and improvement in lean conditions, supports the earlier explanation that two-location increases the probability that the spark hits a more fuel rich region of the cylinder. But of course there is no way to know in a closed cylinder where the combustion

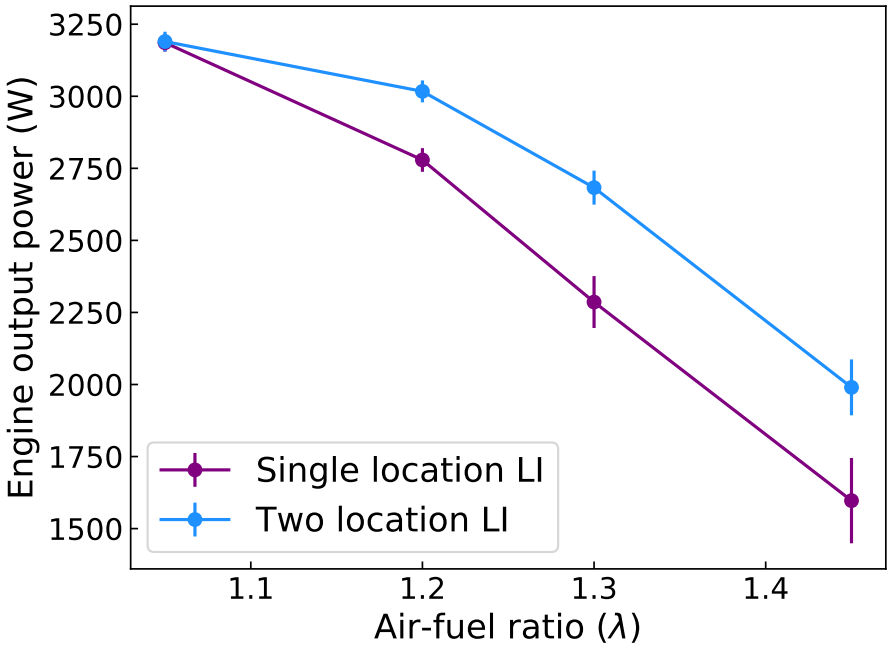

Figure 5.22: Engine output power against λ for single- and two-location LI.

starts, or how the fuel was distributed, we can only see the end result in terms of engine output.

Multi-location LI shows promise but further tests need to carried out across a range of engine parameters. Two-location may not always be optimal. SLM refresh rates are typically 60 Hz, which is fast enough to display a different CGH at every engine cycle, so the position and number of sparks could be changed to whatever is optimal for the current engine conditions. Running at lean air-fuel ratios is useful since this can translate to better fuel efficiency, however it was not possible to directly measure fuel use with the engine system used for these experiments.

5.3 Chapter summary

In this chapter experimental results were presented of work towards multi-location LI. A technique to create multiple sparks simultaneously at different locations inside the cylinder was demonstrated for the first time. By displaying certain CGHs on the SLM, the incoming beam can be modulated to create a diffractive multi-beam pattern,

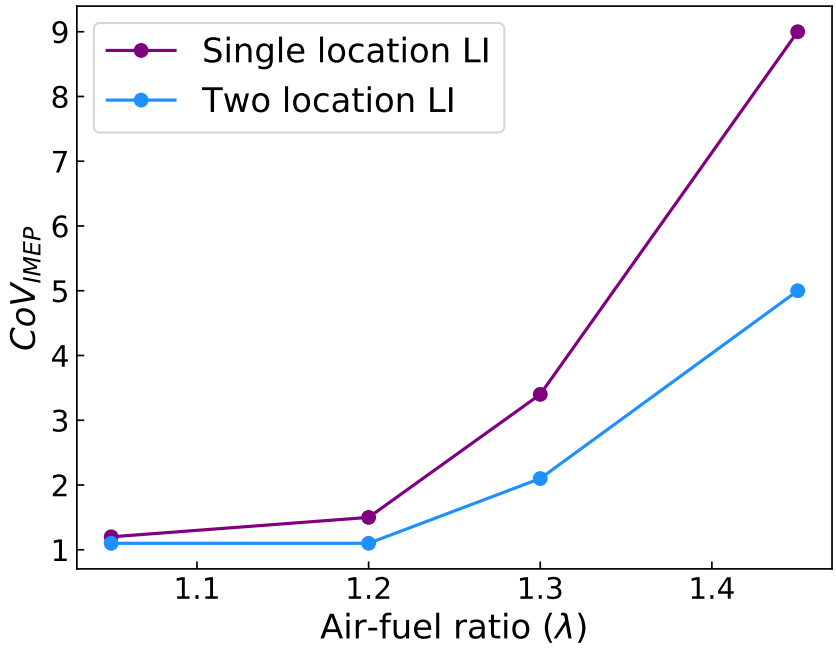

Figure 5.23: COV_{IMEP} against λ for single- and two-location LI.

which when focused creates a certain arrangement of laser air breakdown plasmas. In principle any arrangement of points could be used. Two types of CGHs were initially investigated: Fresnel lens phases, and prism phases. Each of these effectively simulated the effect of the laser beam passing through a lens or prism, but could be controlled dynamically. Complex superpositions of this phases were used to create multi-location air breakdown. Axially and laterally shifted multiple-beam patterns were created. In the axial shift, three-location air breakdown was achieved, which could be achievable inside the engine. However limitations of the equipment prevented these being used for LI.

New equipment was then acquired to attempt LI with this technique. An experiment was carried out to find the optical damage threshold of the SLM in the context of engine tests in this work, and a safe working pulse energy was found. Diffractive multi-beam arrays were created by applying CGHs to and SLM. Linear gratings were used to create lateral arrays with variable number of beams, and separation between them. A $4f$ optical system was designed and built to allow these multi-beams to reach the engine and be focused down. Using a dummy line equivalent to the line into the

engine, the multi-location air breakdown created by this was studied. The maximum number of sparks that could be maintained with 100% probability of breakdown was two, due to the limitations of the SLM. This was then used to ignite the single cylinder test engine. The major finding from the engine test was that two-location LI reduced the probability of misfires, improved engine output power, and reduced COV_{IMEP} at lean air-fuel ratios.

Chapter 6

Wavelength Dependence of Laser Ignition

Laser ignition is usually carried out using the fundamental Nd:YAG wavelength or its harmonics. Previous work in this area was discussed in Section 2.4.3 on page 26. There have been some comparisons between readily available wavelengths, and also suggestions that tuning to a specific wavelength may have dramatic benefits, such as creating air breakdown via resonant multiphoton ionisation.

This chapter covers two pieces of work. First, a comparison of two wavelengths, 1064 nm and 532 nm, in experiments conducted in air, inside a pressure chamber, and in an IC engine. The characteristics of the two lasers were analysed, and experimental results were compared, mainly in terms of the air breakdown threshold pulse energy. The second area of work was an attempt at using an OPO for continuous wavelength tuning, which unfortunately was unsuccessful. The reasons why it didn't work, and how such an experiment could be carried out successfully, will be discussed.

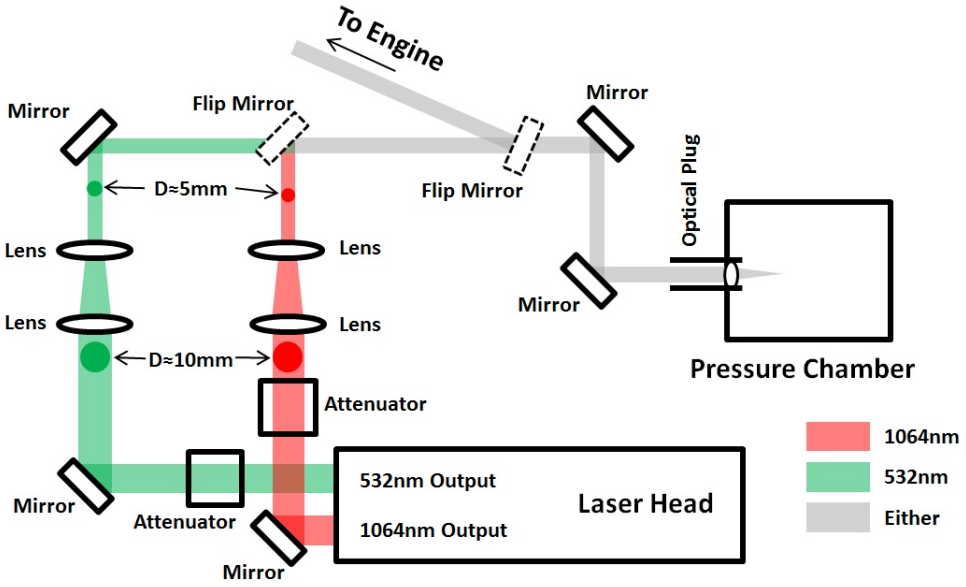

Figure 6.1: Schematic of the experimental setup used during the two wavelength comparison tests.

6.1 1064 nm and 532 nm LI Comparison

This section describes experiments comparing the fundamental output at 1064 nm and the second harmonic at 532 nm of the Litron LPY 764-30. Each output was similar except for the wavelength, and further analysis was used to isolate the difference between the wavelengths specifically.

6.1.1 Experimental Setup

The Litron LPY 764-30 was used again, this time in both 1064 nm and 532 nm modes. See Chapter 3 for further details on this and other equipment used.

Figure 6.1 shows the two wavelength setup.

The laser head can output either wavelength, though not simultaneously. The change between the two was made by making an adjustment inside the laser head.

As shown, both wavelengths passed through appropriately coated attenuator and beam telescope setups, which controlled the energy and reduced the beam size. Next,

they are directed onto the same beam path by mirrors which are added or removed depending on the desired wavelength. The mirrors and telescope lenses were coated to suit either wavelength, and other optics such as the optical plug focussing lens were uncoated for compatibility with both. Finally, the beam reaches the optical plug in either the engine or pressure chamber.

The beam path length from either wavelength output on the laser head to the pressure chamber or engine was $\sim 1.5 - 2\,\mathrm{m}$. Other tests, such as the spark efficiency analysis and imaging using the beam profiler camera, were carried out at roughly the same distance from the output.

The short optical plug was used with the standard $f = 16\,\mathrm{mm}$ sapphire plano-convex lens. Rubber rings were used to create an airtight seal in place of the usual copper washers, which form a seal once heated when used in the engine. The only difference between the two is that the pressure chamber setup has a shorter spark distance, which gives slightly higher transmission.

The energy meter used was the Gentec-EO QE25. It was calibrated individually for each wavelength; a simple multiplier factor associated with each was set in the software before each test.

A Thorlabs BC106-VIS beam profiler camera was used for capturing the profile, and for measuring the beam diameter for calculation of M^2. The incoming beam had to be sufficiently attenuated in order to not damage the camera. A 40 dB neutral density (ND) filter was attached directly to the camera, and a further OD4 ND filter was placed after the attenuator, which initially reduced the pulse energy to 8 mJ.

A Thorlabs DET025A/M photodiode with a 1 ns response time was used to measure the laser pulse length. An attached Tektronix TDS 3054C oscilloscope with a 500 MHz frequency produced the traces shown later. For pulse length measurement, the laser was attenuated to minimum energy and scattered by a white paper target. The photodiode was kept 30 cm away behind an OD2 ND filter, where it could safely measure the pulse.

The Ford single cylinder Boss test engine was again used for the engine tests. The setup and methodology were exactly the same as before, described in Section 3.6 on page 42. Parameters related to the engine were fixed, since these experiments only compared laser properties. Specifics will be described later in Subsection 6.1.5.

6.1.2 Laser Calibration

As discussed earlier, the characteristics of the beam from the Litron laser vary with repetition rate. Experiments described in this chapter used a fixed rate of 8 Hz. Laser characterisation described in this section was done at this fixed rate.

First, the laser pulse length was measured using a fast photodiode and oscilloscope. The pulse length was measured to be 12.6 ± 1.0 ns at 532 nm. This is the FWHM measurement. The pulse length at 1064 nm could not be measured, the manufacturer states that the pulse length is not changed significantly by the harmonic generation, so it was assumed to be the same for both wavelengths. An example photodiode trace from the pulse length measurement is shown in Figure 6.2 on the next page. There is a slight variability between pulses, as shown by the overlapping traces, which is accounted for by the uncertainty on the pulse length value.

The laser beam profile was captured using the Thorlabs BC106-VIS beam profiler camera. Figures 6.3 and 6.4 show the beam profiles at each wavelength. The green has a roughly Gaussian shape elongated along the x axis, while the infrared has a more complex structure with two peaks, and is elongated in the y axis. Equations used to calculate focus spot size assume a Gaussian shape, so they will be less precise with these beams. The $1/e^2$ definition of beam diameter was used, giving values of 3.36 ± 0.18 mm at 532 nm, and 5.05 ± 0.18 mm at 1064 nm. These are averaged between the shorter and longer axes.

The beam quality factor M^2 was also measured using the beam profiler camera. The camera was mounted on a translational stage, and a $f = 300$ mm lens was used to focus the beam near the centre point. In this way a measure of d_{min} was found, from which M^2 was calculated.

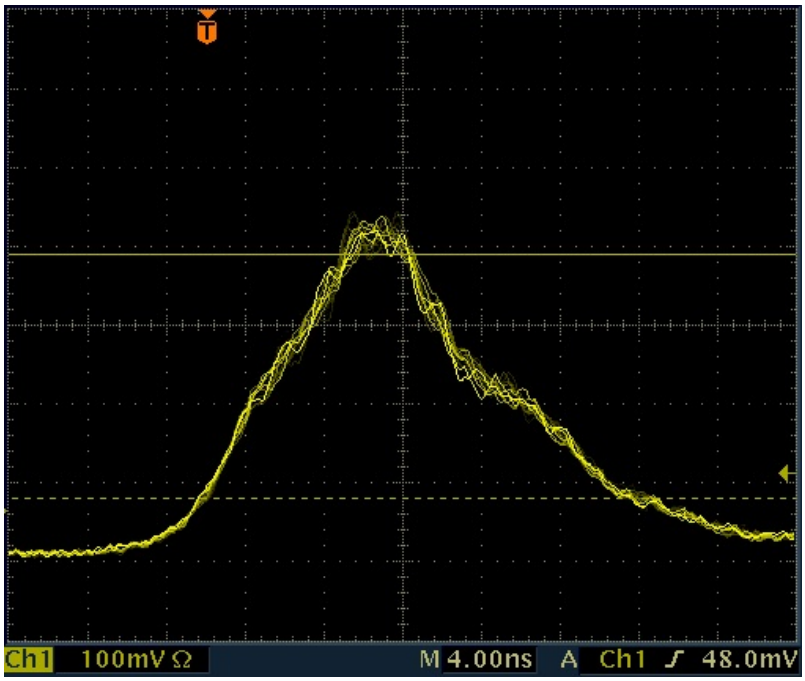

Figure 6.2: Laser pulse length photodiode trace, showing the intensity distribution of the pulse. The time division is 4 ns per square on the horizontal axis, and this trace has a width of 10 divisions or 40 ns.

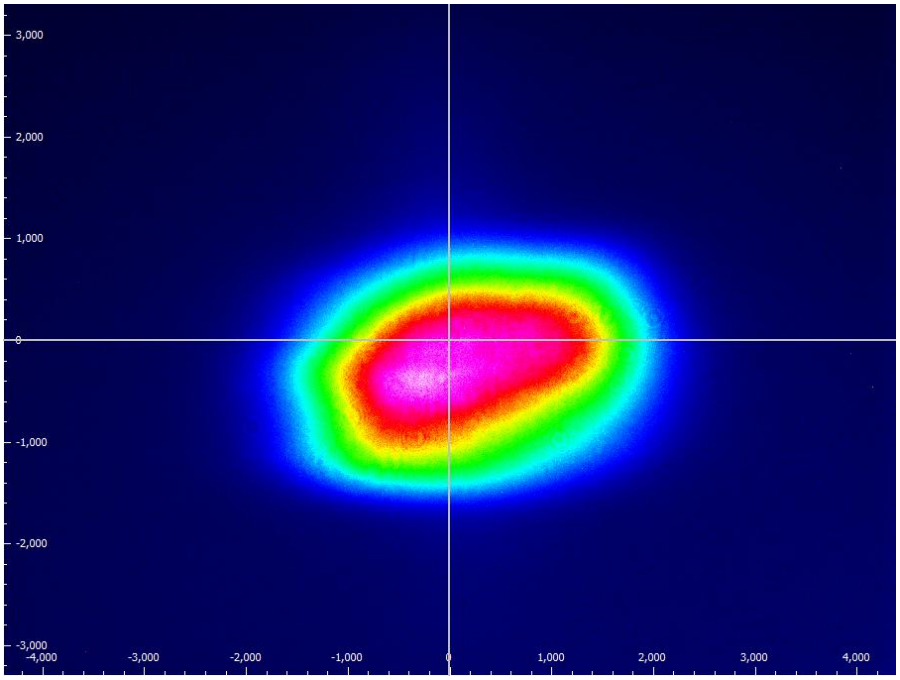

Figure 6.3: Laser beam profile at 532 nm and other fixed parameters described during the wavelength comparison experiments. The scale shown is in micrometers.

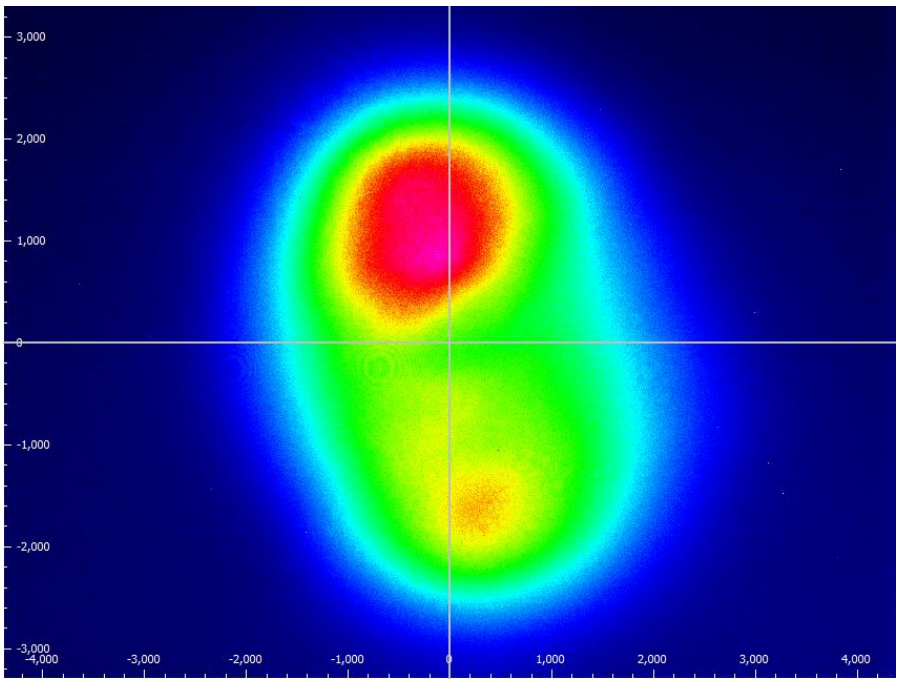

Figure 6.4: Laser beam profile at 1064 nm and other fixed parameters described during the wavelength comparison experiments. The scale shown is in micrometers.

With the laser running at 532 nm and repetition rate $R = 8$ Hz, it was found that $M^2 = 8.12$. At 1064 nm and $R = 8$ Hz, beam quality was $M^2 = 5.79$.

6.1.3 Offline Testing of Transmission and Plasma Absorption

With the experimental setup established, a number of tests were carried out in air before the engine or pressure chamber were used. For these, the optical plug was mounted offline at the end of a beam path equivalent to that used with the pressure chamber.

The transmission at each wavelength had to be measured. Using the plug setup for pressure tests, it was found to be $T \approx 82\%$ for both wavelengths with a new and therefore perfectly clean lens. Threshold breakdown energy in air with this setup was found to be approximately ~ 30 mJ at 532 nm and ~ 33 mJ at 1064 nm. These were therefore taken as the starting points for the range of energies tested.

It is clear when observing a spark in air that at least some of the pulse energy is

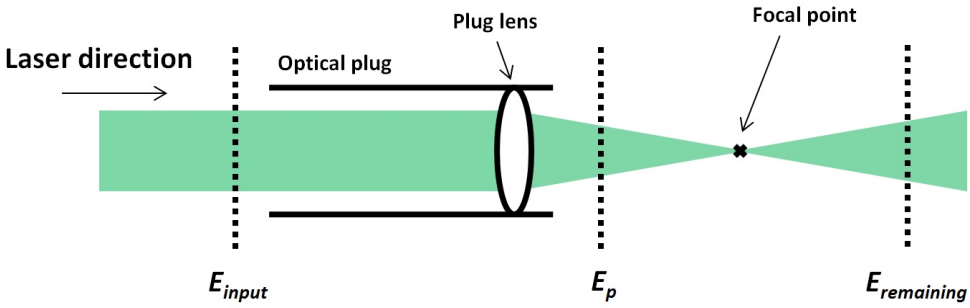

Figure 6.5: Schematic of a beam entering the optical plug, with energy measurement points labelled.

lost, as light is clearly visible behind the spark. The proportion of laser pulse energy transferred to the plasma is known as the plasma absorption percentage. Chen et al. (2000) and Griffiths et al. (2013) have previously studied air plasma formation and measured plasma absorption.

As incident pulse energy increase, absorption increases rapidly from just below threshold energy to just above it, then gradually levels out at higher energy. This is because of the roughly Gaussian shape of the energy distribution over time within each pulse.

There is some threshold intensity at which the plasma starts to form. Below this threshold light passes through and is lost, while above the threshold it is absorbed into the plasma. A higher E_p pulse will hit the threshold sooner, and so a smaller proportion of its energy will be lost. Plasma saturation occurs when the plasma reaches peak density and temperature, past this point the plasma only grows in size. This is expected to occur at greater three times the threshold energy.

Measurements were taken to determine the plasma absorption percentage. The relevant energies are shown in Figure 6.5, where E_{input} is the energy that enters the plug, E_p is the pulse energy delivered to the spark (calculated from the transmission), and $E_{remaining}$ is the energy left after the plasma. This test only has meaning when E_p is above the threshold breakdown energy.

Plasma absorption is then given by the following equation:

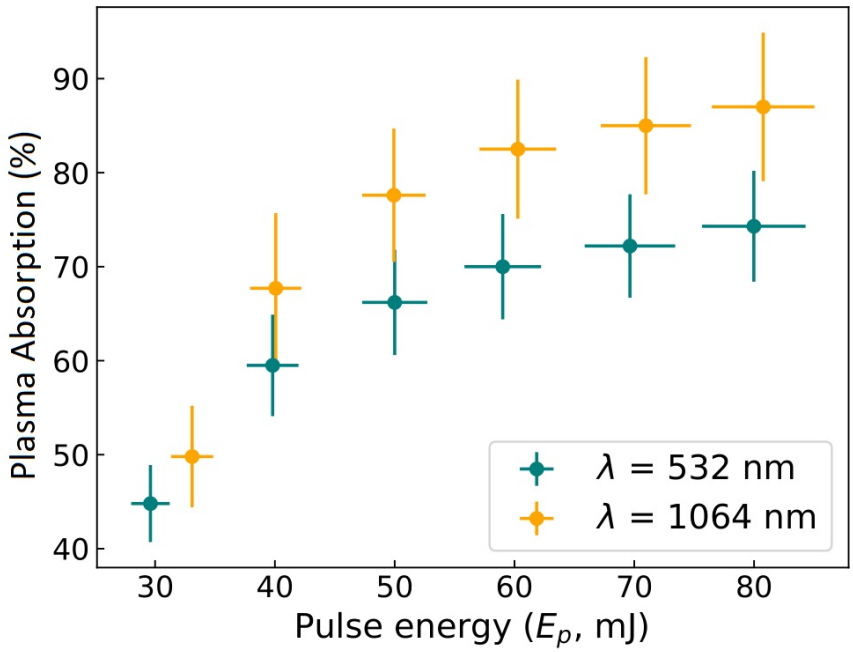

Figure 6.6: Plasma absorption as a percentage of laser pulse energy E_p, against E_p delivered to the focal point.

$$\text{Plasma absorption} = \frac{E_{remaining}}{E_p} * 100 \tag{6.1}$$

In an attempt to measure whether any of the emission from the plasma was affecting the energy reading, a small test was carried out. The energy meter was moved out of the beam path, and placed perpendicular to it, at a similar distance from the spark (~ 50 mm) to when $E_{remaining}$ was measured. Here the meter consistently gave a reading of zero. Given that the minimum detectable energy with this meter was 0.1 mJ, this test showed that practically all of the energy measured was left over from the original pulse.

Results of the plasma absorption test are shown in Figure 6.6. There is a clear upwards trend; a higher E_p produces a higher absorption percentage, though this is not a strictly one-to-one correlation. After a short rapid rise, the trend begins to level off at *approx*40 mJ, and is almost completely level from 60 mJ onwards. Comparing the two wavelengths, 1064 nm is more efficient than 532 nm by 5-10%, with the gap increasing at higher E_p. It is not clear why this is the case, possibly the differences in

laser properties between wavelengths.

These results are in agreement with similar findings in the literature. The plasma absorption trend is the same, and plasma saturation is not expected to be seen as the maximum E_p in these tests was only just three times the threshold.

The pulse to pulse variations in energy measured for $E_{remaining}$ are relatively large, especially at lower E_p, suggesting some randomness in the plasma formation process. This variation is the most significant factor in the large uncertainty on the plasma absorption values.

Henceforth, results will be presented in energy delivered to the focus, E_p, since it is more practical, but if higher energies give significantly different results in tests it may be due to the difference in energy in the plasma.

6.1.4 Pressure Chamber Test

A pressure chamber was used to measure the change in breakdown threshold energy with changing pressure. In this earlier work, such as engine tests presented in Chapter 4, the breakdown threshold pulse energy in air was found to be approximately the same as the lowest stable energy for engine running. This is despite the cylinder pressure being around 10 bar at the ignition point. According to the theory, higher pressure results in lower threshold energy as the density of the air at the focal point will be higher, making ionisation more likely.

A pressure chamber was not available during earlier experiments, so the pressure dependence of air breakdown threshold pulse energy was not known for those tests.

The procedure for the pressure test was to first set the desired pressure using the gauge, then input the laser at low pulse energy. The energy was gradually increased until 100% of the pulses produced air breakdown. Finally, E_{input} was measured and E_p was calculated from it. This was repeated for each wavelength. Sources of error were the manual adjustment of the pressure gauge and the half-wave plate in the attenuator. It was not possible to measure spark efficiency here, as there was no way

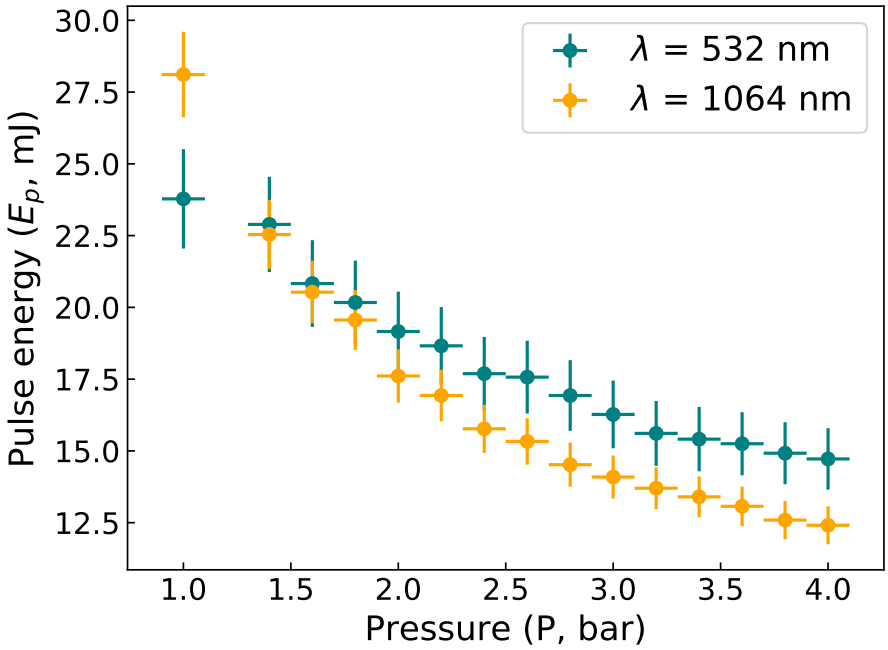

Figure 6.7: Variation of breakdown threshold pulse energy with pressure.

to access the inside of the chamber with the energy meter.

Figure 6.7 shows the variation in the breakdown threshold energy (E_p) with pressure inside the pressure chamber. As shown, there is a downwards trend in threshold energy as pressure increases. Comparing the two wavelengths, infrared has a lower threshold than green across the range. However, differences in the properties of the beams, such as beam quality, are not being taken into account.

Using the equation for d_{min} and the M^2 value measured earlier, it was possible to calculate the peak power density at the focal point in each case. Peak power density during a pulse was calculated from the following equation:

$$\text{Peak power density} = \frac{\text{Peak power}}{\text{Focus spot area}} = \frac{E_p/t_{pulse}}{\pi \frac{d_{min}}{2}^2} \tag{6.2}$$

The energy threshold data was converted to peak power density and plotted against pressure, as shown in Figure 6.8. All thresholds are of the order of 10×10^{11} W/cm^2, in agreement with the literature. The overall trend is the same; a reduction in threshold

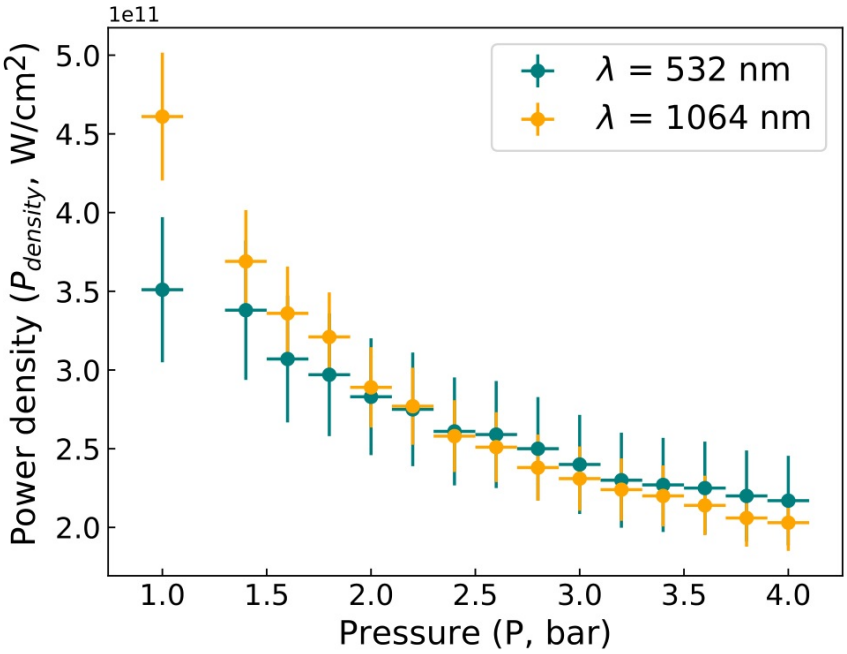

Figure 6.8: Variation of breakdown threshold peak power density with pressure.

power density with pressure, and a more slowly changing downward trend at higher pressure.

The comparison between wavelengths for this quantity shows very similar results, which are within the error on both readings, and therefore any differences may not be significant. Shorter wavelengths focus more tightly, and the 532 nm beam has a worse beam quality, but these factors are accounted for in the calculation of peak power density.

It was expected that the shorter wavelength would give a lower threshold, since the mechanism for the first step in air breakdown is multiphoton ionisation, a process which is partly dependent on photon energy.

Unfortunately as shown in Figure 6.8, the uncertainty on all of this data is fairly large, having been compounded from the uncertainties in the variables used to derive the peak power density. Taking this into account, it is not possible to say there is any difference between using these two wavelengths. These results also do not address the question of why the breakdown threshold in atmosphere and inside the cylinder are

so similar.

6.1.5 Engine Test

The two wavelengths were then tested using the engine. Previous research has not shown significant difference between these, as discussed in 2.4.3.

Engine parameters were fixed throughout the test: engine speed at 1000 rpm, air-fuel ratio at $\lambda = 1.05$ and a spark advance of 15°. These were chosen based on the results presented in Chapter 4 and the design specification of the engine, this was the best performing spark advance at the intended speed and air-fuel ratio of the engine system.

The variables were wavelength (λ) and pulse energy (E_p). The lowest energy used was 30 mJ, as this is the minimum energy required for the engine to run, as discussed earlier. Data was taken for each wavelength in the same engine run, starting at 80 mJ and lowering to 30 mJ. Hence there could be small bias in performance for lower energies as the engine tends to run better after running for several hours, despite trying to make allowances for this. As before, all parameters were adjusted; the engine was given time to warm up and stabilise; and finally ~ 500 engine cycles were recorded.

This time the optical plug was used in the usual engine format, and transmission had to be re-measured accordingly. The plug transmission before and after the 532 nm engine test was $71.6 \pm 3.3\,\%$ and $64.4 \pm 2.8\,\%$ respectively, so an average of these values, $68.0 \pm 4.3\,\%$, was used to calculate E_p during the test.

Similarly for 1064 nm, the transmission before and after was $69.0 \pm 3.1\,\%$ and $70.1 \pm 3.1\,\%$ respectively, giving an average of $69.6 \pm 4.3\,\%$.

Earlier in the chapter the transmission of a new lens was reported as $T \approx 82\%$ for a new lens. Values reported above are for older lenses, where the transmission has been observed to drop over time due to deposits on the lens.

The first result presented compares performance against air-fuel ratio λ. The purpose of this was to eliminate any correlation between these parameters. λ was fixed as much as possible, however due to the nature of the engine there are always small variations between and within tests. Large variations in λ would of course affect performance.

Figure 6.9 on the following page shows engine output power and $IMEP$ plotted against λ. Each point corresponds to a test of a specific wavelength and E_p combination.

There is clearly no trend here, the entire range of values is within 2% of each other, much smaller than the error on these values. Again, the purpose of this is to show that any trends in later results are due to E_p and wavelength changes, not air-fuel ratio.

Engine output power results are shown in Figure 6.10. 532 nm trends upwards while 1064 nm is fairly flat. However the magnitude of the changes is very small, other than between the tests at 80 mJ where there is perhaps an advantage for the green.

Both $IMEP$ and COV_{IMEP} are plotted against E_p in Figure 6.11. $IMEP$ shows a similar trend to power as expected, except 532 nm is consistently higher. There is a clear trend of increasing $IMEP$ with E_p this time, but weakly due to the uncertainty on all values.

COV_{IMEP} in the bottom half of the figure shows an increase in stability when using 532 nm. This is perhaps the biggest improvement in all of the tests. Looking at all of the engine results, performance overall improves marginally when using 532 nm compared with 1064 nm. Additionally this data show a decrease in COV_{IMEP} for both wavelengths as E_p increases.

A similar test was discussed previously in Section 4.2. It is necessary to point out the apparent disagreement between what are similar tests of single-point LI. In the earlier results, when looking at the trend in $IMEP$ and COV_{IMEP} , they improved as E_p increased up to a peak, then got worse past this at higher energies. In the results from this section, $IMEP$ and COV_{IMEP} linearly improve across the same range of E_p.

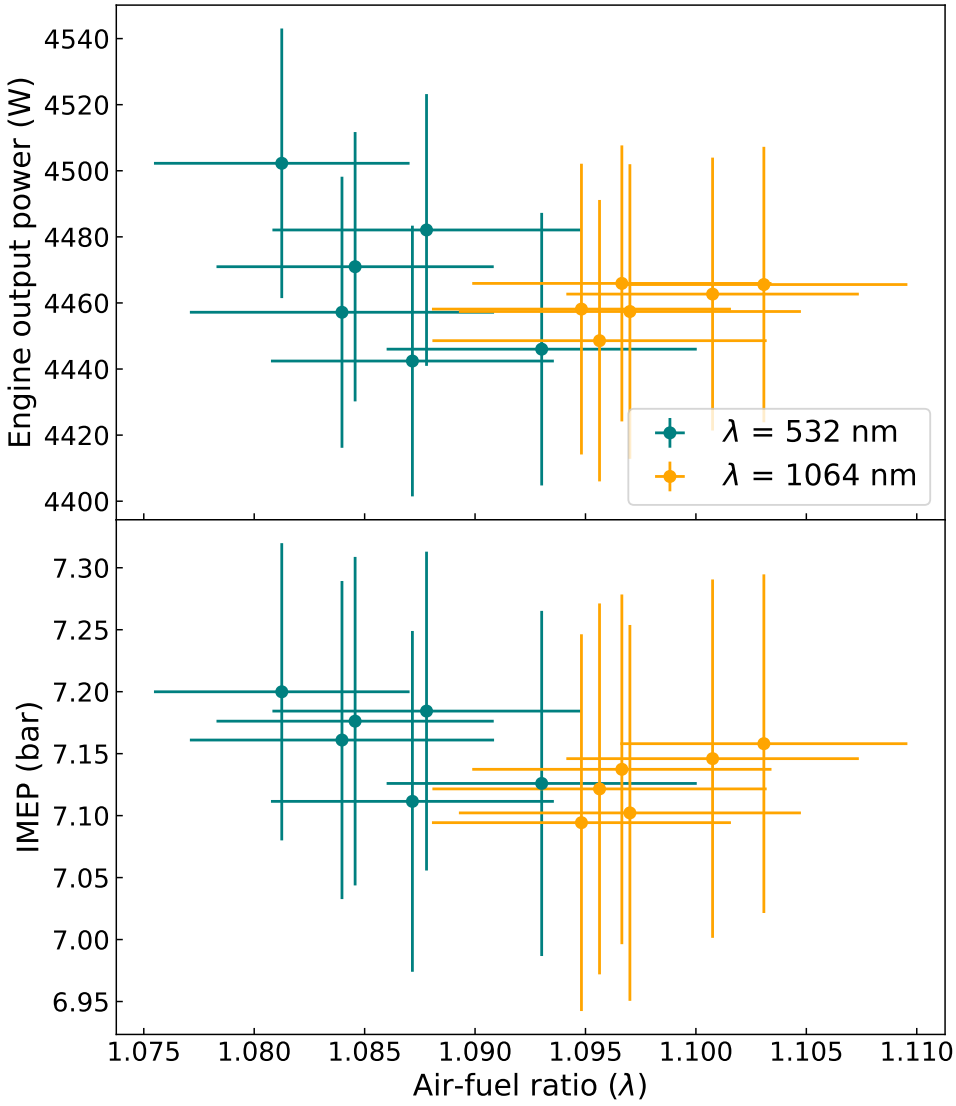

Figure 6.9: Graph of engine output power and $IMEP$ against air-fuel ratio, each point is a different E_p and wavelength combination tested.

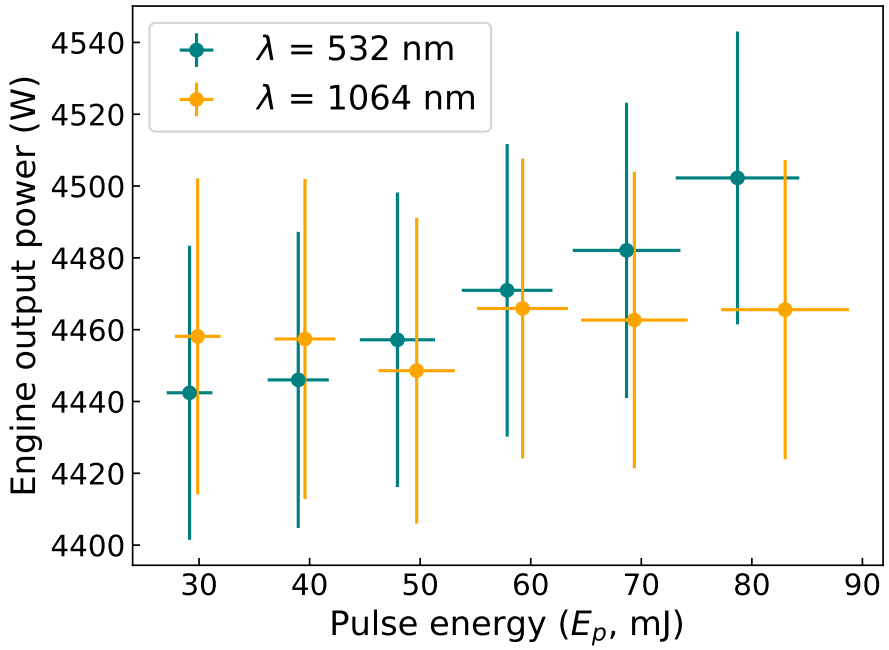

Figure 6.10: Engine output power against laser pulse energy at two wavelengths.

These two tests were taken using much of the same equipment, but about two years apart, during which time many components of the engine and laser systems were replaced or modified. This means that results are not directly comparable.

Looking at the trend in the earlier results, performance improved linearly with increasing E_p up to the point of peak performance. It could be that this point has now moved higher with the engine being modified, which would mean both experiments follow the same trend. Further testing would be required to verify this.

In summary, these engine results and earlier pressure chamber results show little to no difference between using green or infrared for LI. Once a laser spark is created, the laser parameters used in the spark creation become irrelevant. The research interest then might be in finding the wavelength with the lowest breakdown threshold, however the two wavelengths tested here have a similar threshold. A sweep across a large, continuous range of wavelengths was then the next goal.

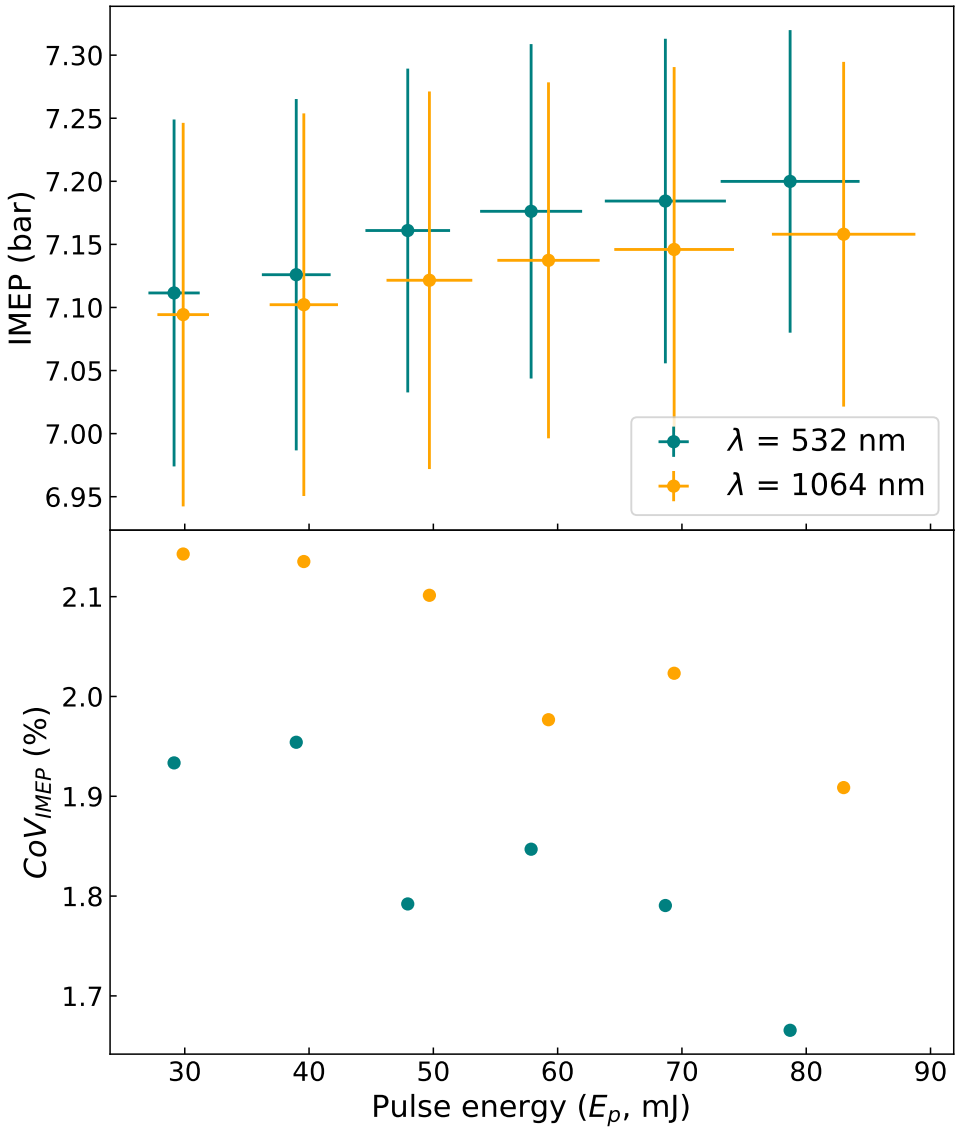

Figure 6.11: $IMEP$ and COV_{IMEP} against laser pulse energy at two wavelengths.

6.2 Continuously Variable Wavelength LI using an Optical Parametric Oscillator

Previous studies on laser ignition have only used one or two discrete wavelengths; a study over a continuous range of wavelengths has never been undertaken before. The two wavelength comparison previously discussed showed no differences, but it is unlikely that picking two wavelengths that are easily obtained would come across different mechanisms such as resonant enhanced multi-photon ionisation (REMPI).

In order to sweep through a range of wavelengths, an optical parametric oscillator (OPO) could be used. Parametric oscillation is a non-linear effect which is utilised by the OPO, that is able to change the wavelength continuously. Changes are dependent on the angle at which the pump beam is incident upon the non-linear crystal in the OPO, which can easily be varied.

The laser pulse produces a spark via air breakdown. The first part of this mechanism is multiphoton ionisation of some of the molecules at the focal point of the lens. This process is dependent on the wavelength of the laser. At certain wavelengths, it was thought that REMPI would take place, which would reduce the breakdown threshold energy significantly.

This would therefore require a lower power laser, allowing a more compact laser system to be used, which would be another step towards practical implementation of a LI system. In the literature review, Section 2.3.4, this was discussed further.

The effects of wavelength on LI can be broken down to two main parts: the ability of a particular wavelength to create air breakdown in the components of the fuel/air mixture, and the amount of energy transmitted through the air-fuel mixture between the entrance window and the focus spot. The objective of this part of the research was to measure the breakdown threshold energy across the range of wavelengths. It was also thought that with a large wavelength wave to test, evidence of REMPI might be observed.

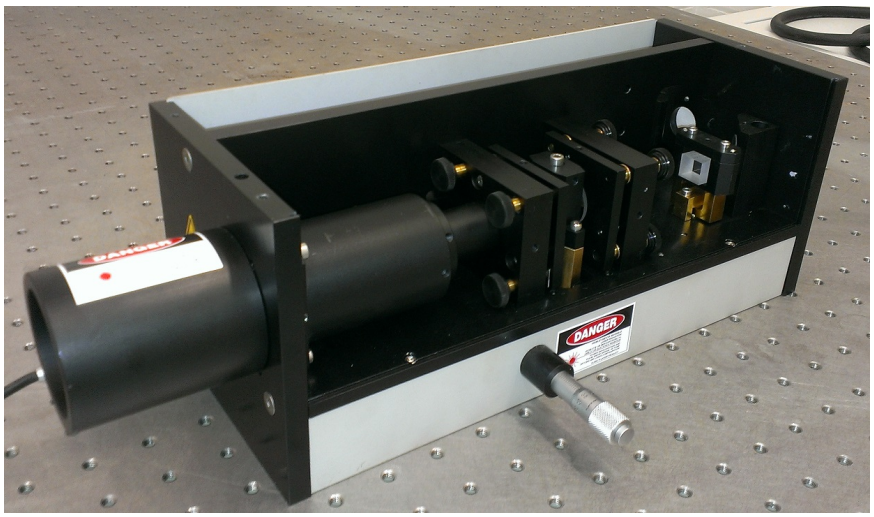

Figure 6.12: Photo of the optical parametric oscillator with casing removed.

6.2.1 Experimental Setup

A system for the study of the effect of wavelength on laser ignition was created using the optical parametric oscillator. When the pump laser passes through the non-linear BBO crystal, part of the energy is converted to two other wavelengths. These two are called the signal (shorter) and idler (longer) wavelengths. The output wavelength is continuously tunable from around 700 nm to 950 nm for the signal, and from 1100 nm to 2400 nm for the idler. However due to the varying properties of each output and variations within each depending on the wavelength chosen, only the signal beam was close to being useful for creating air breakdown.

The pump, signal and idler wavelengths are linked by the following equation:

$$\frac{1}{\lambda_{pump}} = \frac{1}{\lambda_{signal}} + \frac{1}{\lambda_{idler}} \tag{6.3}$$

The OPO used for these tests was a GWU versaScan-L532. An OPO can be designed to be pumped by a specific wavelength, this one is just for 532 nm. Figure 6.12 is a photograph of the OPO with the casing removed.

The laser used was the Litron LPY 764-30 Nd:YAG, operating at 532 nm. A schematic of the experimental setup is shown in Figure 6.13. The inset shows a simplified view

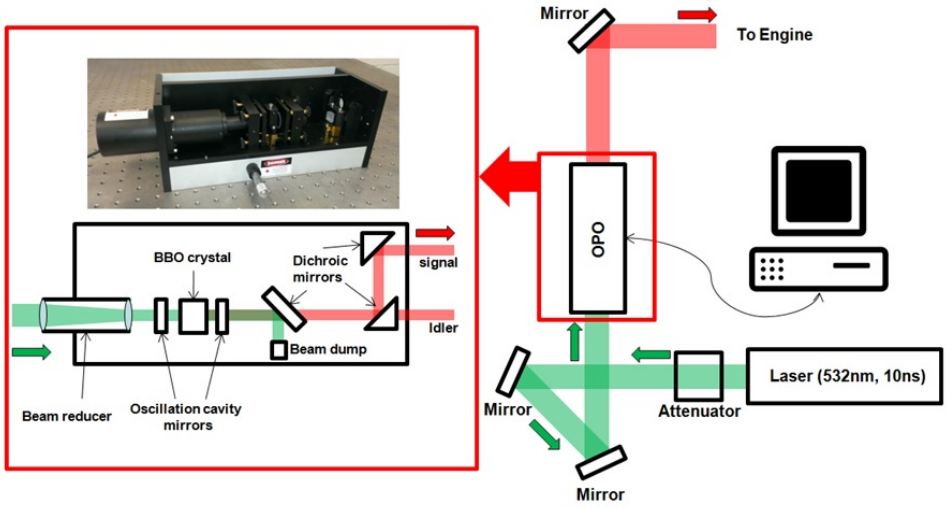

Figure 6.13: Experimental setup for the optical parametric oscillator (OPO) with a 532 nm pump laser.

of the internal components. A small cavity is created around the BBO crystal, where the conversion takes places. After the cavity, the wavelengths are separated and the unwanted pump beam is discarded.

Crystal angle is varied by a motor, which changes the incident angle of input beam on the crystal. This varies the output wavelengths λ_{signal} and λ_{idler}. Once the software is calibrated, the user simply enters the desired wavelength and the motor is controlled automatically. The Thorlabs CCS200 CCD spectrometer was used to measure the signal wavelength.

6.2.2 Results and Discussion

The signal pulse length was measured to be ~ 5 ns at 700 nm, compared with ~ 12 ns of the 532 nm pump laser. In theory a shorter pulse length is better at causing air breakdown.

It was possible to achieve some wavelength conversion. Figure 6.14 demonstrates that the wavelength of the signal output is shifted to red (~ 700 nm). The idler output is infrared, but appears green in the image since the pump laser is not fully filtered out, as it is for the signal beam.

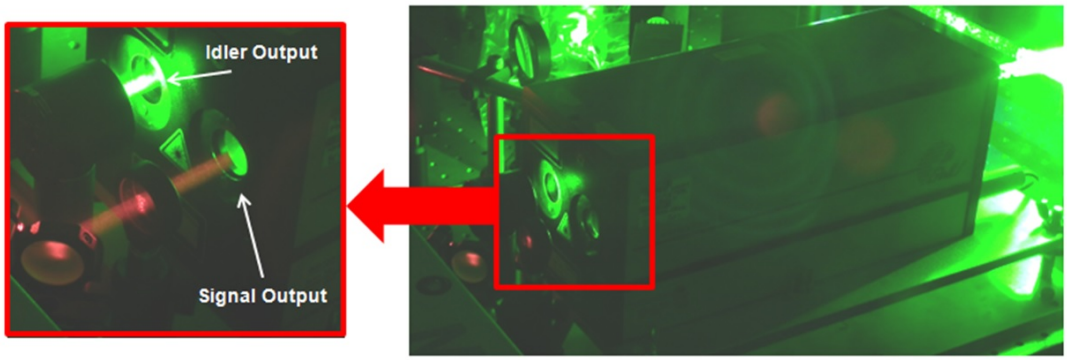

Figure 6.14: Image showing the OPO signal output at $\sim 700\,\mathrm{nm}$, as well as the idler output mixed with the residual pump beam.

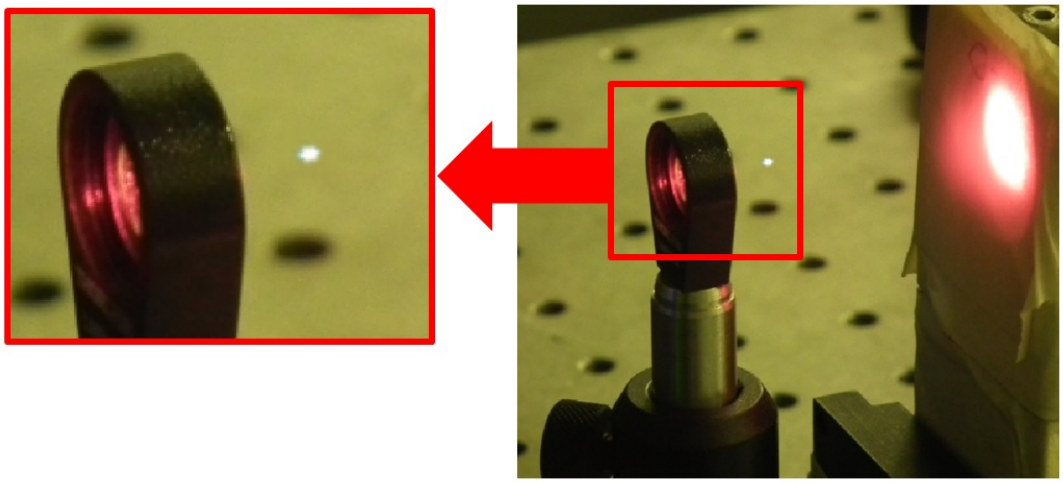

Figure 6.15: Laser air breakdown using the OPO signal output with poor stability ($< 20\%$).

Offline tests were carried out, where a spark was created using a larger coated lens (rather than engine lens) using the 700 nm beam. The lens was placed close to the output of the OPO, however the spark stability was very poor, at $< 20\%$. An image of the spark can be seen in Figure 6.15 on the preceding page.

The manufacturer stated conversion efficiencies to be in the region of 25% for the signal and 15% for the idler; equipment was not available to measure the idler, but for the signal efficiencies measured were closer to 10%. It was not clear why this was so low, but in any case this was ultimately not the main issue with the output laser. The maximum input pulse energy was 250 mJ, while most signal output measured was 22 mJ.

It was thought that using the pressure chamber would allow stable sparking, as previous tests have shown the difference in pulse energy between stable and unstable sparking is fairly small (~ 5 mJ). An optical setup was built much like the one used earlier for the chamber, shown in Figure 6.1, consisting of a telescope and the minimum necessary number of mirrors to direct the beam along the shortest beam path there.

However it was not possible to direct the beam to the chamber in a usable state, due to poor beam quality. The M^2 couldn't be measured since the camera was too small to image the beam and the telescope had almost no effect on the beam size. The divergence was very high, the beam diameter doubled from roughly 8 mm to 16 mm over a distance of 1 m. The main problem was that the laser available for these tests was not suitable for this purpose. The pump beam had poor beam quality and mode, better are preferred for pumping the OPO.

The properties of the output beam are dependent on the properties of the input. A superior pump laser, along with a larger BBO crystal (the one used here had a cross-section of 5×6 mm), should produce a usable signal beam. This should avoid the divergence and clipping issues that caused the experiment described here to fail. The concept of the experiment works, and the results would still be of interest if it could be carried out in the future.

6.3 Chapter summary

This chapter contained results from two tests, one comparing two fixed wavelengths, and one to sweep across a range. There was very little separating 532 nm and 1064 nm in any of the tests. When it came to spark efficiency, the infrared was slightly better, however when breakdown threshold energies were compared there was no significant difference. In the engine tests there were a couple of areas where the green was superior, but overall neither could clearly be shown to be superior outside of error measurements.

The continuous wavelength sweep using an OPO was not possible due to limitations of the equipment. The laser and OPO used were not ideally matched, but with the right equipment it would be possible to carry out the test proposed, and it may produce interesting results.

Chapter 7

Conclusions

This chapter will cover conclusions and ideas for future work. Key findings and novel work from each area of experimentation will be discussed.

7.1 Single-point LI

The first engine tests were carried out in order to find the optimal parameters for LI of the single cylinder test engine. A single-point LI system was established, and parameters including laser pulse energy, spark position, and ignition timing were varied. Engine output power, $IMEP$, and COV_{IMEP} all appear to depend strongly on the laser parameters used. The optimal ignition conditions were found to be $E_p = 50\,\mathrm{mJ}$, 20° SA, and 6 mm spark distance. The purpose of finding these was to have a baseline point of comparison later, when using more advanced optical techniques.

During these tests the self-cleaning of the optical plug lens was observed. If incorporated into a commercial engine, all the components of the LI system would have to survive thousands of hours of operation, and so millions of laser pulses and engine cycles. The lifetimes of these components, their damage mechanisms, their damage thresholds, and their performance whilst partially damaged are all of interest when developing a robust LI system. As well as the effect of the laser itself, the engine con-

ditions could affect the window. Engine vibration can cause components to become misaligned, or heat could cause damage. The window into the cylinder seems to be the biggest issue since combustion deposits material onto its surface.

A challenge that remains is to demonstrate the self-cleaning of the window into the cylinder over long time periods. A potential drawback to LI systems is that the optical window becomes covered by deposits after each combustion event, if this progresses the laser could be fully blocked and the ignition system would fail.

During this work a large data set of stable engine running was never seen, however there was short term evidence of the self-cleaning effect. The sapphire lenses that acted as windows in these experiments have shown to be fairly resistant, but that possibly relied on the lens being receded into the plug. The lens was not flush to the end of the plug, a small cylindrical cavity was created in front of the lens. Whilst this might turn out to be protecting the lens surface, this could create other problems such as soot collecting in the corners, or effects on the flame propagation. Ideally the lens would be flush with the cylinder wall.

7.2 Multi-point LI

In Chapter 5 results of technique which can create multi-location ignition in a flexible and controllable way were presented.

It is possible to modulate a laser beam using a spatial light modulator (SLM) in order to create a diffractive multi-beam pattern, which creates multiple focus spots when passed through a standard lens. The multi-location pattern is dependent on the computer generated hologram (CGH) displayed on the SLM, which can in principle be designed to create a multi-beam pattern. Two types of CGHs were initially investigated: Fresnel lens phases, and prism phases. Each of these effectively simulated the effect of the laser beam passing through a lens or prism, but could be controlled dynamically. Complex superpositions of these phases were used to create multi-location air breakdown. Axially and laterally shifted multiple-beam patterns were created.

In the case of lateral shifts, limitations of the equipment meant that the separation between points was not sufficient to create multiple sparks. With axial shift, a 60 mJ pulse was used to create three simultaneous air breakdown sparks, which could be achievable inside the engine. However limitations of the equipment prevented these being used for LI. Given these limitations, further experiments were carried out using a higher quality SLM.

An experiment was carried out to find the optical damage threshold of the SLM in the context of engine experiment, and a safe working pulse energy of 60 mJ was found. Diffractive multi-beam arrays were created by applying CGHs to a SLM. Linear gratings were used to create lateral arrays with two, three and five beams, and vary separation between them. A $4f$ optical system was designed and built to allow these multi-beams to reach the engine and be focused down. This system shifted the image plane from the SLM surface to the optical plug, avoiding any clipping issues. Using a dummy line equivalent to the engine line, the multi-location air breakdown created by this was studied.

The maximum number of sparks that could be maintained with 100% probability of breakdown was two, due to the limitations of the SLM and laser - the laser's M^2 was poor so the energy required for more than this would be beyond the damage threshold of the SLM. The separation between the two points could be varied up to a maximum of 4 mm. However in the case of small separation ($d \leq 2$ mm), the two plasmas merged into one, so the maximum was used to ensure a true test of multiple locations.

This was then used to ignite the single cylinder test engine, where two-location was compared to single-location LI. The major finding from the engine test was that two-location LI reduced the probability of misfires, improved engine output power, and reduced COV_{IMEP} at lean air-fuel ratios. In particular at $\lambda = 1.2$, two-location LI worked without the misfires from single-location. For comparison, with this engine a spark plug could not ignite at all for air-fuel ratios leaner than this. Although the stability is poor, the engine did run, so perhaps multi-location can be further refined to address this. Now that the technique is established, future work could study its effect across a large range of engine parameters, here only a couple of specific cases

were studied.

A downside to multi-point LI is that a SLM would add significant cost to a piece of equipment that is already expensive, if implemented into a practical system. The technique developed here could apply an arbitrary arrangement of sparks to any engine in a lab environment. Tests could be ran to determine which arrangement is best, and based on this information a custom optic could be engineered to create this pattern in a simpler, lower cost way. Another limitation was the small separation achievable. Larger separations could be achieved with a larger diameter lens or window into cylinder, or by using a SLM with higher pixel density and better optics. A SLM durable enough to go near the engine would open up many more parameters to testing.

It is possible to create more complex CGHs, for example axial and lateral shifts could be combined to create 3D arrays of sparks. This would require a lower M^2 input beam, the SLM to have a higher power handling capability, or an increased SLM resolution, as more complex CGHs have a lower efficiency. The SLM can also shape the beam in other ways, for example into ring or line shapes, which give more possibilities for future work.

With regard to the SLM damage threshold problems, the reason main for the difficulties was the inappropriate laser rather than the technique itself. As previously discussed, poor beam quality greatly increases the required pulse energy for air breakdown. The fundamental output of the Litron laser gave 1 J of energy which is excessive for this application. For example, 5 mJ pulses are able to cause breakdown given the right conditions, in which case the SLM could create 5-10 foci without risking damage.

Multi-pulse LI refers to using multiple sparks in time to ignite an engine. The author also contributed to published work in this area that was not discussed in this thesis (Cheng et al., 2016). Early results showed the effect on performance of two sparks closely spaced in time was similar to that on the multi-location technique. It improved engine stability and allowed operation in leaner air-fuel mixtures. If these two approaches continue to show similar results, then the easiest to implement in a compact laser may supersede the other.

7.3 Effect of Wavelength on LI

Investigations into the effect of varying wavelength on LI were split into two areas. First, a comparison of two fixed wavelengths that were easily obtained directly from the Litron laser. Then an unsuccessful attempt was made to use an optical parametric oscillator to sweep a range of wavelengths for a more in depth investigation.

In the two wavelength comparisons, 532 nm and 1064 nm produced largely similar results. When measuring plasma absorption, the proportion of pulse energy that is absorbed into the plasma, 1064 nm showed an increase of 5-10%. The plasma absorption results also showed that higher energy pulses transfer a higher percentage of their energy into the plasma, so high E_p might be preferred in some cases. Energy delivered to the focus was kept as the measured parameter, but this effect is worth keeping under consideration.

Later in this work, in the comparison of peak power density breakdown thresholds across a range of pressures, which accounted for different beam qualities of the two, there was no difference between 532 nm and 1064 nm. Engine tests showed little variation between the two when comparing engine output power or $IMEP$. COV_{IMEP} was slightly lower in the 532 nm case, and improved engine stability is an important objective. However when taking into account the errors on all of the parameters, it is not possible to claim any differences.

A limitation of this test was that a complete range of engine parameters weren't tested, but given the close results it seems unlikely that it any differences would arise in studies across untested parameters.

When deciding which of these two to use, the most important fact is that 532 nm lasers are 1064 nm lasers with second harmonic generators attached. In the conversion process you throw away half the pulse energy and lose beam quality. With this in mind, 532 nm would have to be more than twice as effective as 1064 nm for it be worth converting. A practical system therefore should always use infrared, as long as the intended mechanism of spark formation is multiphoton ionisation. For experimentation

purposes however, either could be used since they effectively produce the same result. Experiments presented in this thesis were carried out using 532 nm due to easier compatibility with optics and other equipment available. The results in Chapter 6 show that using only 532 nm should produce the same results as if 1064 nm was used.

An optical parametric oscillator was used to create a continuously tunable laser source from 700 nm to 950 nm. Unfortunately the beam quality was so poor that it was not possible to use this for any LI experiments. The pump laser used was not well suited to this use, it had too poor of a beam mode and high M^2, which are not ideal for pumping an OPO. Alignment of the internal components of the OPO to optimise the output was very delicate. Since the crystal would be moving, it was not possible to achieve good alignment at all output wavelengths, so a compromise position has to be reached. However even the best alignment for a given wavelength led to poor results.

The literature suggests that different air breakdown mechanisms, such as resonant enhanced multiphoton ionisation (REMPI) could be used at certain wavelengths, and the research into the effect of wavelength on LI has been limited so far, so there would be value in repeating this test with more appropriate equipment. Perhaps the same argument as in the 532 nm case might apply to any better performing or even resonant wavelengths found. If the only way to build a laser that generates them is through a wasteful conversion process, with a loss of E_p and M^2, the advantage they produce would have to be very significant. There would also be cost and complexity concerns for practical implementation.

7.4 Future Work

The work presented in this thesis has demonstrated new LI techniques that have advantages over single-point ignition, but further research will be required for these concepts to be implemented in a practical system.

Various ideas for future work have been discussed so far in this chapter, but there are a few main areas to suggest.

There is a clear path for future investigation into multi-point LI. The SLM based system is very flexible and many different patterns could be achieved and tested. Testing and especially implementing LI at varying wavelengths would be more challenging but could potentially lower the laser energy requirements by a significant amount. For a given engine, a customised solution including multiple ignition points at a specific wavelength might give better results than just an off the shelf laser. A laboratory setup like the ones described in this thesis could be used to determine the ideal laser, which would then inform the design of the compact laser used. This would require, for example, a fixed optic such as a grating which could be placed behind the lens/window into the cylinder.

At a more fundamental level, further parameters could be tested using this work as a starting point. Two-location ignition was tested, but only with a relatively small spark separation. Varying the separation and orientation of the sparks within the cylinder might find more significant results. This could then be repeated for three sparks or more. Each of these sets of location parameters would then need to be tested across a range of engine conditions, in order to find the most optimal form of multi-location ignition. Ignition timing especially should depend greatly on the position of the sparks.

There is still a lack of research on the self-cleaning effect on windows into the cylinder. Long term tests are needed, with varying engine parameters, of a window flush to the wall of the cylinder. This hasn't been done for gasoline engines, and other engine such as natural gas fuelled are not comparable due to different combustion products being left behind. Window self-cleaning is a key issue that needs to be addressed by a mass-produced compact laser solution.

Further investigation could also be carried out into the effect of wavelength. The OPO experiments mentioned earlier were not successful, but it should be possible to follow this method with a better laser and produce useful results. An appropriately high beam quality laser could be used as a pump source to generate continuous wavelengths 700 nm to 950 nm. Comparing these in terms of air breakdown threshold pulse energy and engine performance would be an important result.

References

Beaudou, B., Gerome, F., Wang, Y. Y., Alharbi, M., Bradley, T. D., Humbert, G., Auguste, J. L., Blondy, J. M., and Benabid, F. (2012). Milli-joule laser pulse delivery and spark ignition through kagome fiber. In *2012 Conference on Lasers and Electro-Optics(CLEO 2012)*.

Bihari, B., Biruduganti, M., and Gupta, S. (2015). Natural gas engine performance ignited by a passively q-switched microlaser. In *Laser Ignition Conference*, page T5A.5. Optical Society of America.

Biruduganti, M., Gupta, S., Bihari, B., Kanehara, K., Polcyn, N., and Hwang, J. (2015). Performance evaluation of a denso developed micro-laser ignition system on a natural gas research engine. In *Laser Ignition Conference*, page T5A.4. Optical Society of America.

Carroll, S., Dodd, R., Shenton, A. T., Dearden, G., Scarisbrick, A. D., and Keen, S. (2005). Laser Ignition in an Automotive Engine: Analysis and Control of C.O.V. in I.M.E.P. and P.P.P. In *Proceedings, Japanese SAE Annual Congress*, number 33 in 05, pages 11–14.

Chen, Y. L., Lewis, J. W. L., and Parigger, C. (2000). Spatial and temporal profiles of pulsed laser-induced air plasma emissions. *Journal of Quantitative Spectroscopy and Radiative Transfer*, 67(2):91–103.

Cheng, H., Kuang, Z., Page, V., Lyon, E., Dearden, G., and Shenton, T. (2014a). An Investigation of Multi-pulse Laser Ignition in a GDI engine. In *The 2nd. Laser Ignition Conference (LIC'14)*, Yokohama, Japan, Apr. 22 - 24, 2014.

Cheng, H., Kuang, Z., Page, V., Lyon, E., Dearden, G., and Shenton, T. (2014b). Multiple Pulse Laser Ignition in GDI Lean Combustion. In *PMC2014 2nd Biennial Conference on Powertrain Mapping and Calibration*, Bradford UK.

Cheng, H., Kuang, Z., Page, V., Lyon, E., Dearden, G., and Shenton, T. (2016). Multiple pulse laser ignition in gdi lean combustion. *International Journal of Powertrains (IJPT)*, 6(1):55–68.

Cheng, H., Vincent, P., Kuang, Z., Lyon, E., Dearden, G., and Shenton, T. (2015). Multiple Pulse Laser Ignition Control Application in GDI Lean Combustion. In *Laser Ignition Conference*, page W2A.2. Optical Society of America.

Dale, J. D., Smy, P. R., and Clements, R. M. (1978). Laser Ignited Internal Combustion Engine - An Experimental Study. *SAE Technical Paper*, (780329):1–10.

Dammann, H. and Grtler, K. (1971). High-efficiency in-line multiple imaging by means of multiple phase holograms. *Optics Communications*, 3(5):312 – 315.

Damon, E. K. and Tomlinson, R. G. (1963). Observation of Ionization of Gases by a Ruby Laser. *Applied Optics*, 2(5):546–547.

Dearden, G., Kuang, Z., Lyon, E., Cheng, H., Page, V., and Shenton, T. (2016). Multi-point laser ignition for in-combustion event feedback control of an automobile engine. In *Laser Ignition Conference*, Yokohama, Japan, May 18 - 20, 2016.

Dearden, G. and Shenton, T. (2013). Laser ignited engines: progress, challenges and prospects. *Optics Express*, 21(S6):A1113–A1125.

Dodd, R., Mullett, J., Carroll, S., Dearden, G., Shenton, A. T., Watkins, K. G., Triantos, G., and Keen, S. (2007). Laser ignition of an IC test engine using an Nd: YAG laser and the effect of key laser parameters on engine combustion performance. *Lasers in Engineering*, 17:213–231.

Efron, U. (1994). *Spatial Light Modulator Technology: Materials, Devices, and Applications*. Optical Science and Engineering. Taylor & Francis.

Forch, B. E. (1994). Resonant laser ignition of reactive gases. In Locke Randy, J., editor, *Laser Applications in Combustion and Combustion Diagnostics II*, volume 2122 of *Laser Applications in Combustion and Combustion Diagnostics II*, pages 118–128. Society of Photo-Optical Instrumentation Engineers.

Forch, B. E. and Miziolek, A. W. (1986). Oxygen-Atom 2 Photon Resonance Effects in Multiphoton Photchemical Igntion of Premixed H2/O2 Flows. *Optics Letters*, 11(3):129–131.

Forch, B. E. and Miziolek, A. W. (1987). Ultraviolet Laser Ignition of Premixed Gases by Efficient and Resonant Multiphoton Photochemical Formation of Microplasmas. *Combustion Science and Technology*, 52(1–3):151–159.

Forch, B. E. and Miziolek, A. W. (1991). Laser-based ignition of H2O2 and D2O2 premixed gases through resonant multiphoton excitation of H and D atoms near 243 nm. *Combustion and Flame*, 85(12):254–262.

Gold, A. and Bebb, H. B. (1965). Theory of Multiphoton Ionization. *Physical Review Letters*, 14(3):60–63.

Griffiths, J., Lawrence, J., and Fitzsimons, P. (2013). Effect of ignition location on the in-process removal of combustion deposits from the output window of a gas turbine laser ignition system. *Optics & Laser Technology*, 48:326–330.

Hayasaki, Y., Sugimoto, T., Takita, A., and Nishida, N. (2005). Variable holographic femtosecond laser processing by use of a spatial light modulator. *Applied Physics Letters*, 87(3):031101.

Hecht, E. (2002). *Optics,4/e*. Pearson Education.

Heywood, J. (1988). *Internal Combustion Engine Fundamentals*. McGraw-Hill Education.

Hummelt, J. S. and Scharer, J. E. (2010). Excitational energy transfer enhancing ionization and spatial-temporal evolution of air breakdown with UV laser radiation. *Journal of Applied Physics*, 108(9):093305 1–8.

Joshi, S., Wilvert, N., and Yalin, A. P. (2012). Delivery of high intensity beams with large clad step-index fibers for engine ignition. *Applied Physics B: Lasers and Optics*, 108(4):925–932.

Keldysh, L. V. (1965). Ionization in the Field of a Strong Electromagnetic Wave. *Soviet Physics JETP-USSR*, 20(5):1307–1314.

Khoo, I. and Saleh, B. (2007). *Liquid Crystals: Physical Properties and Nonlinear Optical Phenomena*. Wiley Series in Pure and Applied Optics. Wiley.

Kopecek, H., Maier, H., Reider, G., Winter, F., and Wintner, E. (2003). Laser ignition of methane-air mixtures at high pressures. *Experimental Thermal and Fluid Science*, 27(4):499–503.

Kuang, Z., Liu, D., Perrie, W., Edwardson, S., Sharp, M., Fearon, E., Dearden, G., and Watkins, K. (2009a). Fast parallel diffractive multi-beam femtosecond laser surface micro-structuring. *Applied Surface Science*, 255(13):6582 – 6588.

Kuang, Z., Lyon, E., Cheng, H., Page, V., Shenton, T., and Dearden, G. (2014). Multi-point Laser ignition of internal combustion engines using a spatial light modulator. In *The 2nd. Laser Ignition Conference (LIC'14)*, Yokohama, Japan, Apr. 22 - 24, 2014.

Kuang, Z., Lyon, E., Cheng, H., Page, V., Shenton, T., and Dearden, G. (2017). Multi-location laser ignition using a spatial light modulator towards improving automotive gasoline engine performance. *Optics and Lasers in Engineering*, 90:275 – 283.

Kuang, Z., Lyon, E., Hua, C., page, V., Shenton, T., and dearden, G. (2015). Diffractive Multi-point Laser ignition of internal combustion engines using a spatial light modulator. In *Laser Ignition Conference*, page W2A.4. Optical Society of America.

Kuang, Z., Perrie, W., Leach, J., Sharp, M., Edwardson, S. P., Padgett, M., Dearden, G., and Watkins, K. G. (2008). High throughput diffractive multi-beam femtosecond laser processing using a spatial light modulator. *Applied Surface Science*, 255(5, Part 1):2284 – 2289.

Kuang, Z., Perrie, W., Liu, D., Edwardson, S., Cheng, J., Dearden, G., and Watkins, K. (2009b). Diffractive multi-beam surface micro-processing using 10 ps laser pulses. *Applied Surface Science*, 255(22):9040 – 9044.

Kuang, Z., Perrie, W., Liu, D., Fitzsimons, P., Edwardson, S. P., Fearon, E., Dearden, G., and Watkins, K. G. (2012). Ultrashort pulse laser patterning of indium tin oxide thin films on glass by uniform diffractive beam patterns. *Applied Surface Science*, 258(19):7601 – 7606.

Lackner, M., Kofler, H., Ranner, H., Winter, F., Klausner, J., and Herdin, G. (2005). The optical spark plug: window-related issues. In *Proc. Eur. Combustion Mtg - Book of Abstracts ECM 2005*, page 248. Combustion Institute.

Leach, J., Sinclair, G., Jordan, P., Courtial, J., Padgett, M. J., Cooper, J., and Laczik, Z. J. (2004). 3d manipulation of particles into crystal structures using holographic optical tweezers. *Opt. Express*, 12(1):220–226.

Leach, J., Wulff, K., Sinclair, G., Jordan, P., Courtial, J., Thomson, L., Gibson, G., Karunwi, K., Cooper, J., Laczik, Z. J., and Padgett, M. (2006). Interactive approach to optical tweezers control. *Appl. Opt.*, 45(5):897–903.

Lee, J. H. and Knystaut, R. (1969). Laser Spark Ignition of Chemically Reactive Gases. *AIAA Journal*, 7(2):312–317.

Leeuwen, R. V., Xu, B., Chen, T., Wang, Q., Seurin, J.-F., Xu, G., Zhou, D., and Ghosh, C. (2016). Vcsel-pumped passively q-switched monolithic solid-state lasers.

Liedl, G., Schuoecker, D., Geringer, B., Graf, J., Klawatsch, D., Lenz, H. P., Piock, W. F., Jetzinger, M., and Kapus, P. (2005). Laser-induced ignition of gasoline direct-injection engines. In *Proc. SPIE 5777, XV International Symposium on Gas Flow, Chemical Lasers, and High-Power Lasers*, volume 5777, pages 955–960.

Lyon, E., Kuang, Z., Cheng, H., Page, V., Shenton, T., and Dearden, G. (2014). Multi-point laser spark generation for internal combustion engines using a spatiallight modulator. *Journal of Physics D: Applied Physics*, 47(47):475501.

Ma, J. X., Alexander, D. R., and Poulain, D. E. (1998). Laser spark ignition and combustion characteristics of methane-air mixtures. *Combustion and Flame*, 112(4):492–506.

Meyerand, R. G. and Haught, A. F. (1963). Gas Breakdown at Optical Frequencies. *Physical Review Letters*, 11(9):401–403.

Morsy, M. H. (2012). Review and recent developments of laser ignition for internal combustion engines applications. *Renewable and Sustainable Energy Reviews*, 16(7):4849–4875.

Morsy, M. H. and Chung, S. H. (2003). Laser-induced multi-point ignition with a single-shot laser using two conical cavities for hydrogen/air mixture. *Experimental Thermal and Fluid Science*, 27(4):491–497.

Morsy, M. H., Chung, S. H., Ko, Y. S., and Yoon, K. J. (1999a). An Experiment on the Combustion Characteristics with Laser-Induced Spark ignition. *KSME International Journal*, 13(1):82–89.

Morsy, M. H., Ko, Y. S., and Chung, S. H. (1999b). Laser-induced ignition using a conical cavity in CH4-air mixtures. *Combustion and Flame*, 119(4):473–482.

Mullett, J. D., Dearden, G., Dodd, R., Shenton, A. T., Triantos, G., and Watkins, K. G. (2009). A comparative study of optical fibre types for application in a laser-induced ignition system. *Journal of Optics A: Pure and Applied Optics*, 11(5):1–10.

Mullett, J. D., Dickinson, P. B., Shenton, A. T., Dearden, G., and Watkins, K. G. (2008). Multi-Cylinder Laser and Spark Ignition in an IC Gasoline Automotive Engine: A Comparative Study. *SAE International*, (2008-01-0470):1–11.

Mullett, J. D., Dodd, R., Williams, C. J., Triantos, G., Dearden, G., Shenton, A. T., Watkins, K. G., Carroll, S. D., Scarisbrick, A. D., and Keen, S. (2007). The influence of beam energy, mode and focal length on the control of laser ignition in an internal combustion engine. *Journal of Physics D: Applied Physics*, 40(15):4730–4739.

Page, V., CHENG, H., Shenton, T., Lyon, E., Kuang, Z., and dearden, G. (2015). Neural Network Prediction of Engine Performance for Second Pulse Fire/No Fire

Decision Making in Dual Pulse Laser Ignited Engines. In *Laser Ignition Conference*, page Th4A.3. Optical Society of America.

Page, V., Lyon, E., Cheng, H., Shenton, T., Kuang, Z., and Dearden, G. (2014). Calibration of Ignition Location and Pulse Energy in the Laser Ignited Engine. In *PMC2014 2nd Biennial Conference on Powertrain Mapping and Calibration*, Bradford UK.

Pavel, N., Tsunekane, M., Kanehara, K., and Taira, T. (2011a). Composite all-ceramics, passively Q-switched Nd:YAG Cr4+:YAG monolithic micro-laser with two-beam output for multi-point ignition. In *2011 Conference on Lasers and Electro-Optics (CLEO 2011)*, 2011 Conference on Lasers and Electro-Optics (CLEO 2011). IEEE Computer Society.

Pavel, N., Tsunekane, M., and Taira, T. (2011b). Composite, all-ceramics, high-peak power Nd:YAG Cr4+:YAG monolithic micro-laser with multiple-beam output for engine ignition. *Optics Express*, 19(10):9378–9384.

Phuoc, T. X. (2000a). Laser spark ignition: Experimental determination of laser-induced breakdown thresholds of combustion gases. *Optics Communications*, 175(4):419–423.

Phuoc, T. X. (2000b). Single-point versus multi-point laser ignition: Experimental measurements of combustion times and pressures. *Combustion and Flame*, 122(4):508–510.

Phuoc, T. X. (2006). Laser-induced spark ignition fundamental and applications. *Optics and Lasers in Engineering*, 44(5):351–397.

Ramsden, S. A. and Savic, P. (1964). A Radiative Detonation Model for the Development of a Laser-Induced Spark in Air. *Nature*, 203(495):1217–1219.

Ranner, H., Tewari, P. K., Kofler, H., Lackner, M., Wintner, E., Agarwal, A. K., and Winter, F. (2007). Laser cleaning of optical windows in internal combustion engines. *Optical Engineering*, 46(10):104301 1–8.

Ronney, P. D. (1994). Laser versus conventional ignition of flames. *Optical Engineering*, 33(2):510–521.

Ryu, S. K., Won, S. H., and Chung, S. H. (2009). Laser-induced multi-point ignition with single-shot laser using conical cavities and prechamber with jet holes. *Proceedings of the Combustion Institute*, 32(2):3189–3196.

Schwarz, E., Muri, I., Tauer, J., Kofler, H., and Wintner, E. (2010). Laser-induced ignition by optical breakdown. *Laser Physics*, 20(6):1545–1553.

Shneider, M. N., Zhang, Z., and Miles, R. B. (2007). Plasma induced by resonance enhanced multiphoton ionization in inert gas. *Journal of Applied Physics*, 102(12):123103 1–7.

Stakhiv, A., Gilber, R., Kopecek, H., Zheltikov, A. M., and Wintner, E. (2004). Laser ignition of engines via optical fibers? *Laser Physics*, 14(5):738–747.

Steen, W. (1991). *Laser material processing.* Springer-Verlag.

Taira, T. (2011). Giant micro-photonics for laser ignitions. In *2012 International Conference on Optical MEMS and Nanophotonics (OMN 2012)*, International Conference on Optical MEMS and Nanophotonics, pages 232–233. IEEE Computer Society.

Thiyagarajan, M. and Scharer, J. (2008). Experimental investigation of ultraviolet laser induced plasma density and temperature evolution in air. *Journal of Applied Physics*, 104(1):0133031–12.

Tsunekane, M. and Taira, T. (2011). Laser performance of composite Nd:YAG Cr:YAG ceramics for laser ignition. In *Conference on Lasers and Electro-Optics, CLEO Pacific Rim 2011*, 2011 Int. Quantum Electron. Conf., IQEC 2011 and Conf. Lasers and Electro-Optics, CLEO Pacific Rim 2011 Incorporating the Australasian Conf. Optics, Lasers and Spectroscopy and the Australian Conf., pages 641–642. IEEE Computer Society.

Tsunekane, M. and Taira, T. (2013). High peak power, passively Q-switched Yb:YAG Cr:YAG micro-lasers. *IEEE Journal of Quantum Electronics*, 49(5):454–461.

Way, J., Hummelt, J., and Scharer, J. (2009). Experimental measurements of multi-photon enhanced air breakdown by a subthreshold intensity excimer laser. *Journal of Applied Physics*, 106(8):083303 1–8.

Weinberg, F. J. and Wilson, J. R. (1971). A preliminary investigation of the use of focused laser beams for minimum ignition energy studies. *Proceedings of the Royal Society of London Series a-Mathematical and Physical Sciences*, 321(1544):41–52.

Weinrotter, M., Iskra, K., Al-Janabi, A. H., Kopecek, H., and Wintner, E. (2004). Laser ignition of engines: multipoint, fiber delivery and diagnostics. *Advanced Laser Technologies*, 5850:88–99.

Weinrotter, M., Kopecek, H., Tesch, M., Wintner, E., Lackner, M., and Winter, F. (2005a). Laser ignition of ultra-lean methane/hydrogen/air mixtures at high temperature and pressure. *Experimental Thermal and Fluid Science*, 29(5):569–577.

Weinrotter, M., Kopecek, H., and Wintner, E. (2005b). Laser ignition of engines. *Laser Physics*, 15(7):947–953.

Yalin, A. P. (2013). High power fiber delivery for laser ignition applications. *Optics Express*, 21(S6):A1102–A1112.

Yalin, A. P., DeFoort, M., Willson, B., Matsuura, Y., and Miyagi, M. (2005). Use of hollow-core fibers to deliver nanosecond Nd:YAG laser pulses to form sparks in gases. *Optics Letters*, 30(16):2083–2085.